ADVANCES IN THE USE OF CONVOLUTION METHODS IN WELL TEST ANALYSIS

A Thesis

by

ADAIYIBO EMMANUEL KIO

Submitted to the Office of Graduate and Professional Studies of
Texas A&M University
in partial fulfillment of the requirements for the degree of

MASTER OF SCIENCE

Chair of Committee,	Thomas A. Blasingame
Committee Members,	Peter Valkó
	Maria Barrufet
Head of Department,	A. Daniel Hill

August 2017

Major Subject: Petroleum Engineering

ABSTRACT

This thesis formalizes and extends a prior work in the effort to create explicit solutions to directly compute the effects of wellbore storage and phase redistribution (phase redistribution is treated as a special case of the wellbore storage problem and is of secondary priority in this work). The objectives of this work are to: derive approximate solutions in the Laplace domain that can be *inverted* directly to the real domain; validate these approximate solutions against the exact solutions for wellbore storage; develop correlations to improve approximate solutions which do not perform well in their original form; develop schemes to "deconvolve" the effects of wellbore storage using either a direct "inversion" to remove these effects or one of the approximations to determine the undistorted solution as a root-solving problem.

The key element of this work is the development of the approximate solutions for the wellbore storage distortion case in the Laplace domain (*i.e.*, part of the first objective). As a starting point, we retrace the work of SPE 21826 and we note that these solutions hinge on the use of approximations for the constant rate (undistorted) solution (p_{sD}). In this work we utilize three scenarios to approximate the $p_{sD}(t_D)$ function for the purpose of the Laplace transform formulation: the "constant" $p_{sD}(t_D)$ case which considers $p_{sD}(t_D)$ to be constant; the "linear" $p_{sD}(t_D)$ case which considers $p_{sD}(t_D)$ to be defined by a linear relationship of t_D; and the "quadratic" $p_{sD}(t_D)$ case which considers $p_{sD}(t_D)$ to be defined by a quadratic relationship of t_D.

As in SPE 21826, each of these solutions has been recast and compared to the exact solution for cases of effects of wellbore storage and phase redistribution (the second objective).

The development of correlations to improve the derived explicit (real domain) solutions has proven problematic, for example, the simplest case is that of the "constant" $p_{sD}(t_D)$, where the solution is given as:

$$p_{wCD}(t_D) = p_{sD}(t_D)\left[1 - \exp\left[\frac{-t_D}{p_{sD}(t_D)C_D}\right]\right] \quad \text{("constant" } p_{sD}(t_D) \text{ case)}$$

The most interesting aspect of this result is that it is exact at very early and very late times, but has errors as high as 15.6 percent in terms of $p_{wCD}(t_D)$ and as high as 25.9 percent in terms of $p_{wCD}'(t_D)$. The goal is to ensure errors less than 1.5 percent for $p_{wCD}(t_D)$. This led to the effort to develop correlations (the third objective) for an "additive" error term (ε), where this function would be in terms of the variable $[t_D/(p_{sD}(t_D)C_D)]$, which appears to be a unique correlation variable for wellbore storage cases. Several correlations are presented in this work.

The last goal of this work is to provide a wellbore storage "deconvolution" scheme (the fourth objective) which uses a permutation of the methodology used to derive the approximate $p_{wCD}(t_D)$ solutions in order to derive the $p_{sD}(t_D)$ function in terms of the $p_{wCD}(t_D)$ solutions, and/or uses the $p_{wCD}(t_D)$ approximate solutions

as "root solutions" to solve for the input $p_{sD}(t_D)$ function. Demonstrative cases are provided for this "deconvolution" process.

DEDICATION

To my loving wife, Patricia, and my daughters, Agbani and Ibim.

Live as if you were to die tomorrow.
Learn as if you were to live forever.

— **Mahatma Gandhi**

ACKNOWLEDGEMENTS

I would like to thank:

Dr. T. A. Blasingame, without whom this work, nay my degree, would not be a reality. He provided funding, food, teaching, advice, guidance, humor, a plan and an attention to detail that has fundamentally made me a different person than the one who came to the university two years ago. His work ethic and dedication to family have been a shining example worthy of emulation. As a student with a young family, it is something that has made a strong impression. He walks his talk. He is not unwilling to do what he asks of you. Most importantly, he cared about me, the person, not just the student. For that, I will always be grateful. I sought an advisor and got an advisor and another dad.

Dr. P. P. Valkó, who preached the gospel of Mathematica to me, changed the way I saw computing and gave me a tool without which this work would have been much harder. He never complained about the many problems for which I needed his help and was always available to guide and encourage me.

Dr. M. A. Barrufet, for her excellent teaching, willingness to answer questions and support all through my studies.

Dr. W. Ayers, for his excellent teaching and for serving on my committee until he retired.

My mum, Mrs. Agbani Batubo, my dad. Mr. P. M. O. Batubo. and my siblings whose dedication to education, love, thoughts, prayers and well-wishes have steered me to where I am today.

My wife, Patricia Kio, who encouraged me to apply to the Masters program while I was still unsure and who, as a consequence of that good advice, has seen less of me in the past two years than she would have liked. My kids who have made great sacrifices for me to be here, through no fault of theirs.

My good friend, Shola Babalola, without whom my life here would have had a rocky start. My countrymen in the Department of Petroleum Engineering – Kingsley Madiebo, Femi Olorode, Feyi Olalotiti-Lawal, Femi Oyedokun, Paul Ofoche, Joshua Ebin, and Ebun Andrew, whose unique experiences and friendship have helped me all through my studies here.

The Blasingame Group, for being the best family I could have had away from home. Alex Valdes-Perez, Alvaro Betancourt, Nefeli Moridis, Matias Brolli, Jorge Garcia, Basayir al-Lawati, Hefdhi Abdennadher, Nattapon Lortong and Andrew Sivon are the best mates one can hope for.

The Department of Petroleum Engineering for awarding me a fellowship that was instrumental in my coming here and Texas A&M University for letting me have an experience that few people on earth are privileged to have.

CONTRIBUTORS AND FUNDING SOURCES

This work was supervised by a thesis committee consisting of Dr. T. A Blasingame, my advisor, Dr. P. P. Valkó of the Department of Petroleum Engineering and Dr. M. A. Barrufet of the Departments of Petroleum and Chemical Engineering.

Graduate study was supported by a Fellowship from the Department of Petroleum Engineering of Texas A&M University and a Graduate Research Assistantship from Dr. T. A. Blasingame.

TABLE OF CONTENTS

Page

LIST OF FIGURES

CHAPTER I
INTRODUCTION

1.1 Introduction

The computation of wellbore pressure responses in the presence of wellbore storage, skin and/or wellbore phase redistribution effects requires solving the diffusivity equation that describes flow through porous media. Solving the diffusivity equation for reservoir engineering purposes often requires the inversion of the Laplace space solutions, which can be done analytically or numerically. Generally, these solutions are often impossible to invert analytically and need to be inverted numerically using algorithms such as Stehfest (1970) and Gaver-Wynn-Rho (2004). Numerical inversions can be computationally intensive and time-consuming. Therefore, any methods of solving the various forms of the diffusivity equation that reservoir engineers deal with, that produces results comparable with numerical inversion solutions, without the attendant time and computing power, would be considered significant progress.

This work leans heavily on SPE 21826 (Blasingame et al. 1991) and extends it significantly. Blasingame *et al*. worked on the development of the methods that this thesis retraces, validates, improves on and extends. Ultimately this work aims to provide simple and easy-to-implement methods for obtaining approximate wellbore storage and phase distribution solutions that are accurate and do not require Laplace transform inversions in their implementation.

The relations developed in this work are verified for the computation of wellbore storage and skin effects for unfractured wells in homogeneous reservoirs (Agarwal et al. 1970), fractured wells in homogeneous reservoirs (Ozkan and Raghavan, 1989), and for wells in naturally fractured reservoirs (Bourdet and Gringarten, 1980 and Warren and Root, 1963).

Also, explicit techniques to compute pressure response in the presence of wellbore phase redistribution effects are validated. This calculation uses only the wellbore storage and wellbore phase redistribution dimensionless pressures to compute the total wellbore dimensionless pressure. Blasingame *et al*. (1991) opined that this result is useful in that it is possible to compute the effects of wellbore phase redistribution without a numerical inversion algorithm to invert the Laplace space solution and the result may provide insight into the analysis of pressure test data which exhibit the effects of wellbore phase redistribution.

The work goes ahead to attempt to develop empirical correlations, using the above-mentioned results as a starting point, and compare the obtained results with those obtained from the numerical inversion of the Laplace space solutions. The correlation results were an improvement on the closed-form approximate methods.

As in SPE 21826, this work does not develop methods to interpret well test data, it is expected that the development of several analysis techniques for wellbore storage distorted pressure data should arise from the computational formulae derived in this work. In particular, the relations derived in this work should be useful in interpreting the “unit slope” line on a type curve plot, and some relations may be useful for convolution and deconvolution analysis. In fact, deconvolution is attempted in this work based on the approximate methods developed and interesting results were obtained.

1.2 Objectives

The objectives of this work are:

- Derive approximate solutions in the Laplace domain that can be *inverted* directly to the real domain.
- Validate these approximate solutions against the exact solutions for wellbore storage.
- Develop correlations to improve approximate solutions which do not perform well in their original form.
- Develop schemes to "deconvolve" the effects of wellbore storage using either:
  - A direct "inversion" to remove these effects, or
  - Using one of the approximations to determine the undistorted solution as a root-solving problem.

1.3 Basic Concepts and Dimensionless Variables

For the purpose of completeness, it is important to provide some background for some of the reservoir engineering concepts that that are mentioned and applied throughout this work. It is also important to define the dimensionless variables that are used. All units that are not dimensionless are in standard "field units" — *i.e.*, pressures in psia, rates in barrels, permeability in millidarcies, time is in hours, and length in feet.

Dimensionless Wellbore Pressure

The dimensionless wellbore pressure, p_D, for a constant rate flow system is defined as

$$p_D = \frac{kh\Delta p}{141.2\, qB\mu} \quad \text{.....(1.1)}$$

where the pressure drop, Δp, for drawdown tests is

$$\Delta p = p_i - p_{wf} \text{ ,.....(1.2)}$$

and for buildup tests,

$$\Delta p = p_{ws} - p_{wf} \text{ .....(1.3)}$$

Where k is the reservoir permeability, h is the reservoir thickness, q is the flow rate, B is the formation volume factor, μ is the reservoir fluid viscosity, p_i is the initial reservoir pressure, p_{wf} is the wellbore flowing pressure, and p_{ws} is the wellbore shut-in pressure.

Wellbore Skin

Wellbore skin was described as the additional pressure in the immediate area surrounding the wellbore, due to a reduction in permeability, as a result of the formation damage that occurs during drilling and completion operations (van Everdingen, 1953). This pressure drop is given by the equation

$$\Delta p_{skin} = \frac{141.2qB\mu}{kh} s \,, \qquad (1.4)$$

where s is the dimensionless Skin Factor. The skin factor was defined by Hawkins (Lee et al. 2003) as

$$s = \left[\frac{k}{k_s} - 1\right] \ln\left[\frac{r_s}{r_w}\right], \qquad (1.5)$$

for a vertical wellbore of radius r_w, with two concentric zones of permeability around it –zone with altered permeability, k_s, and a radius, r_s, measured from the center of the wellbore, immediately around the wellbore, and zone with original reservoir permeability, k, further out. This concept is illustrated in **Figure 1.1**.

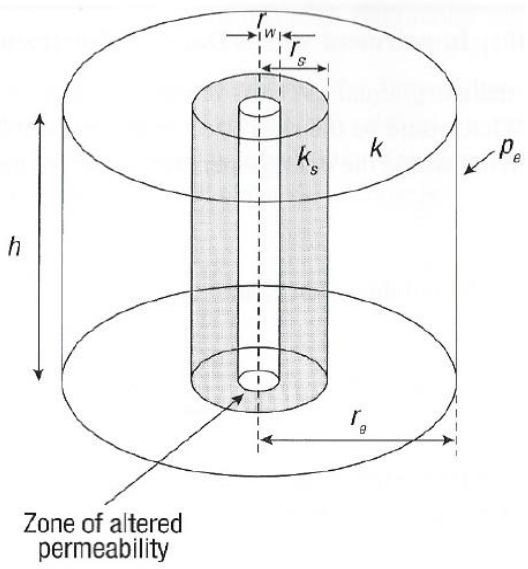

Figure 1.1 — Near Wellbore Zone of Altered Permeability (Reproduced from Economides et. al., 2013)

Dimensionless Wellbore Pressure with Skin Effects

For the constant rate solution, the skin factor has been demonstrated to be an additive function to the wellbore pressure response (Lee et al. 2003). The dimensionless wellbore pressure, p_{sD}, for a constant rate flow system with skin effects, s, is, therefore, defined as

$$p_{sD} = p_D + s \quad \text{.....(1.6)}$$

Wellbore Storage

Wellbore Storage is the phenomena that accounts for the difference between surface and bottomhole flowrates due primarily to the compressibility of the fluid within the wellbore. Occurring immediately after any change in the flowrate, the expansion or compression of the fluid causes a delay in the measured rates of the fluid. Wellbore storage is of significant interest due to its nature to mask reservoir behavior, at early-time, typically during well tests (*e.g.*, shut-in tests), but also during early flowback operations (Wiewiorowski, 2016).

The ability of the wellbore to store or unload fluids per unit change in pressure is the wellbore storage coefficient, C in bbl/psi (Lee, Rollins and Spivey, 2003), and it is given as

$$C = \frac{144 A_{wb}}{5.615 \rho}, \quad \text{.....(1.7)}$$

where A_{wb} is the wellbore area in square feet and ρ is the wellbore fluid density in lbm/ft^3.

Dimensionless Wellbore Storage Coefficients

The dimensionless wellbore storage coefficient, C_D, based on a wellbore radius, r_w, is given as

$$C_D = \frac{0.8936 C}{\phi c_t h r_w^{\,2}}, \quad \text{.....(1.8)}$$

and the dimensionless wellbore storage coefficient, C_{LfD}, based on fracture half-length, L_f, is given as

$$C_{LfD} = \frac{0.8936 C}{\phi c_t h L_f^{\,2}}, \quad \text{.....(1.9)}$$

where ϕ is the reservoir porosity, and c_t is the total compressibility of the reservoir and fluid system.

Dimensionless Time Functions

The dimensionless time, t_D, based on the wellbore radius, r_w, and time, t, is given as

$$t_D = \frac{0.0002637kt}{\phi\mu c_t {r_w}^2} \quad \text{.....(1.10)}$$

and the dimensionless time, t_{LfD}, based on the fracture half-length, L_f, t, is given as

$$t_{LfD} = \frac{0.0002637kt}{\phi\mu c_t {L_f}^2} \quad \text{.....(1.11)}$$

Dimensionless Flow Rate

The dimensionless flow rate is defined as

$$q_D = \frac{qB\mu}{0.00798kh(p_i - p_{wf})}, \quad \text{.....(1.12)}$$

Dimensionless Sandface Flow Rate Function with Wellbore Storage and Skin Effects

For a well with constant wellbore storage, the dimensionless sandface flow rate, q_{wCD}, is defined as

$$q_{wCD} = 1 - C_D \frac{dp_{wD}}{dt_D}, \quad \text{.....(1.13)}$$

where p_{wD} is the total dimensionless pressure (Agarwal et al. 1970).

Dimensionless Wellbore Pressure with Wellbore Storage and Skin Effects

The dimensionless wellbore pressure, p_{wCD}, for a constant rate flow system with wellbore storage and skin effects is defined as

$$p_{wCD} = \int_0^{t_D} \frac{d}{d\tau}\left[q_{wCD}(\tau)\right] p_{sD}\left(t_D - \tau\right) d\tau \quad \text{.....(1.14)}$$

The right hand side of Eq. 1.14 is the convolution integral. In well test analysis, convolution was introduced by van Everdingen and Hurst in 1949 to provide a mechanism in which to combine the constant rate solution with the constant pressure solution (Wiewiorowski, 2016).

Dimensionless Sandface Flow Rate Function with Wellbore Storage, Skin and Phase Redistribution Effects

For a well with wellbore storage and wellbore phase redistribution, the dimensionless sandface flow rate, q_{wCD}, is defined as

$$q_{w\phi D} = 1 - C_D\left(\frac{dp_{wD}}{dt_D} - \frac{dp_{\phi D}}{dt_D}\right). \quad (1.15)$$

where p_{wD} is the total dimensionless pressure with wellbore storage, skin, and wellbore phase redistribution effects while $p_{\varphi D}$ is the dimensionless pressure with wellbore phase redistribution effects (Fair, 1981).

Dimensionless Wellbore Pressure with Wellbore Storage, Skin and Phase Redistribution Effects

The dimensionless wellbore pressure, p_{wD}, for a constant rate flow system with wellbore phase redistribution and skin effects is defined as

$$p_{wD} = \int_0^{t_D} \frac{d}{d\tau}\left[q_{w\phi D}(\tau)\right] p_{sD}(t_D - \tau)\, d\tau \quad (1.16)$$

Dimensionless Pressure Derivative Functions

The dimensionless derivative function, p_D', which is used in the type curve analysis, is defined as

$$p_D' = \frac{dp_D}{d(\ln t_D)} \quad (1.17)$$

It can also be written as

$$p_D' = t_D \frac{dp_D}{dt_D} \quad (1.18)$$

We note that both forms of p_D' are mathematically equivalent.

Numerical Laplace Transform Inversion

All numerical Laplace transform inversions done in this work were obtained using the Gaver-Wynn-Rho algorithm, developed by Valko and Abate (2004), and implemented in Wolfram Mathematica.

CHAPTER II
LITERATURE REVIEW

This chapter aims to provide a brief study of wellbore storage and wellbore phase redistribution studies, as pertinent to this work.

2.1 Pressure Buildup Analysis with Wellbore Storage Distortion

Wellbore Storage is the phenomena that accounts for the difference between surface and bottomhole flowrates due primarily to the compressibility of the fluid within the wellbore. Occurring immediately after any change in the flowrate, the expansion or compression of the fluid causes a delay in the measured rates of the fluid. Wellbore storage is of significant interest due to its nature to mask reservoir behavior, at early-time, typically during well tests (*e.g.*, shut-in tests), but also during early flowback operations (Wiewiorowski, 2016).

van Everdingen and Hurst (1949) first developed solutions for wellbore storage effects in their classic paper about the application of Laplace transforms to solving the diffusivity equations that petroleum engineers have. In that work, they posited that to obtain the relation between flowing bottomhole pressure and the rate of production from a formation, it is necessary to correct the rate of production as measured in the flow tanks for the amount of oil obtained from the annulus between casing and tubing. They determined that the rate of unloading of the annulus $q_{\Delta(T)}$, expressed in cubic centimeters per second corrected to reservoir conditions was given by

$$q_{\Delta(T)} = C\frac{d\Delta p}{dT}, \quad (2.1)$$

where Δp is the pressure drop and C is the volume of fluid unloaded from the annulus per atmosphere bottom hole pressure drop her unit sand thickness (i.e. wellbore storage).

They defined dimensionless wellbore storage as

$$C_D = \frac{0.8936C}{\phi c_t h r_w{}^2}, \quad (2.2)$$

with all parameters in field units. They also, wrote the convolution integral describing the dimensionless bottomhole pressure affected by wellbore storage, p_{wD}, as

$$p_{wD} = \int_0^{t_D}\left[1 - C_D\frac{dp_{wD}(\tau)}{d\tau}\right]\frac{dp_D(t_D-\tau)}{dt_D}d\tau, \quad (2.3)$$

and demonstrated how to solve for p_{wD} using Laplace transforms.

van Everdingen (1953) introduced the steady-state skin effect as an "additive" pressure drop at the sandface in his work explaining the effect of skin on the productive capacity of a well and proposing an exponential model for sandface flow rate. Agarwal et al. (1970) and Wattenbarger and Ramey (1970) used the steady-state skin effect, explained by van Everdingen, in the convolution integral equation, and developed analytical and numerical methods for dealing with wellbore storage and skin in wells with unsteady flow.

McKinley (1971) worked on calculating wellbore transmissibility from build-up data with wellbore storage distortion and developed type curve analysis for it.

Ramey (1965), in his work on non-Darcy flow and wellbore storage effects extended van Everdingen's work to drawdown in gas wells.

2.2 Pressure Buildup Analysis with Wellbore Phase Redistribution

Stegmeier and Matthews (1958) described wellbore phase redistribution as a wellbore storage phenomenon occurring when both liquid and gas flow through the tubing. When such a well is shut-in at the surface, gravity cause the liquid to fall to the bottom and the gas to rise to the surface. The gas that rises to the surface tries to expand and, consequently, exerts pressure on the liquid, as there is little room for expansion and the liquid is relatively incompressible. That pressure that is temporarily exerted causes a "hump" in the pressure profile.

Fair (1981), in his work on wellbore phase redistribution went further than Stegmeier and Matthews (1958), carrying out analysis of wellbore phase redistribution by including it as wellbore storage in the dimensionless diffusivity equation. The dimensionless flow rate was then given as

$$q_D(t_D) = 1 - C_D\left[\frac{dp_{wD}}{d_{tD}} - \frac{dp_{\phi D}}{d_{tD}}\right], \quad (2.4)$$

where $p_{\phi D}$ is the pressure caused by phase redistribution, given by:

$$p_{\phi D}(t_D) = C_{\phi D}[1 - e^{-t_D/\alpha_D}], \quad (2.5)$$

where α_D is the time in which 63% of the total change has occurred,

$$p_{\phi D} = \frac{khp_{\phi}}{141.2qB_o\mu} \quad (2.6)$$

$$C_{\phi D} = \frac{khC_{\phi}}{141.2qB\mu} \quad (2.7)$$

$$t_D = \frac{0.00264kt}{\phi\mu c_t {r_w}^2} \quad \text{.....(2.8)}$$

$$\alpha_D = \frac{0.00264k\alpha}{\phi\mu c_t {r_w}^2} \quad \text{.....(2.9)}$$

with all non-dimensionless parameters in field units.

CHAPTER III
APPROXIMATIONS FOR $p_{wCD}(t_D)$

In this chapter, we follow the work done in SPE 21826 (Blasingame et al) to develop rigorous analytical approximations for the dimensionless pressure function that includes the effects of wellbore storage and skin, $p_{wCD}(t_D)$. As a recognition of the imperfection inherent in these approximations, correlations are developed to create better approximations that, while not derived through a rigorous mathematical process, are more accurate than the analytical approximations. As a special case of the wellbore storage and skin problem, an explicit solution for the computation of the effects of wellbore storage and phase redistribution is also developed.

3.1 Analytical Approximations of $p_{wCD}(t_D)$

The convolution integral for wellbore storage is given as

$$p_{wCD}(t_D) = \int_0^{t_D} \frac{d}{d\tau}\left[q_{wCD}(\tau)\right] p_{sD}(t_D - \tau)\, d\tau \quad \text{.....(3.1)}$$

where

$$q_{wCD}(t_D) = 1 - C_D \frac{d}{dt_D}\left[p_{wCD}(t_D)\right] \quad \text{.....(3.2)}$$

and

$$p_{sD}(t_D) = p_D(t_D) + S \quad \text{.....(3.3)}$$

Taking the Laplace transforms of Eqs. 2.1 and 2.2 and rearranging gives

$$\bar{p}_{wCD}(u) = \frac{1}{\left[\dfrac{1}{\bar{p}_{sD}(u)} + C_D u^2\right]}, \quad \text{.....(3.4)}$$

which can also be written as

$$\bar{p}_{wCD}(u) = \frac{\bar{p}_{sD}(u)}{[1 + C_D u^2 \bar{p}_{sD}(u)]} \quad \text{.....(3.5)}$$

Appendix A details the derivation of Eqs. 3.4 and 3.5.

It is clear from these equations that the *nature* of $\bar{p}_{sD}(u)$ i.e. $p_{sD}(t_D)$ determines the nature of $\bar{p}_{wCD}(u)$ i.e. $p_{wCD}(t_D)$. Therefore, the solutions that are developed are based on making reasonable approximations of $p_{sD}(t_D)$ transforming those approximations into Laplace space, and solving Eq. 3.4 or 3.5.

Case 1: $p_{wCD}(t_D)$ Approximation Based on Constant $p_{sD}(t_D)$

The simplest approximation that can be made for the $p_{sD}(t_D)$ function is that it is constant near a particular time of interest, say between two data points. This equation can be written as

$$p_{sD}(t_D) = a \,, \qquad (3.6)$$

where a is constant.

Appendix B develops this idea in detail and results in the approximation for $p_{wCD}(t_D)$ given as

$$p_{wCD}(t_D) = p_{sD}(t_D)\left[1 - \exp\left[\frac{-t_D}{p_{sD}(t_D)C_D}\right]\right] \qquad (3.7)$$

Eq. 3.7 states that the $p_{wCD}(t_D)$, function is an exponentially increasing function of the $p_{sD}(t_D)$ relation. As stated in SPE 21826, this is a somewhat intuitive result since we know that the $p_{wCD}(t_D)$, function increases monotonically over time until it is identical to the $p_{sD}(t_D)$ function.

The dimensionless pressure derivative function, $p_{wCD}'(t_D)$ can be computed by

$$p_{wCD}'(t_D) = t_D \frac{dp_{sD}(t_D)}{dt_D}\left[1 - \exp\left[\frac{-t_D}{p_{sD}(t_D)C_D}\right]\right] + \frac{t_D}{p_{sD}(t_D)C_D}\left[p_{sD}(t_D) - t_D \frac{dp_{sD}(t_D)}{dt_D}\right]\exp\left[\frac{-t_D}{p_{sD}(t_D)C_D}\right] \qquad (3.8)$$

Eq. 3.8 is good for computing the pressure derivative, $p_{wCD}'(t_D)$, but it might be more convenient to employ numerical means for that computation.

The dimensionless sandface flow rate can be computed by

$$q_{wCD}(t_D) = 1 - \exp\left[\frac{-t_D}{p_{sD}(t_D)C_D}\right]. \qquad (3.9)$$

In the next chapter, the results from these relations would be compared to results obtained from the numerical Laplace transform inversion solutions.

Case 2: $p_{wCD}(t_D)$ Approximation Based on Linear $p_{sD}(t_D)$

The second approximation for the $p_{sD}(t_D)$ function assumes that the $p_{sD}(t_D)$ function is linear near a particular time of interest, say between two data points. This equation can be written as

$$p_{sD}(t_D) = a + bt_D, \quad (3.10)$$

where are a and b are constants that can be easily determined.

Differentiating Eq. 3.10 with respect to t_D gives

$$b = \frac{d}{dt_D}\left[p_{sD}(t_D)\right] \quad (3.11)$$

a can, therefore, be determined by substituting b from Eq. 3.11 into Eq. 3.10. This gives

$$a = p_{sD}(t_D) - t_D \frac{d}{dt_D}\left[p_{sD}(t_D)\right] \quad (3.12)$$

Appendix B develops this idea in detail and results in the approximation for $p_{wCD}(t_D)$ given as

$$p_{wCD}(t_D) = \frac{y}{x}[1-\exp(-xt_D)] + \frac{z}{x^2}[1-\exp(-xt_D)] \quad (3.13)$$

where the generalized coefficients for this case, x,y, and z, are defined as

$$x = \frac{1+yC_D}{aC_D} \quad (3.14) \qquad y = \frac{1}{C_D} \quad (3.15) \qquad z = \frac{b}{aC_D} \quad (3.16)$$

Eq. 3.12 can also be expressed without any coefficients as

$$p_{wCD}(t_D) = \frac{p_{sD}(t_D) + C_D t_D\left[\frac{d}{dt_D}\left[p_{sD}(t_D)\right]\right]^2}{\left[1+C_D\left[\frac{d}{dt_D}\left[p_{sD}(t_D)\right]\right]\right]^2} + \exp\left[-\frac{t_D + C_D t_D\left[\frac{d}{dt_D}\left[p_{sD}(t_D)\right]\right]}{C_D\left[p_{sD}(t_D) - t_D\frac{d}{dt_D}\left[p_{sD}(t_D)\right]\right]}\right]\left[\frac{t_D\frac{d}{dt_D}\left[p_{sD}(t_D)\right] - p_{sD}(t_D)}{\left[1+C_D\left[\frac{d}{dt_D}\left[p_{sD}(t_D)\right]\right]\right]^2}\right] \quad (3.17)$$

Appendix G details the development of Eq. 3.17. It is mathematically equivalent to Eq. 3.13 and more inconvenient to implement, but is presented here for the purpose of completeness.

An expression for the dimensionless pressure derivative, $p_{wCD}'(t_D)$, is not developed here because the analytical differentiation of either of Eqs. 3.13 or 3.17 would yield very complex results. It is more efficient to find the pressure derivative by numerical methods.

The dimensionless sandface flow rate, $q_{wCD}(t_D)$, can be computed by the substitution of results obtained from the numerical differentiation of $p_{wCD}(t_D)$ into Eq. 3.2.

In the next chapter, the results from these relations would be compared to results obtained from the numerical Laplace transform inversion solutions.

Case 3: $p_{wCD}(t_D)$ Approximation Based on Quadratic $p_{sD}(t_D)$

The second approximation for the $p_{sD}(t_D)$ function assumes that the $p_{sD}(t_D)$ function is linear near a particular time of interest, say between two data points. This equation can be written as

$$p_{sD}(t_D) = a_0 + a_1 t_D + a_2^* t_D^2 \quad \text{.....(43)}$$

where are a_0, a_1, and a_2* are constants that can be determined by the process detailed in Appendix D where the details of this approximation are documented

The complexity of this approximation suggests that it would be difficult to implement without a spreadsheet or software package to do the calculations.

In the next chapter, the results from these relations would be compared to results obtained from the numerical Laplace transform inversion solutions.

3.2 Empirical Approximations of $p_{wCD}(t_D)$

As would be seen in the next chapter, although the approximations are good, they are not perfect. In order to improve the accuracy of these approximations, correlations were developed for term an "additive" discrepancy term (ε), where this function would be in terms of the variable $[t_D/(p_{sD}(t_D)C_D)]$. This discrepancy function would, in theory, be the difference between the actual $p_{wCD}(t_D)$ obtained from numerical methods and the approximate $p_{wCD}(t_D)$ obtained from Section 3.1.

The approximate $p_{wCD}(t_D)$ solution chosen for improvement is the constant $p_{sD}(t_D)$ solution given by Eq. 3.7.

$$p_{wCD}(t_D) = p_{sD}(t_D)\left[1 - \exp\left[\frac{-t_D}{p_{sD}C_D}\right]\right]. \quad \text{.....(3.7)}$$

The improved approximation would be of the form

$$p_{wCD}(t_D) = p_{sD}(t_D)\left[\left[1 - \exp\left[\frac{-t_D}{p_{sD}C_D}\right]\right] - \varepsilon\left[\frac{t_D}{p_{sD}C_D}\right]\right], \quad \text{.....(3.8)}$$

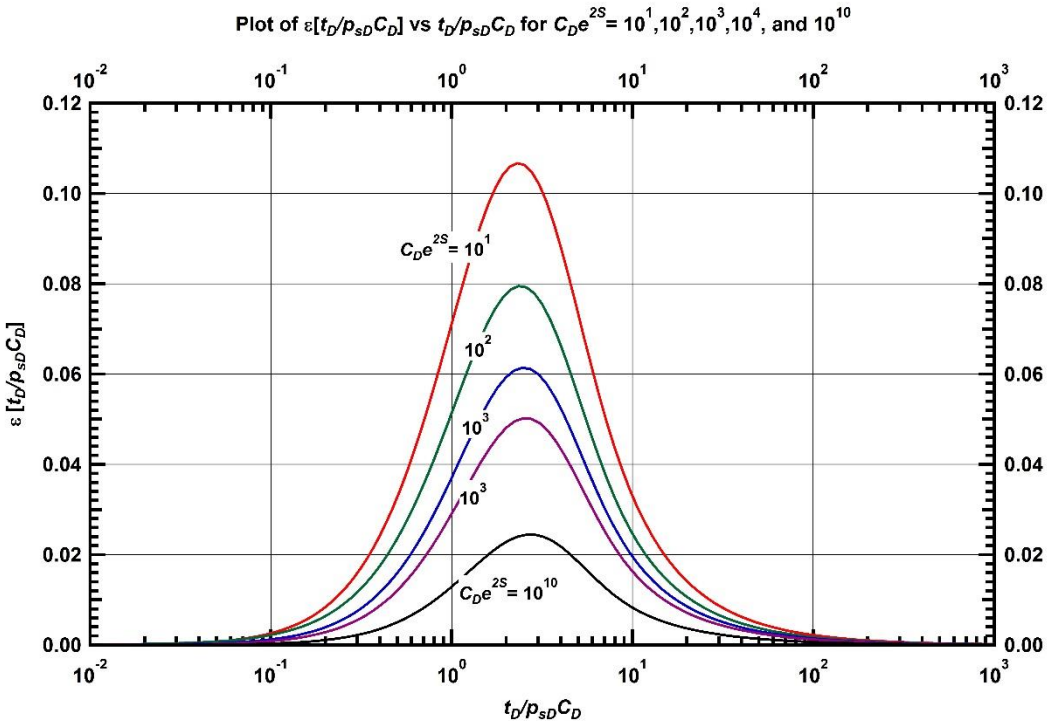

Figure 3.1 — Plot showing ε vs. $t_D/(p_{sD}\,C_D)$ for C_De^{2s} values of 10^1, 10^2, 10^3, 10^4 and 10^{10}

A semilog plot of $\varepsilon[t_D/(p_{sD}\,C_D)]$ vs. $t_D/(p_{sD}\,C_D)$ for C_De^{2s} values of 10^1, 10^2, 10^3, 10^4 and 10^{10} is shown in **Figure 3.1**. All other values of C_De^{2s} show a similar shape. This plot suggests that $\varepsilon[t_D/(p_{sD}\,C_D)]$ is either normally distributed (Gaussian distribution) or distributed in a fashion that is similar in shape to the normal distribution. This implies that a mathematical equation describing the normal distribution or one that describes a shape such as this could accurately model $\varepsilon[t_D/(p_{sD}\,C_D)]$.

There are several equations of varying mathematical complexity that could describe a function shaped like this and two were chosen for this work – normal distribution and modified normal distribution. Detailed developments of both approximate correlations can be found in Appendix F.

Normal Distribution Adjustment Correlation for $p_{wCD}(t_D)$

The normal distribution is given by Abramowitz and Stegun (1972) as

$$p=\frac{\alpha}{\sigma\sqrt{2\pi}}\exp\left[-\frac{1}{2}\left[\frac{x-m}{\sigma}\right]^2\right] \qquad (3.10)$$

Where p is the probability distribution function, α is a scaling factor, m is the mean of the distribution, σ is the variance of the distribution and x is value of the data point.

In our case, the normal distribution equation describing $\varepsilon[t_D/(p_{sD}\,C_D)]$ would be

$$\varepsilon\left[\frac{t_D}{p_{sD}C_D}\right]=\frac{\alpha}{\sigma\sqrt{2\pi}}e^{-\frac{1}{2}\left[\frac{\ln\left[\frac{t_D}{p_{sD}C_D}\right]-m}{\sigma}\right]^2} \qquad (3.11)$$

An improved approximation of $p_{wCD}(t_D)$, obtained from combining Eqs. 3.8 and 3.11, can, therefore, be written as

$$p_{wCD}(t_D)=p_{sD}(t_D)\left[\left[1-\exp\left[\frac{-t_D}{p_{sD}C_D}\right]\right]-\frac{\alpha}{\sigma\sqrt{2\pi}}e^{-\frac{1}{2}\left[\frac{\ln\left[\frac{t_D}{p_{sD}C_D}\right]-m}{\sigma}\right]^2}\right] \qquad (3.12)$$

where the parameters α, m, and, σ are given by the following correlations and shown in **Figures 3 2** and **3.3**.

$$\alpha = \frac{26}{77.1579}\exp\left[-\frac{|1.43087\ln C_D + 1|}{9.50843}\right] + 0.03772, \text{for } C_D < 1, \quad \text{.....(3.13a)}$$

$$\alpha = \frac{1.6}{\ln C_D + 4.4}, \text{for } C_D \geq 1, \quad \text{.....(3.13b)}$$

$$m = 0.90, \text{for } C_D < 10^3, \quad \text{.....(3.14a)}$$

$$m = 1.00, \text{for } C_D \geq 10^3, \quad \text{.....(3.14b)}$$

$$\sigma = \frac{58}{21\sqrt{2\pi}} e^{-\frac{1}{2}\left[\frac{\ln C_D - 1}{21}\right]^2}, \text{for } C_D < 10^6, \quad \text{.....(3.15a)}$$

$$\sigma = 0.94, \text{for } C_D \geq 10^6 \quad \text{.....(3.15b)}$$

The dimensionless pressure derivative, $p_{wCD}'(t_D)$ and dimensionless sandface flow rate, $q_{wCD}(t_D)$, can be computed by numerical methods.

In the next chapter, the results from these relations would be compared to results obtained from the numerical Laplace transform inversion solutions.

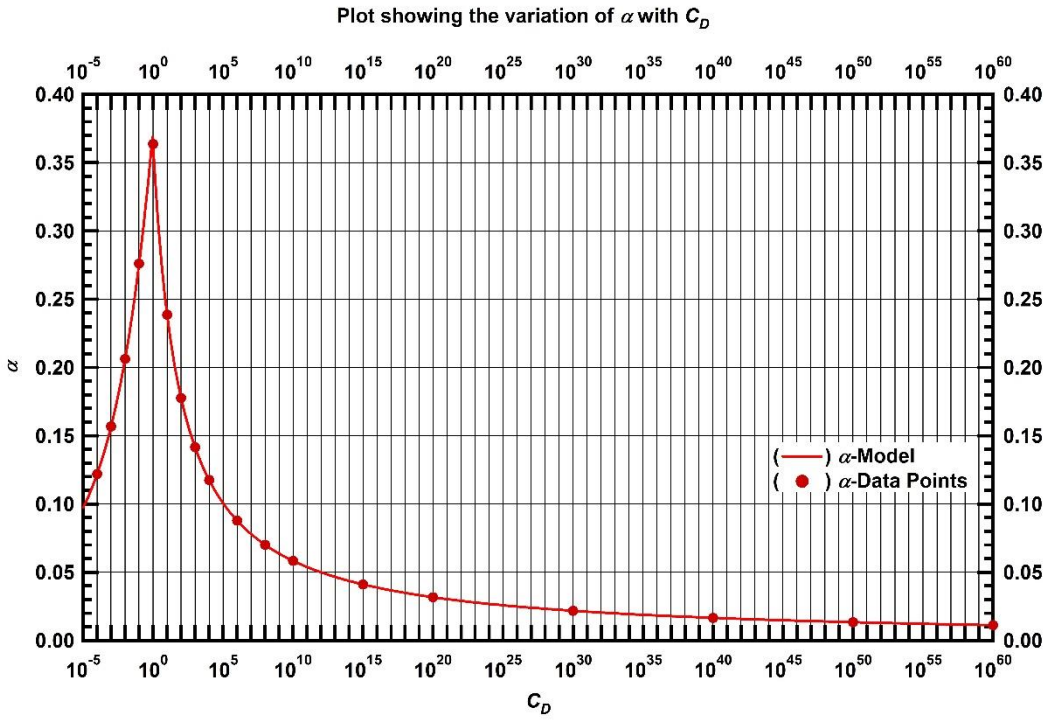

Figure 3.2 — Plot showing the variation of α with C_D.

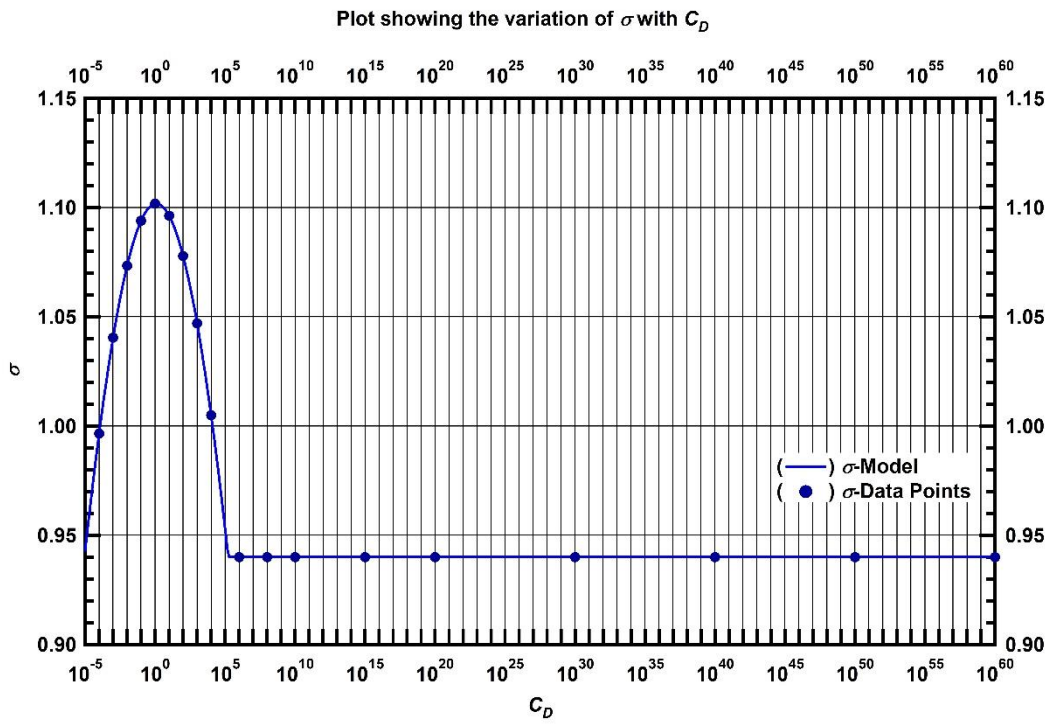

Figure 3.3 — Plot showing the variation of m with C_D.

Modified Normal Distribution Adjustment Correlation for $p_{wCD}(t_D)$

The modified normal distribution, developed in this work, can be written as

$$p = \frac{\alpha_1}{\sigma_1\sqrt{2\pi}}\exp\left[-\frac{1}{2}\left[\frac{x-m_1}{\sigma_1}\right]^2\right] + \frac{\alpha_2}{\sigma_2\sqrt{2\pi}}\exp\left[-\frac{1}{2}\left[\frac{x-m_2}{\sigma_2}\right]^2\right] \quad \text{.....(3.16)}$$

This is essentially the addition to two normal distribution equations, where p is the probability distribution function, α_1 and α_2 are the scaling factors, m_1 and m_2 are the means of the distributions, σ_1 and σ_2 are the variances of the distributions and x is value of the data point.

In our case, the normal distribution equation describing $\varepsilon[t_D/(p_{sD}\,C_D)]$ would be

$$\varepsilon\left[\frac{t_D}{p_{sD}C_D}\right] = \frac{\alpha_1}{\sigma_1\sqrt{2\pi}}\exp\left[-\frac{1}{2}\left[\frac{\ln\left[\frac{t_D}{p_{sD}C_D}\right]-m_1}{\sigma_1}\right]^2\right] + \frac{\alpha_2}{\sigma_2\sqrt{2\pi}}\exp\left[-\frac{1}{2}\left[\frac{\ln\left[\frac{t_D}{p_{sD}C_D}\right]-m_2}{\sigma_2}\right]^2\right]$$

.....(3.17)

An improved approximation of $p_{wCD}(t_D)$, obtained from combining Eqs. 3.8 and 3.17 can, therefore, be written as

$$p_{wCD}(t_D) = p_{sD}(t_D)\left[\left[1-\exp\left[\frac{-t_D}{p_{sD}C_D}\right]\right]-\frac{\alpha_1}{\sigma_1\sqrt{2\pi}}\exp\left[-\frac{1}{2}\left[\frac{\ln\left[\frac{t_D}{p_{sD}C_D}\right]-m_1}{\sigma_1}\right]^2\right]\right] + \frac{\alpha_2}{\sigma_2\sqrt{2\pi}}\exp\left[-\frac{1}{2}\left[\frac{\ln\left[\frac{t_D}{p_{sD}C_D}\right]-m_2}{\sigma_2}\right]^2\right] \quad \text{.....(3.18)}$$

Where the parameters α_1, α_2, m_1, m_2, σ_1, and σ_2 are given by the following correlations and shown in **Figures 3.4** and **3.5**.

$$\alpha_1 = \frac{67}{46.79328048}\exp\left[-\frac{|0.17712654\ln C_D|}{6.491984578}\right] + 0.06176, \text{for } C_D < 1, \quad \text{.....(3.19a)}$$

$$\alpha_1 = \frac{7.25627685}{\ln C_D + 4.82070369}, \text{ for } C_D \geq 1, \quad \text{.....(3.19b)}$$

$$\alpha_2 = \frac{67}{46.79328048}\exp\left[-\frac{|0.17712654\ln C_D|}{6.491984578}\right] + 0.06176, \text{for } C_D < 1, \quad \text{.....(3.20a)}$$

$$\alpha_2 = \frac{4.02500168}{\ln C_D + 6.45174628}, \text{ for } C_D \geq 1, \quad \text{.....(3.20b)}$$

$$m_1 = 0.33475819\,\text{erf}(0.00017879 C_D) + 3.43607917, \quad \text{.....(3.21)}$$

$$m_2 = 0.16\,\text{erf}(0.000038895 C_D) + 1.44896298, \quad \text{.....(3.22)}$$

$$\sigma_1 = 1.58, \quad \text{.....(3.23)}$$

$$\sigma_2 = 0.79. \quad \text{.....(3.24)}$$

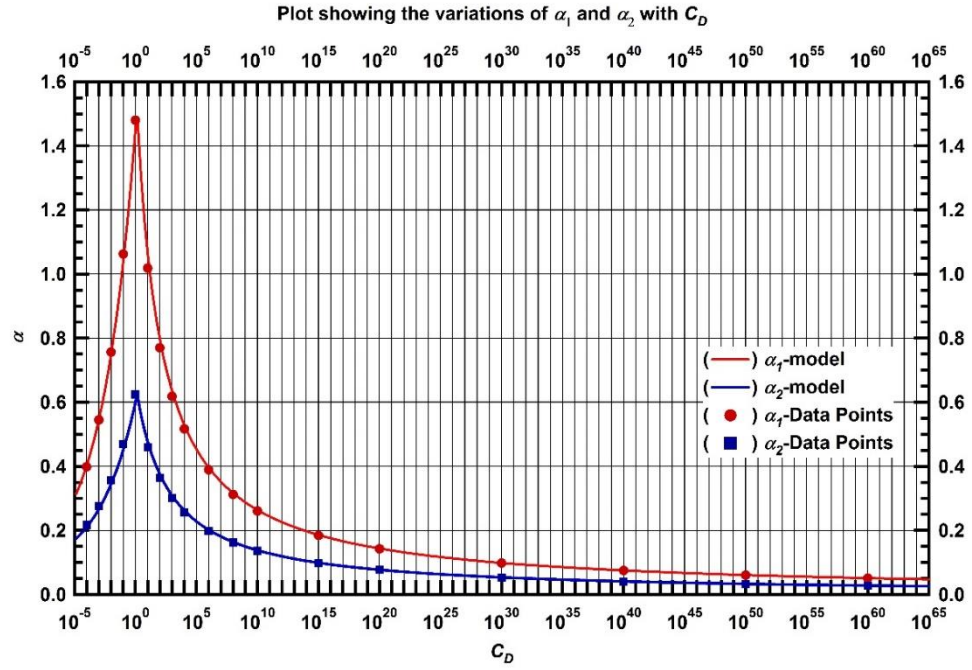

Figure 3.4 — Plot showing the variation of α_1 and α_2 with C_D.

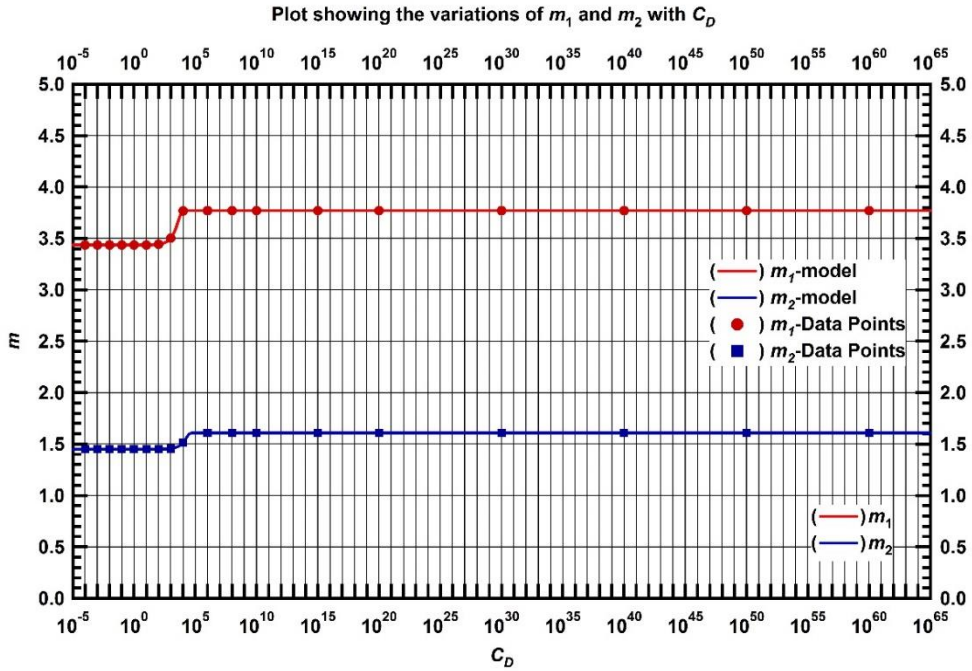

Figure 3.5 — Plot showing the variation of m_1 and m_2 with C_D.

3.3 Explicit Calculation of the Wellbore Phase Redistribution Dimensionless Pressure, $p_{wD}(t_D)$

In this section, we verify two formulae which can be used to explicitly compute the total dimensionless pressure for a system with wellbore storage, skin and wellbore phase redistribution effects. These relations are developed rigorously.

These formulae were constructed in such a way that the total dimensionless pressure, p_{wD}, is given as

$$p_{wD}(t_D) = p_{wCD}(t_D) + p_{w\phi D}(t_D) \quad \text{.....(3.1)}$$

where $p_{w\phi D}(t_D)$ is the dimensionless wellbore storage pressure and the dimensionless wellbore phase redistribution pressure, $p_{w\phi D}(t_D)$ is given as

$$p_{w\phi D}(t_D) = C_D \sum_{i=1}^{n} \left[\frac{d}{dt_D}[p_{\phi D}(t_{D,i}) - \frac{d}{dt_D}[p_{\phi D}(t_{D,i-1})] \right] p_{wCD}(t_{D,i-1}) \quad \text{.....(3.2)}$$

or, alternatively as

$$p_{w\phi D}(t_D) = C_D \sum_{i=1}^{n} \left[\frac{d}{dt_D}[p_{wCD}(t_{D,i})] - \frac{d}{dt_D}[p_{wCD}(t_{D,i-1})] \right] p_{\phi D}(t_{D,i-1}) \quad \text{.....(3.3)}$$

Also, the dimensionless phase redistribution pressure, $p_{\phi D}(t_D)$ is given by Fair (1981) as

$$p_{\phi D}(t_D) = C_{\phi D} \left[1 - \exp\left[\frac{-t}{\alpha_{\phi D}} \right] \right] \quad \text{.....(3.4)}$$

Our experience suggests that, when using the model of $p_{\phi D}(t_D)$ given by Eq. 3.4, Eq. 3.3 will yield the most accurate results for $p_{\phi D}(t_D)$ relative to results obtained from numerical Laplace transform inversion.

CHAPTER IV
VALIDATION OF RESULTS

In this chapter, we validate the approximations for $p_{wCD}(t_D)$ developed in the previous chapter. As was done in SPE 21826, each of these solutions are compared to the exact solutions for cases of effects of wellbore storage and phase redistribution for chosen reservoir systems. While SPE 21826 did a qualitative comparison for purposes of validation, this thesis goes further. Both qualitative and quantitative comparisons are done in order to ascertain the accuracy of these approximations and correlations, and determine which is best suited for the different reservoir systems.

In the qualitative comparisons, visual inspections of the curves are done to

- See if there is general agreement between the approximate and actual solutions.
- Locate the areas where the solutions match up well and where they do not.

For quantitative comparisons, we quantify by how much the approximate solution is off from the actual solution, by calculating the error. For the determination of error, we introduce the term Absolute Relative Error (*ARE*), in percent, which is the absolute value of the difference between the actual solution, obtained using numerical methods, and the approximate solution. Absolute Relative Error (*ARE*) is given as

$$ARE = \frac{\left| p_{wCD_{Actual}} - p_{wCD_{Approximate}} \right|}{p_{wCD_{Actual}}} \times 100 \quad \text{.....(4.1)}$$

All of the verification cases use the infinite-acting (transient) flow solutions for the chosen reservoir system.

4.1 Validation of Analytical Approximations

Unfractured Wells in an Infinite-Acting Homogeneous Reservoir

The infinite-acting homogeneous reservoir solution with wellbore storage and skin effects is the simplest and probably best-documented case of the convolution integral solution. There is ample discussion of the subject and solutions by several authors, one of which is van Everdingen and Hurst (1949). The consensus is that an analytical solution to the problem is impossible and solutions have to be obtained by numerical methods, hence the use of numerical Laplace transform inversions. This work aims to develop approximations and correlations, which accurately describe the pressure response distorted by wellbore storage and skin effects, which can be utilized without the need for numerical inversions.

As was done in SPE 21826, the behavior of $p_{wCD}(t_D)$ for $10^{-1} \le t_D/C_D \le 10^4$ for 13 values of C_De^{2S} ranging from 10^1 to 10^{60} is plotted. These parameters will be used for all of the unfractured well cases for the $p_{wCD}(t_D)$, $p_{wCD}'(t_D)$ and $q_{wCD}(t_D)$ solutions.

Case 1: $p_{wCD}(t_D)$ Approximation Based on Constant $p_{sD}(t_D)$

Case 1 hinges on the assumption that the $p_{sD}(t_D)$ function can be considered constant near a particular time of interest. It has to be noted that this does not imply a constant $p_{sD}(t_D)$ for the well, which would make no physical sense. The assumption applies only for a "brief" time period of interest (for instance, between two well test data points), and is useful in obtaining the approximation.

Figure 4.1 shows the behavior of the $p_{wCD}(t_D)$ function, computed using Eq. 3.7. It is clear that there is general agreement between the actual solutions and approximate solutions, especially in very early times and late times. However between the time period $1 \leq t_D/C_D \leq 5 \times 10^1$, there is some deviation by the approximate solutions from the actual solutions. This can clearly be seen in the *ARE* plot shown in **Figure 2** where when C_De^{2S} is 10^1, the error is as high as 15.6%. For larger values of C_De^{2S} the error drops significantly. This shows that the case 1 approximation (linear $p_{sD}(t_D)$ assumption) can accurately predict the $p_{wCD}(t_D)$ solution.

Figure 4.3 shows the behavior of the $p_{wCD}'(t_D)$ function for case 2. This function was computed analytically, as the closed-form of the derivative function (Eq. 3.8) is simple enough to be dealt with that way. As with the $p_{wCD}(t_D)$ function, there is general agreement between the actual and approximate solutions. Also, the approximate derivative solutions deviates over the same parameter range as the $p_{wCD}(t_D)$ function i.e. $1 \leq t_D/C_D \leq 5 \times 10^1$. In this case the deviation is more pronounced, because the errors inherent in a function are naturally amplified in their derivative function. It will also be noted that the error is highest when the derivative curve is about to go into radial flow stabilization, i.e. when the value of $p_{wCD}'(t_D)$ is 0.5. The time period at which this happens varies for different values of C_De^{2S}. **Figure 4.4** shows that when C_De^{2S} is 10^1, that error is about 25.9%. It also shows that, unlike the errors that occur in the time period $1 \leq t_D/C_D \leq 5 \times 10^1$, the errors close to radial flow stabilization do not decrease significantly with an increase in C_De^{2S}. However, for all most practical uses of the derivative function, this error would be within engineering accuracy. The results in Figures 4.3 and 4.4 suggest that the case 1 approximation (constant $p_{sD}(t_D)$ assumption) can accurately predict the $p_{wCD}(t_D)$ solution and the resulting $p_{wCD}'(t_D)$ solution is also accurate

Figure 4.5 shows the behavior of the $q_{wCD}(t_D)$ function for case 1, computed using Eq. 3.9. As expected, the errors inherent in the $p_{wCD}(t_D)$ and $p_{wCD}'(t_D)$ solutions are present in the $q_{wCD}(t_D)$ solution. As with the $p_{wCD}'(t_D)$ function, the $q_{wCD}(t_D)$ function magnifies the errors in the $p_{wCD}(t_D)$ function due to the differentiation that is carried out in the computation. The accuracy of the the $q_{wCD}(t_D)$ function should be considered the most sensitive test of the approximate solutions and should not detract from the use of the $p_{wCD}(t_D)$ and $p_{wCD}'(t_D)$ functions obtained using this approximation. The errors associated with each function i.e. $p_{wCD}(t_D)$ and $p_{wCD}'(t_D)$ should be within the accuracy needed for most reservoir engineering applications.

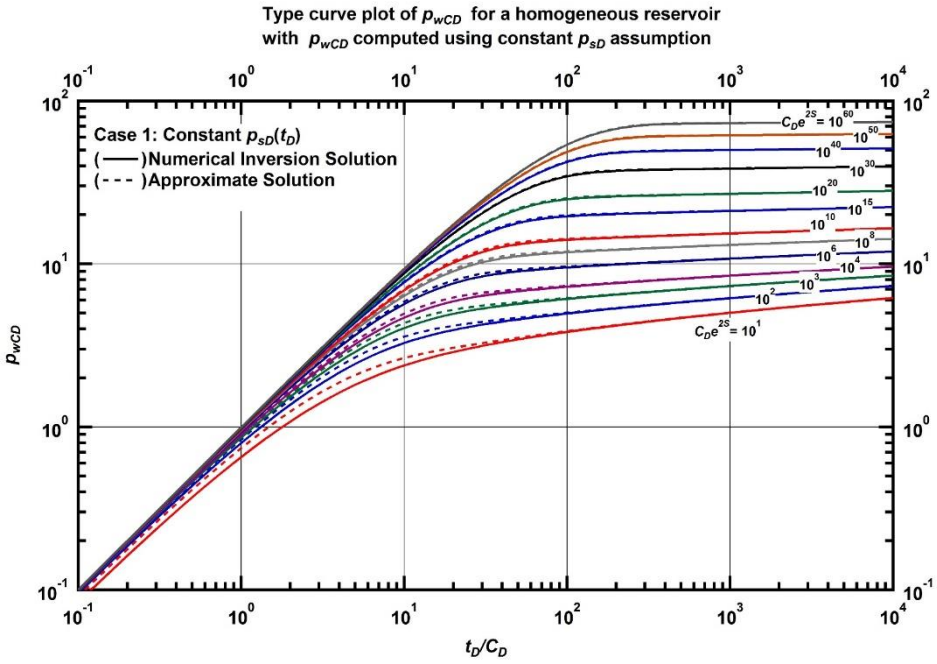

Figure 4.1 — Type curve plot of p_{wCD} for a homogeneous reservoir. p_{wCD} computed using constant p_{sD} assumption.

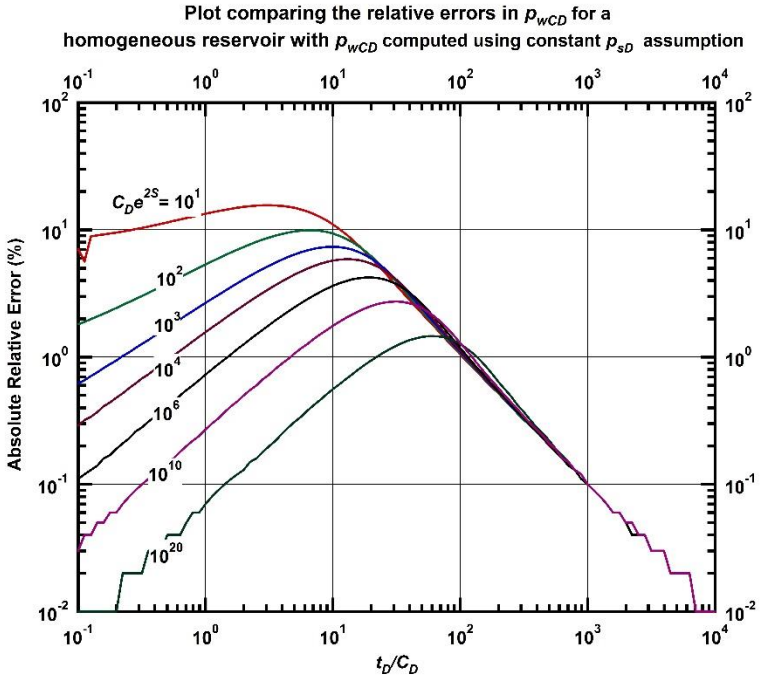

Figure 4.2 — Plot comparing the relative errors in p_{wCD} for a homogeneous reservoir with p_{wCD} computed using constant p_{sD} assumption.

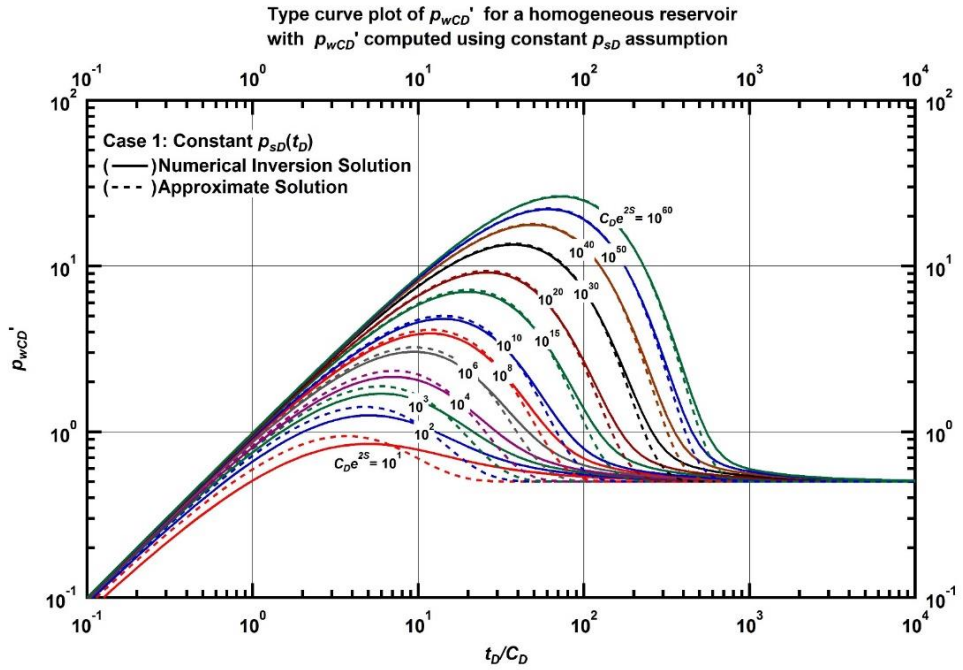

Figure 4.3 — Type curve plot of p_{wCD}' for a homogeneous reservoir. p_{wCD}' computed using constant p_{sD} assumption.

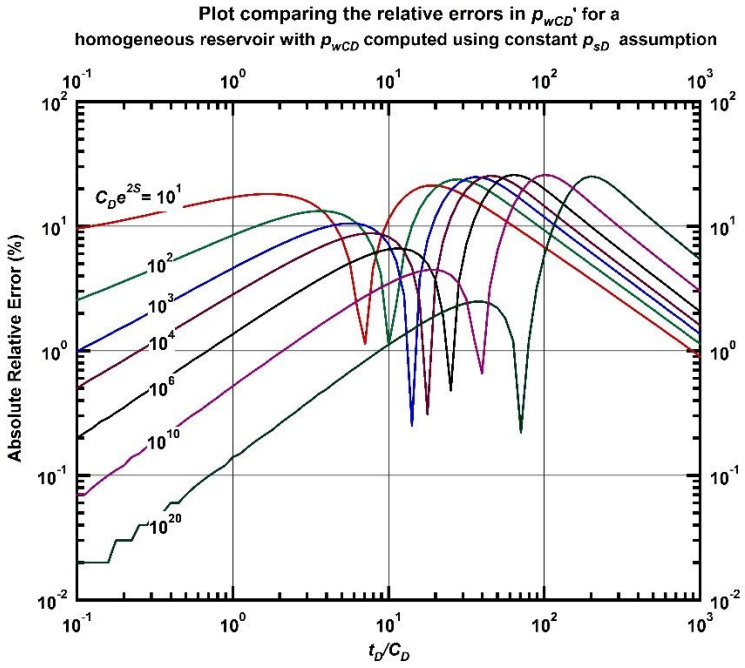

Figure 4.4 — Plot comparing the relative errors in p_{wCD}' for a homogeneous reservoir with p_{wCD} computed using constant p_{sD} assumption.

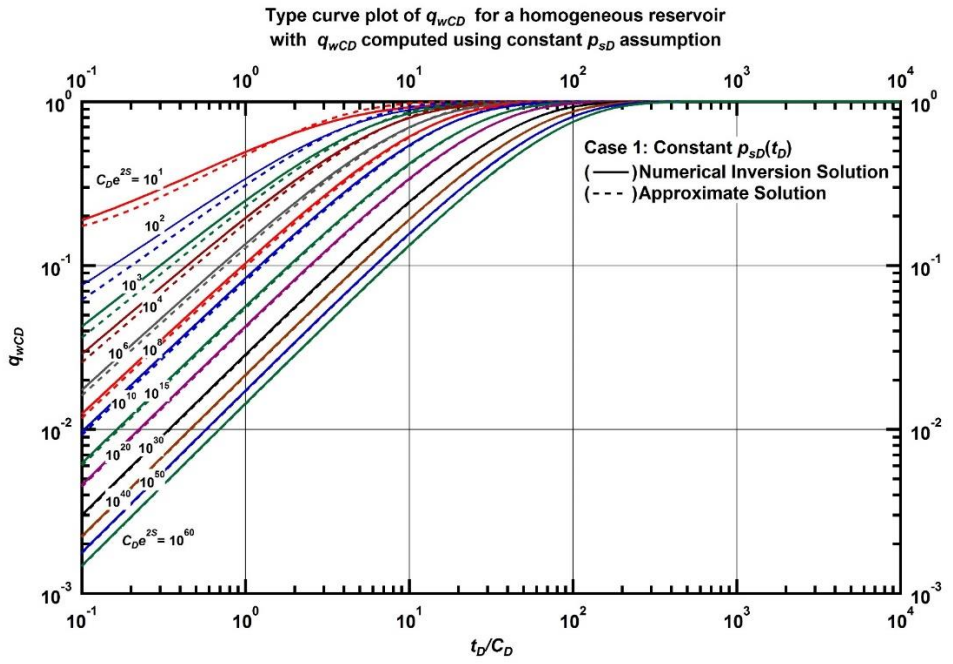

Figure 4.5 — Type curve plot of q_{wCD} for a homogeneous reservoir. q_{wCD} computed using constant p_{sD} assumption.

Case 2: $p_{wCD}(t_D)$ Approximation Based on Linear $p_{sD}(t_D)$

The premise of the this approximation is the assumption that the $p_{sD}(t_D)$ function can be described by the equation of a straight line near a particular time of interest. As in case 1, this does not imply a linear $p_{sD}(t_D)$ for the well. It applies for a "brief" time period of interest and is the simplifying assumption necessary to develop the approximation.

Figure 4.6 shows the behavior of the $p_{wCD}(t_D)$ function, computed using Eq. 3.13. We note that the $p_{wCD}(t_D)$ functions compare well with the numerical inversion solution even though in the period $1 \le t_D/C_D \le 10^1$ there is a slight deviation from the actual solutions by the approximate solutions. However, **Figure 4.7** shows that these deviations are a lot smaller than those encountered in the constant $p_{sD}(t_D)$ approximation and they diminish significantly with an increase in C_De^{2S}. The case 2 approximation can accurately predict the $p_{wCD}(t_D)$ solution.

Figure 4.8 shows the behavior of the $p_{wCD}'(t_D)$ function for case 2. This function was computed numerically, as the closed-form of the derivative function is not a simple expression and makes for tedious computing. As with the $p_{wCD}(t_D)$ function, there is very good agreement between the actual and approximate solutions. Also, the approximate derivative solutions deviates over the same parameter range as the $p_{wCD}(t_D)$ function i.e. $1 \le t_D/C_D \le 10^1$, and as with the constant $p_{sD}(t_D)$ case the deviation is more pronounced here than in the

$p_{wCD}(t_D)$ solution. The error noted in the area where the derivative curve is about to go into radial flow stabilization, is also noticed here, but as can be seen in **Figure 4.9**, it is significantly less than that observed in the constant $p_{sD}(t_D)$ case, and does not pose a problem for most reservoir engineering calculation applications. Due to this good agreement between the approximate and numerical inversion solutions, the case 2 approximation for $p_{wCD}(t_D)$ and $p_{wCD}'(t_D)$ functions is an accurate approximation.

Figure 4.10 shows the behavior of the $q_{wCD}(t_D)$ function for case 2, which was computed using Eq. 3.2. As we noted earlier, the $q_{wCD}(t_D)$ function is the most sensitive quantity that we can compare. As with case 1, there is some disagreement between approximate and inverted solution and it should be noted that although the approximate $q_{wCD}(t_D)$ function deviates rather significantly in some places, this should not rule out the use of $p_{wCD}(t_D)$ and $p_{wCD}'(t_D)$ function functions obtained by the use of this constant $p_{sD}(t_D)$ approximation.

The errors associated with each function i.e. $p_{wCD}(t_D)$, $p_{wCD}'(t_D)$ and $q_{wCD}(t_D)$, should be should be within the accuracy needed for most reservoir engineering applications.

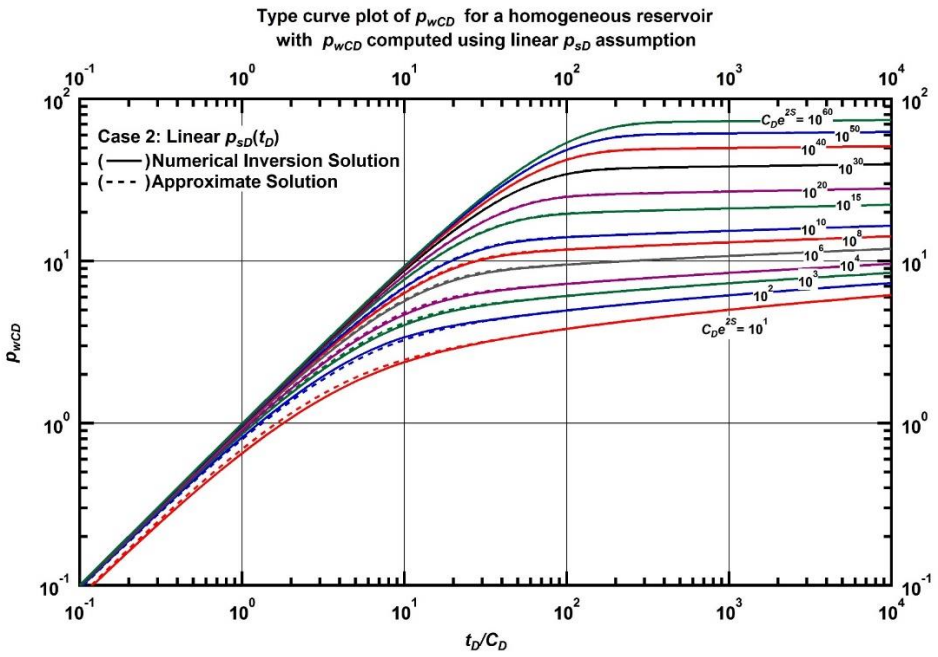

Figure 4.6 — Type curve plot of p_{wCD} for a homogeneous reservoir. p_{wCD} computed using linear p_{sD} assumption

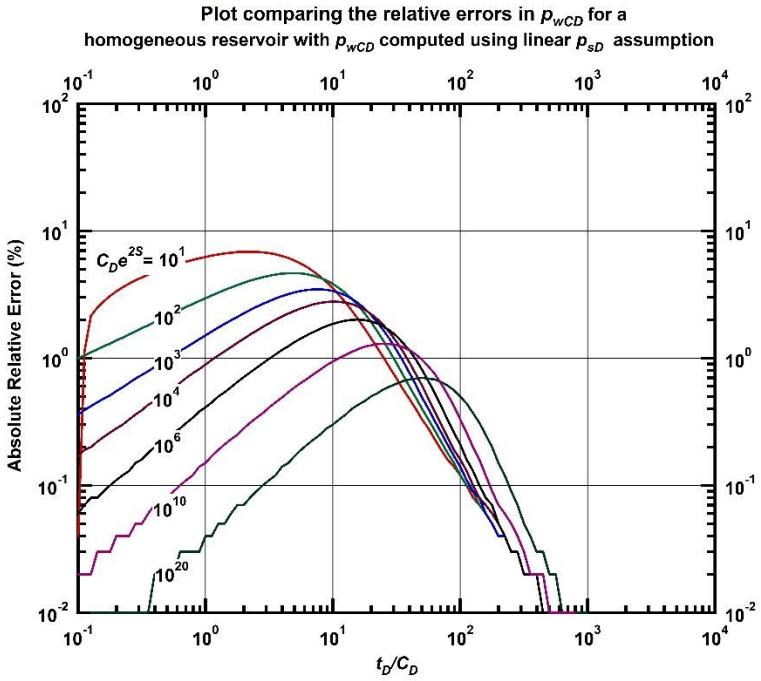

Figure 4.7 — Plot comparing the relative errors in p_{wCD} for a homogeneous reservoir with p_{wCD} computed using linear p_{sD} assumption.

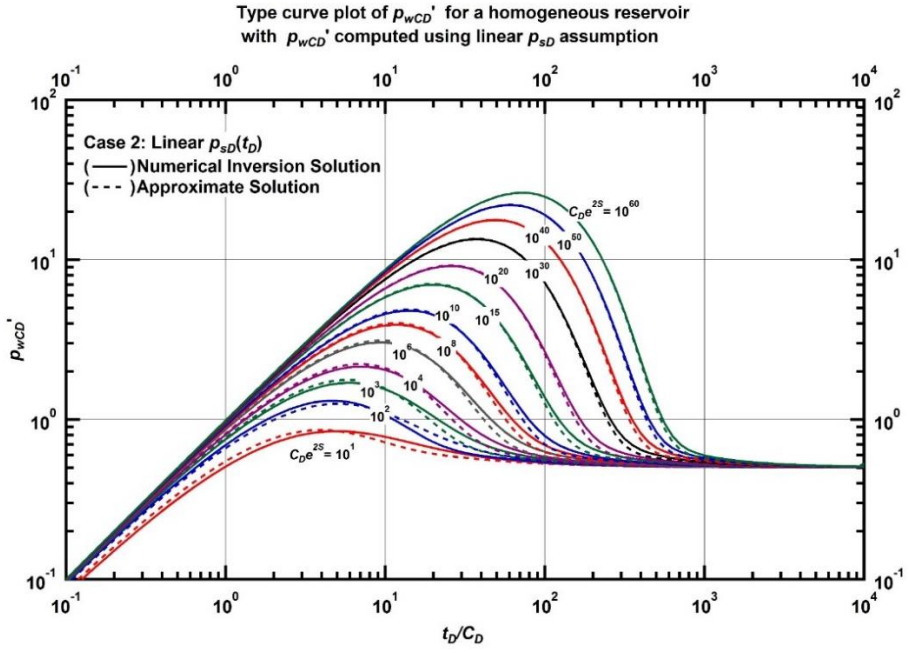

Figure 4.8 — Type curve plot of p_{wCD}' for a homogeneous reservoir. p_{wCD}' computed using linear p_{sD} assumption.

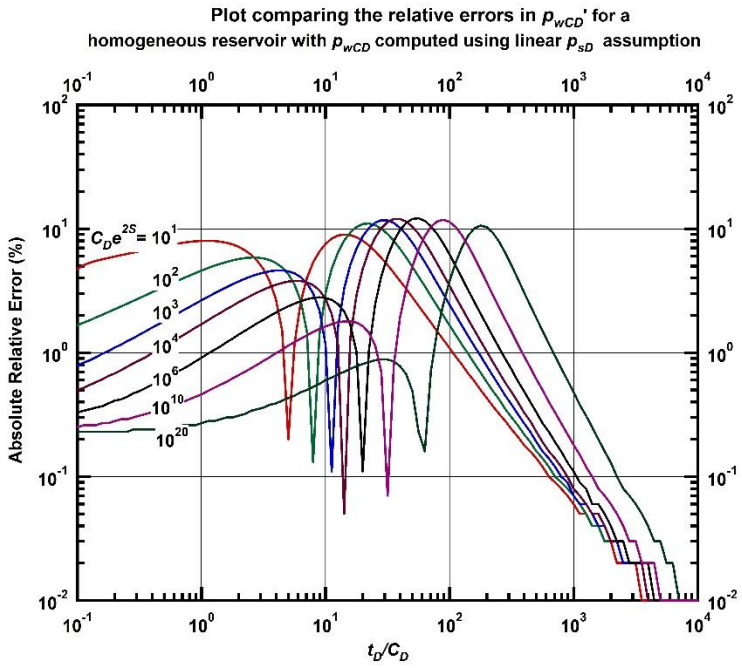

Figure 4.9 — Plot comparing the relative errors in p_{wCD}' for a homogeneous reservoir with p_{wCD} computed using linear p_{sD} assumption.

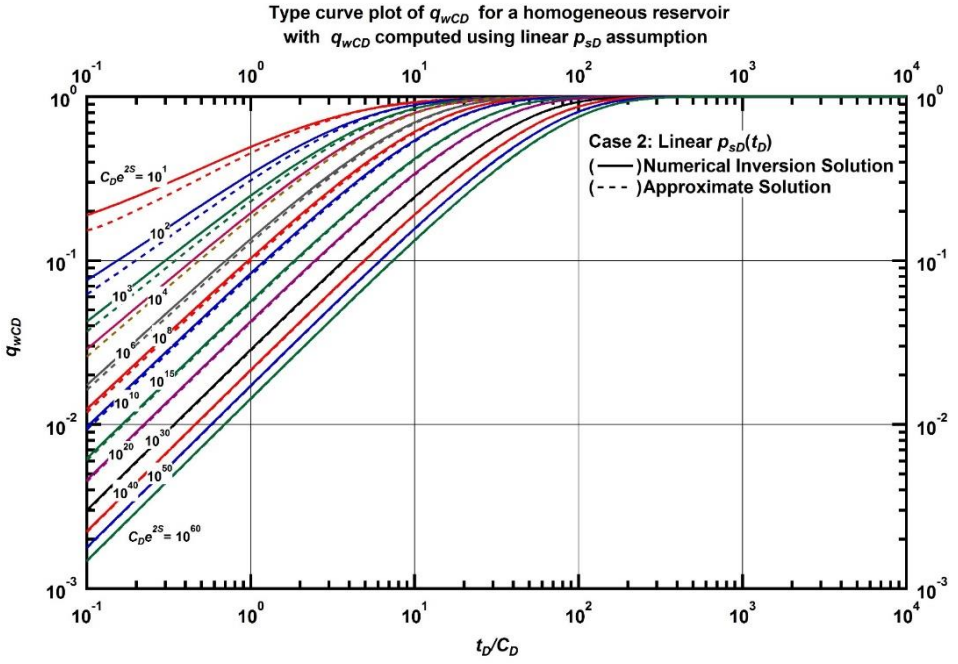

Figure 4.10 — Type curve plot of q_{wCD} for a homogeneous reservoir. q_{wCD} computed using linear p_{sD} assumption.

Case 3: $p_{wCD}(t_D)$ Approximation Based on Quadratic $p_{sD}(t_D)$

This approximation is based on the assumption that the $p_{sD}(t_D)$ function varies as a quadratic function of time near a particular time of interest, say between three adjacent well testing data points. As in cases 1 and 2, this only applies for a "small" time period of interest and is the simplifying assumption necessary to develop the approximation.

Figure 4.11 shows the behavior of the $p_{wCD}(t_D)$ function, computed using the procedure given in Appendix D. It can be observed that the $p_{wCD}(t_D)$ functions compare very well with the numerical inversion solution even though in the period $1 \leq t_D/C_D \leq 10^1$ there is a very slight deviation from the actual solutions by the approximate solutions. **Figure 4.12** shows that these deviations are small and they diminish significantly with an increase in C_De^{2S}. This agreement between numerical solutions and the approximation suggests that the case 3 approximation can accurately predict the $p_{wCD}(t_D)$ solution.

Figure 4.13 shows the $p_{wCD}'(t_D)$ function. The $p_{wCD}'(t_D)$ functions are computed numerically, as the closed-form derivative function would be difficult to compute otherwise. There is generally an excellent agreement of approximate and numerically inverted $p_{wCD}'(t_D)$ functions. The slight deviation that occurs during the time period $1 \leq t_D/C_D \leq 10^1$ is barely perceptible The error noted in the area where the derivative curve is about to go into radial flow stabilization, is also noticed here, but as can be seen in **Figure 4.14**, it is significantly less than that observed in cases 1 and 2. Due to this good agreement between the approximate and numerical inversion solutions, the case 3 approximation for $p_{wCD}(t_D)$ and $p_{wCD}'(t_D)$ functions is an accurate approximation.

Figure 4.15 shows the behavior of the $q_{wCD}(t_D)$ function for case 3, computed using Eq. 3.2 and the numerical differentiation of the $p_{wCD}(t_D)$ function. As was noted in case 2, the errors inherent in the $p_{wCD}(t_D)$ function are amplified in the $q_{wCD}(t_D)$ function, and the disagreement in this case is identical to that of case 2. This agreement between numerical solutions and the approximation suggests that the case 3 approximation can accurately predict the $p_{wCD}(t_D)$ solution and the errors associated with each function i.e. $p_{wCD}(t_D)$, $p_{wCD}'(t_D)$ and $q_{wCD}(t_D)$, should be should be within the accuracy needed for most reservoir engineering applications.

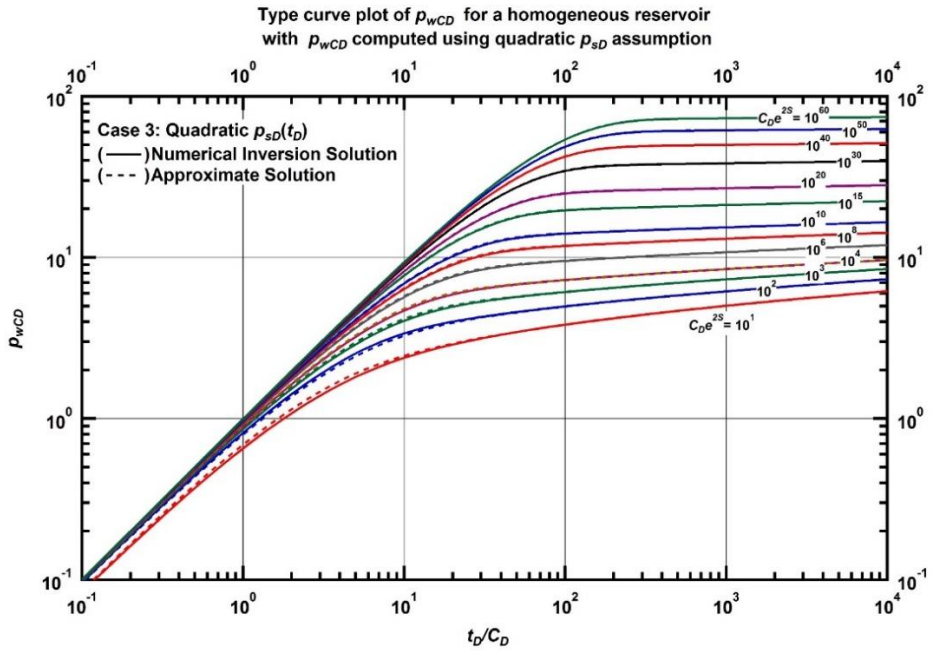

Figure 4.11 — Type curve plot of p_{wCD} for a homogeneous reservoir. p_{wCD} computed using qudaratic p_{sD} assumption.

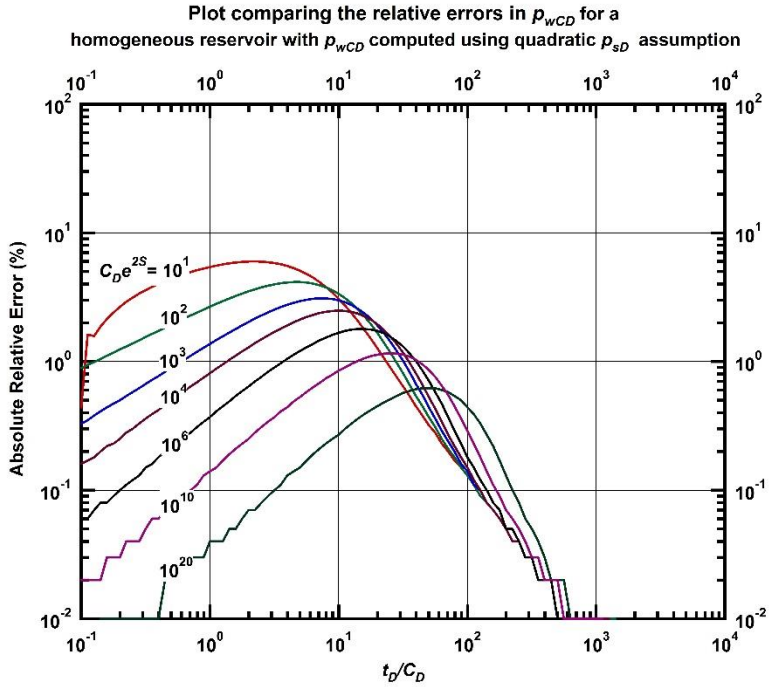

Figure 4.12 — Plot comparing the relative errors in p_{wCD} for a homogeneous reservoir with p_{wCD} computed using quadratic p_{sD} assumption.

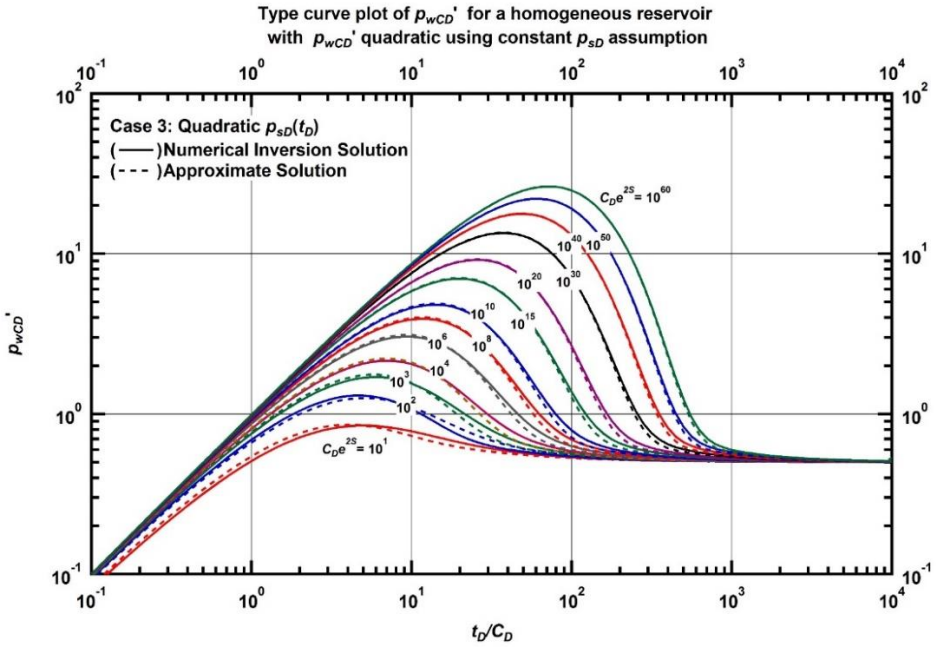

Figure 4.13 — Type curve plot of p_{wCD}' for a homogeneous reservoir. p_{wCD}' computed using qudaratic p_{sD} assumption.

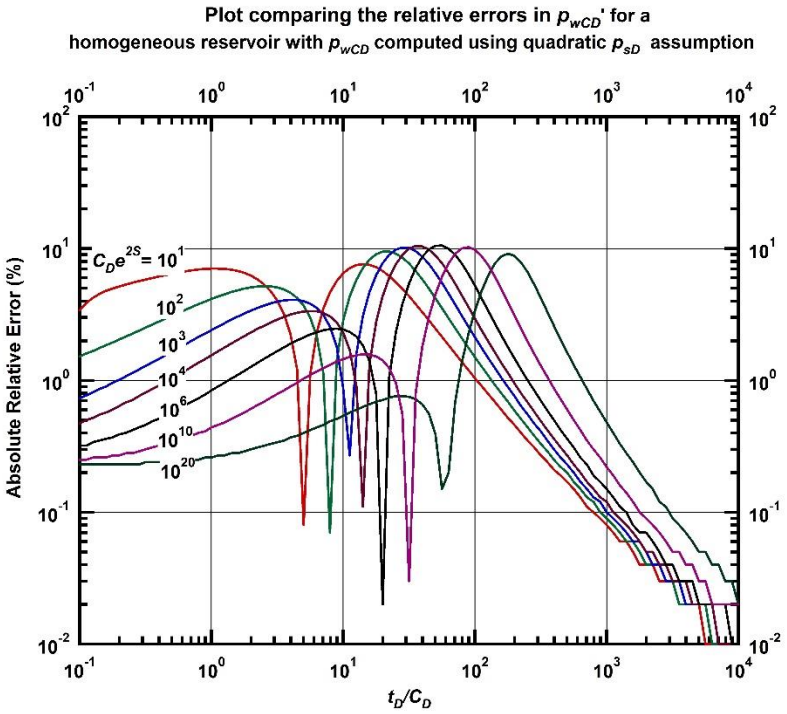

Figure 4.14 — Plot comparing the relative errors in p_{wCD}' for a homogeneous reservoir with p_{wCD} computed using quadratic p_{sD} assumption.

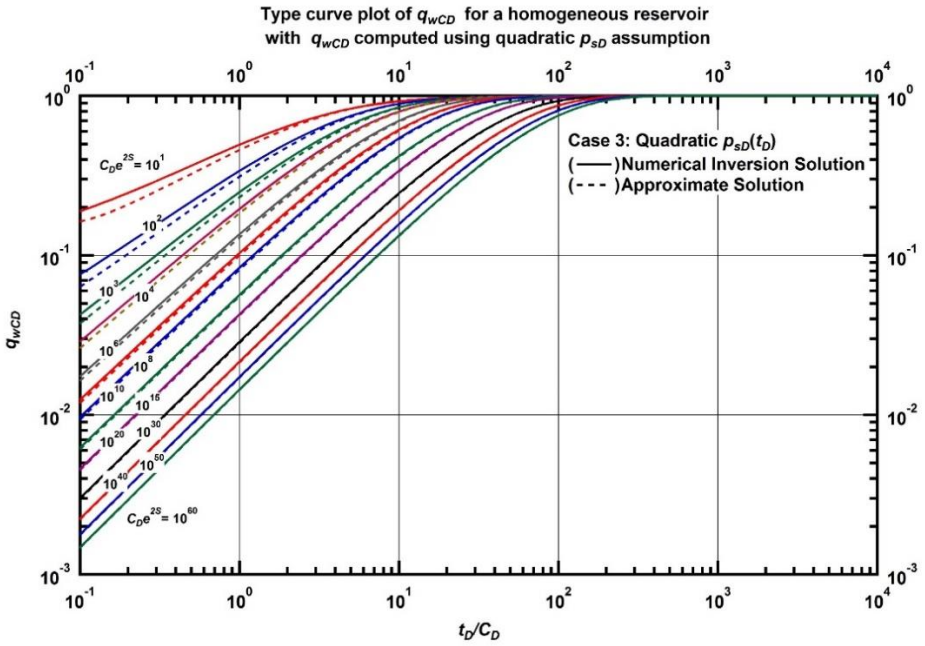

Figure 4.15 — Type curve plot of q_{wCD} for a homogeneous reservoir. q_{wCD} computed using qudaratic p_{sD} assumption.

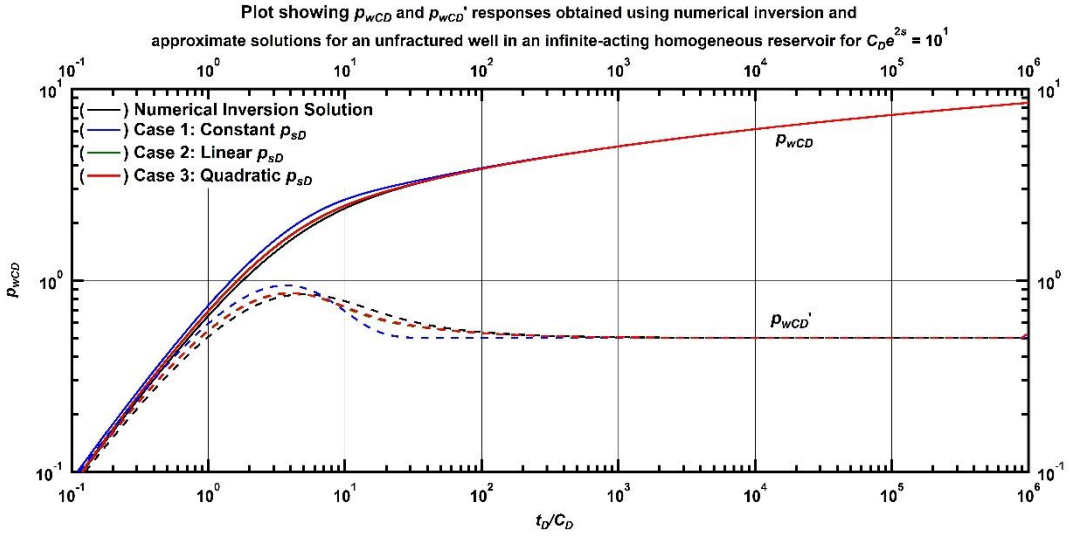

Figure 4.16 — Plot showing p_{wCD} and p_{wCD}' responses obtained using numerical inversion and approximate solutions for an unfractured well in an infinite-acting homogeneous reservoir for $C_De^{2S} = 10^1$.

From the foregoing, it is clear that although the three cases are good approximations, there is a difference in their accuracies. **Figure 4.16** shows the p_{wCD} and p_{wCD}' responses from the three approximations compared

to the numerical responses for $C_De^{2S} = 10^1$. **Figures 4.17** and **4.18** compare the differences in Absolute Relative Error in the approximations for $p_{wCD}(t_D)$ and $p_{wCD}'(t_D)$ respectively, for when C_De^{2S} is 10^1. It is noted that there is a significant difference in accuracy between the case 1 approximation and the cases 2 and 3 approximations. The difference between cases 2 and 3 is less significant, although, case 3 is slightly more accurate. **Figures 4.19** and **4.20** show the same trends for when C_De^{2S} is 10^{20}, and **Figures 4.21** and **4.22** do the same for when C_De^{2S} is 10^{60}.

In SPE 21826, Blasingame et al. (1991) recommended the use of the case 2 approximation due to the fact it is computationally easier than case 3 and they yield similar results. The author agrees with this analysis as the increased difficulty in the implementation of case 3 is not concomitant with the marginal improvement of its results from the case 2 results

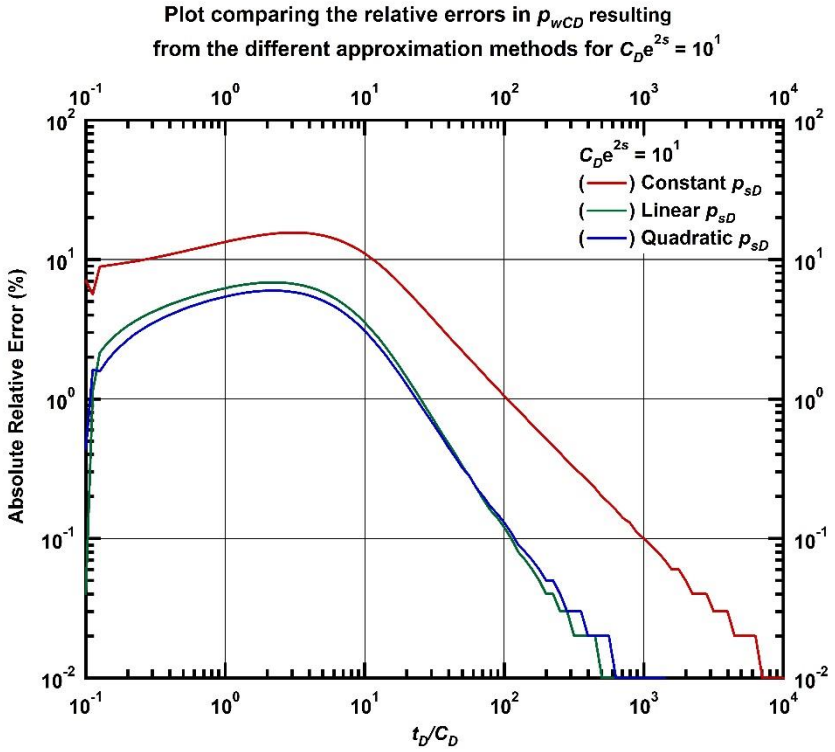

Figure 4.17 — Plot comparing the relative errors in p_{wCD} resulting from the different approximation methods in an unfractured homogeneous reservoir for $C_De^{2S} = 10^1$.

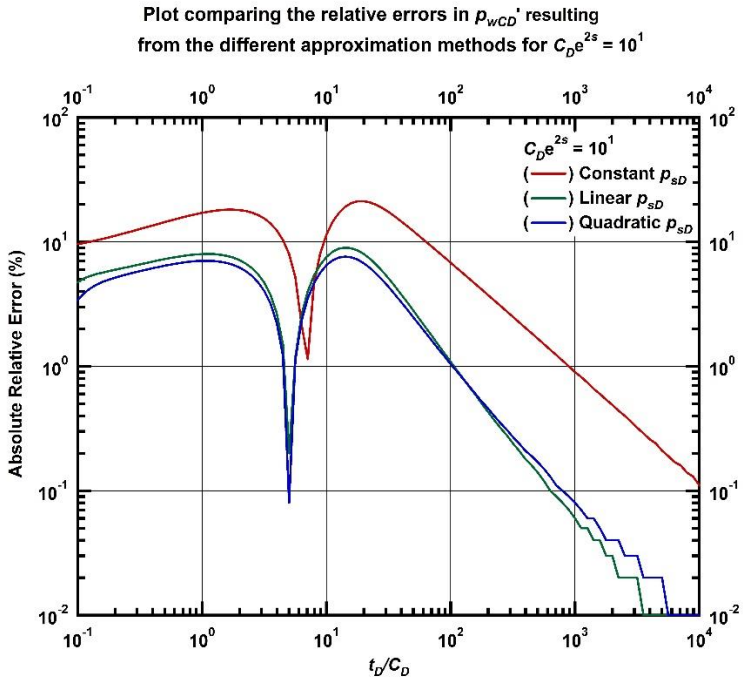

Figure 4.18 — Plot comparing the relative errors in p_{wCD}' resulting from the different approximation methods in an unfractured homogeneous reservoir for $C_De^{2S} = 10^1$.

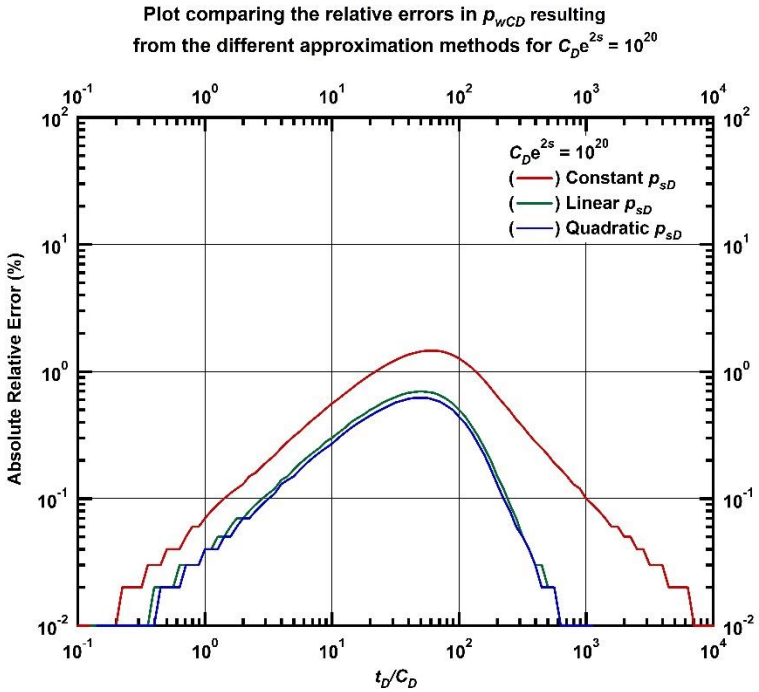

Figure 4.19 — Plot comparing the relative errors in p_{wCD} resulting from the different approximation methods in an unfractured homogeneous reservoir for $C_De^{2S} = 10^{20}$.

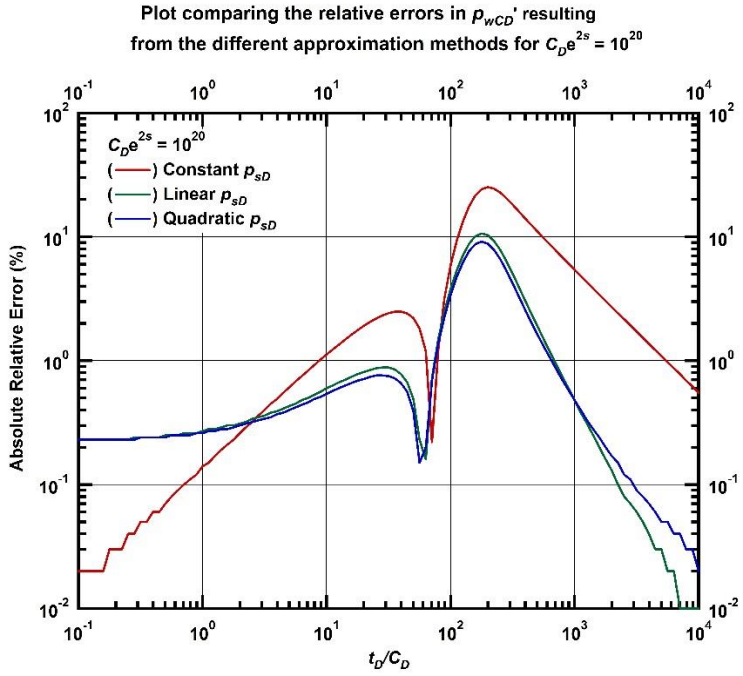

Figure 4.20 — Plot comparing the relative errors in p_{wCD}' resulting from the different approximation methods in an unfractured homogeneous reservoir for $C_De^{2S} = 10^{20}$.

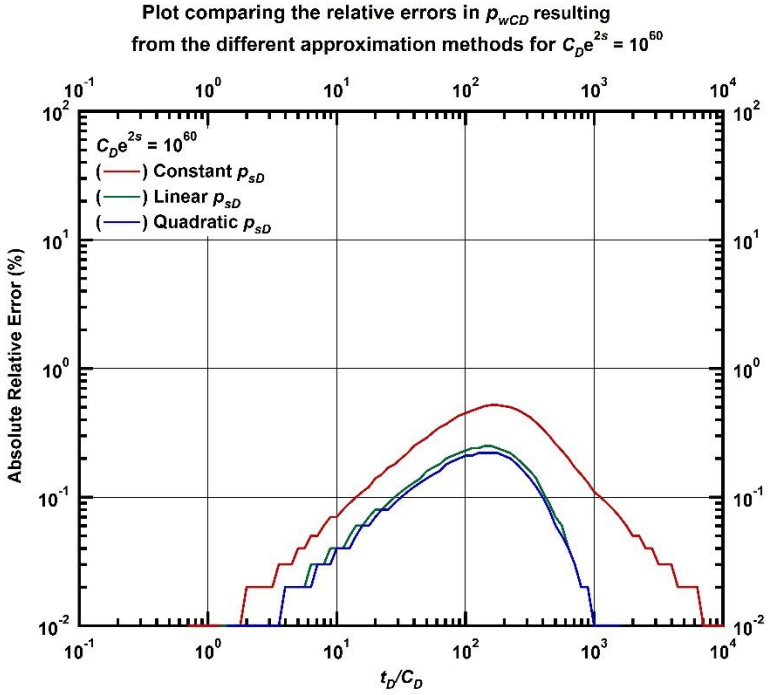

Figure 4.21 — Plot comparing the relative errors in p_{wCD} resulting from the different approximation methods in an unfractured homogeneous reservoir for $C_De^{2S} = 10^{60}$.

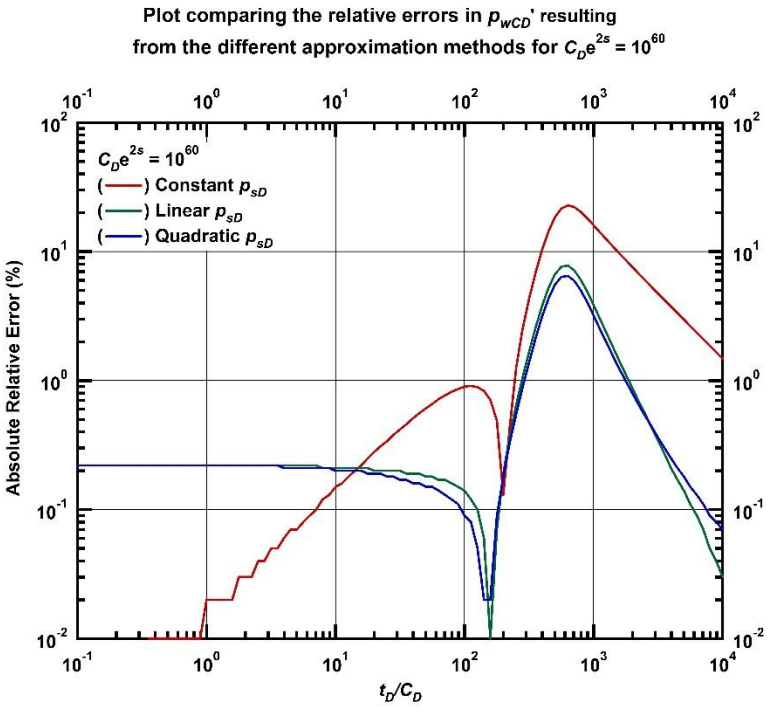

Figure 4.22 — Plot comparing the relative errors in p_{wCD}' resulting from the different approximation methods in an unfractured homogeneous reservoir for $C_De^{2S} = 10^{60}$.

Fractured Wells in an Infinite-Acting Homogeneous Reservoir

This section considers the case of a well with a vertical fracture of infinite conductivity in an infinite-acting homogeneous reservoir. In SPE 21826 the Laplace space solution for this problem obtained by Ozkan and Raghavan (1989) was used in the to determine the actual and approximate $p_{wCD}(t_{LfD})$ solutions. In this section, we rework that problem at to determine the most accurate and consistent model of the $p_{wCD}(t_{LfD})$ function for an unfractured well in an infinite-acting homogeneous reservoir.

As was done in SPE 21826, the behaviors of $p_{wCD}(t_{LfD})$ for $10^{-2} \le t_{LfD}/C_{fD} \le 10^{3}$ for 6 values of C_{fD} ranging from 3 x 10^{-3} to 1 are plotted. These parameters will be used for all of the unfractured well cases for the $p_{wCD}(t_{LfD})$, $p_{wCD}'(t_{LfD})$ and $q_{wCD}(t_{LfD})$ solutions.

Case 1: $p_{wCD}(t_{LfD})$ Approximation Based on Constant $p_{sD}(t_{LfD})$

Figure 4.23 shows the behavior of the $p_{wCD}(t_{LfD})$ function, computed using the case 1 approximation (Eq. 3.7). For the time period $t_{LfD}/C_{fD} \le 10^{1}$ and for all C_{fD}, the does not accurately predict the $p_{wCD}(t_{LfD})$ solution for the. This is can also be seen in **Figure 4.24** that shows high error values for all C_{fD} in that time period. As explained by Blasingame et al., this is likely due to this period being the linear flow region for the no

wellbore storage case, and the assumption of a constant $p_{sD}(t_{LfD})$ function is insufficient for this period. This disagreement suggests that the linear $p_{sD}(t_{LfD})$ is not a good approximation of the $p_{wCD}(t_{LfD})$ function.

Figure 4.25 shows the behavior of the $p_{wCD}'(t_{LfD})$ function and there is a significant deviation between the actual and the approximate solutions for $t_{LfD}/C_{fD} \leq 10^1$ and for all C_{fD}. This behavior is as expected, because of the significant errors that were observed in the $p_{wCD}(t_{LfD})$ solution in the same time period. **Figure 4.26** confirms these observations, showing significant errors for all C_{fD}.

Figure 4.26 shows the behavior of the $q_{wCD}(t_{LfD})$ function, and embodies the same lack of accuracy observed in the $p_{wCD}(t_{LfD})$ and $p_{wCD}'(t_{LfD})$ solutions.

For all practical purposes, therefore, the case 1 approximation cannot be be used for the description of the fractured well in a homogeneous reservoir problem in the time period $t_{LfD}/C_{fD} \leq 10^1$.

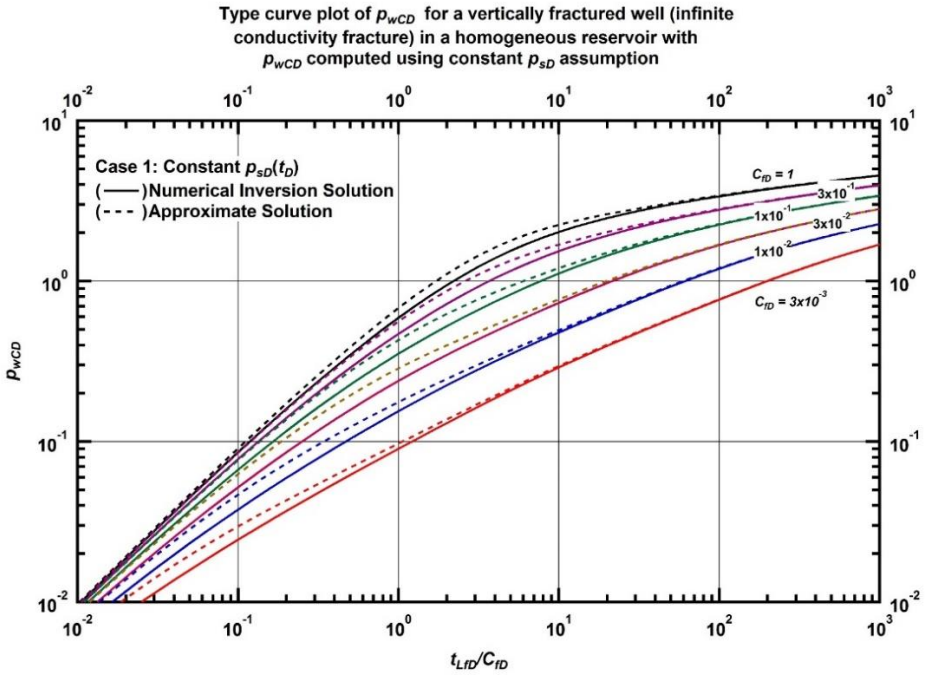

Figure 4.23 — Type curve plot of p_{wCD} for a vertically fractured well (infinite conductivity fracture) in a homogeneous reservoir p_{wCD} computed using constant p_{sD} assumption.

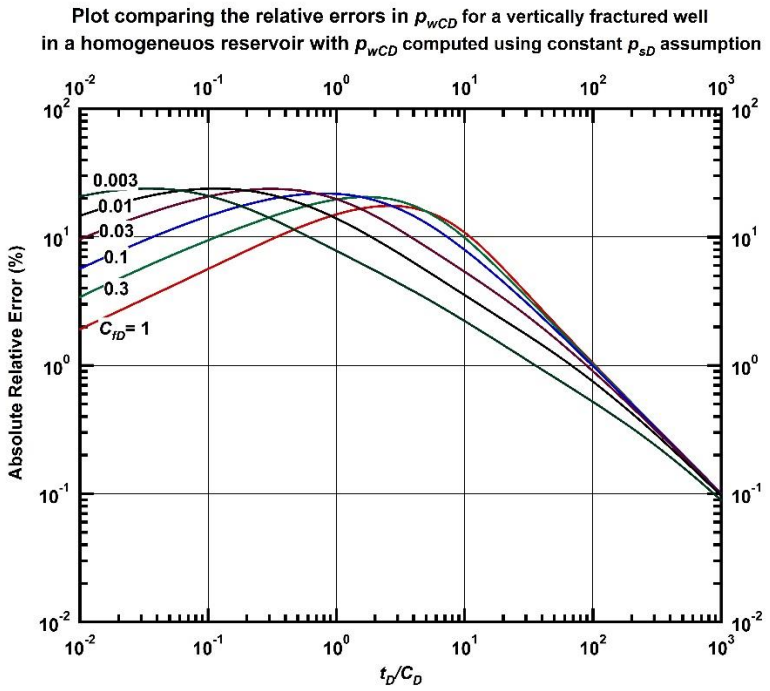

Figure 4.24 — Plot comparing the relative errors in p_{wCD} for a vertically fractured well (infinite conductivity fracture) with p_{wCD} computed using constant p_{sD} assumption.

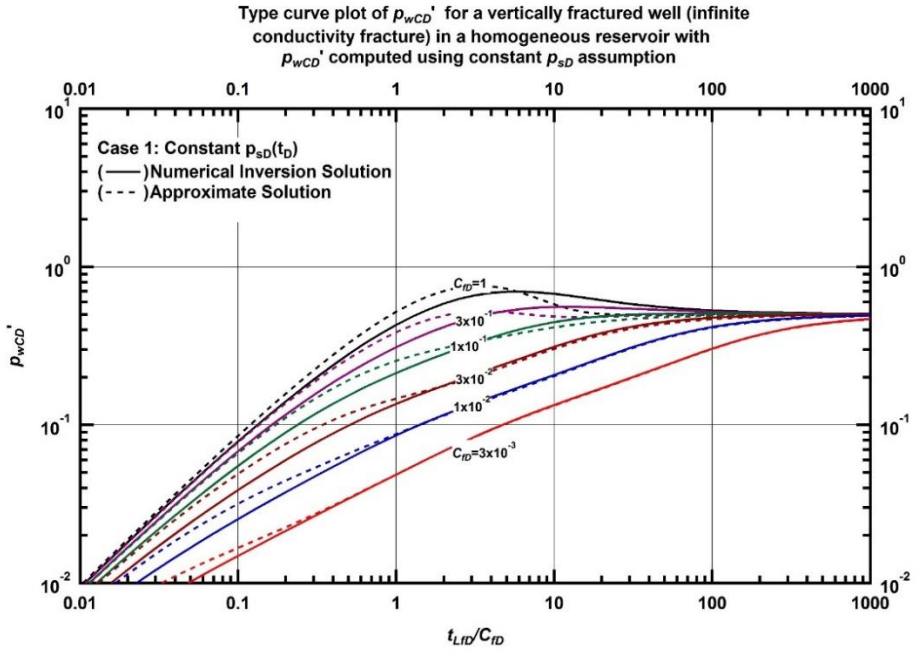

Figure 4.25 — Type curve plot of p_{wCD}' for a vertically fractured well (infinite conductivity fracture) in a homogeneous reservoir p_{wCD}' computed using constant p_{sD} assumption.

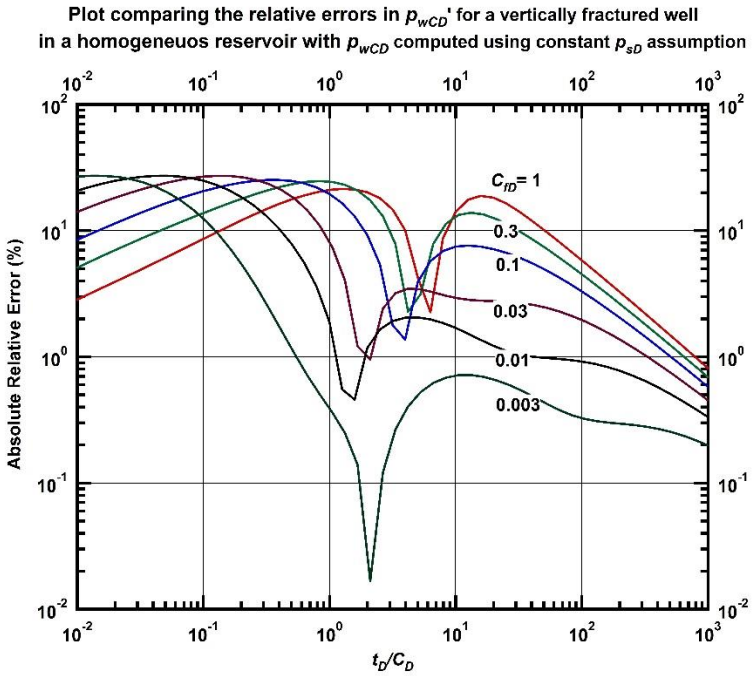

Figure 4.26 — Plot comparing the relative errors in p_{wCD}' for a vertically fractured well (infinite conductivity fracture) with p_{wCD} computed using constant p_{sD} assumption.

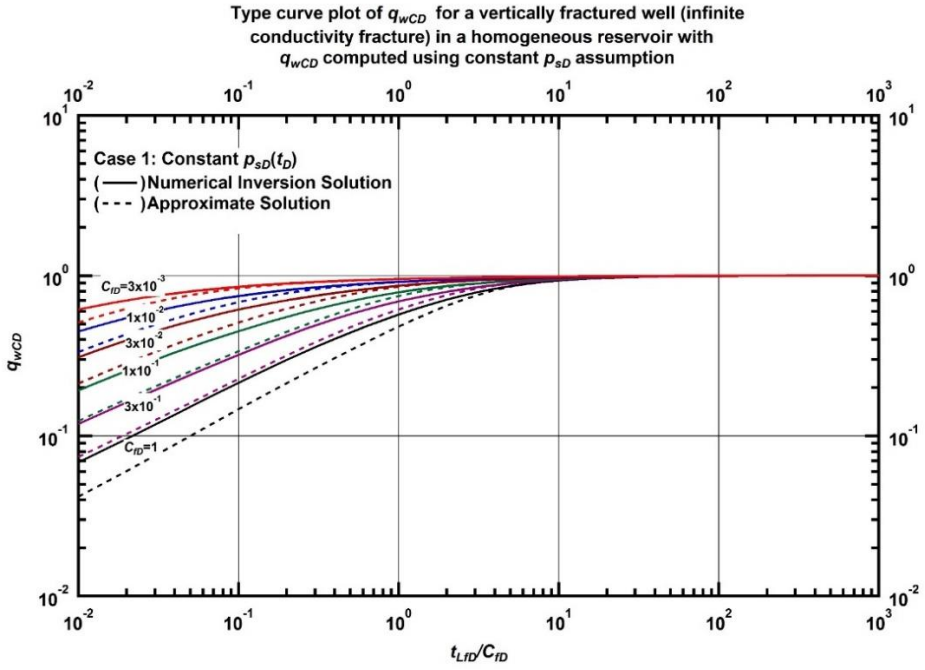

Figure 4.27 — Type curve plot of q_{wCD} for a vertically fractured well (infinite conductivity fracture) in a homogeneous reservoir q_{wCD} computed using constant p_{sD} assumption.

Case 2: $p_{wCD}(t_{LfD})$ Approximation Based on Linear $p_{sD}(t_{LfD})$

Figure 4.28 shows the behavior of the $p_{wCD}(t_{LfD})$ function computed using the case 2 approximation (Eq. 3.13). We note that there is excellent agreement between the actual and approximate $p_{wCD}(t_{LfD})$ results. The maximum deviation is about 6.1% for when C_{fD} is 1 and diminishes as the value of C_{fD} decreases, according to **Figure 4.29**. This is a significant improvement from the case 1 approximation, strongly suggests that the case 2 approximation is an accurate approximation for the fractured well $p_{wCD}(t_{LfD})$ function.

Figure 4.30 shows the behavior of the $p_{wCD}'(t_{LfD})$ function estimated using numerical differentiation methods. There is slightly more deviation in this function than in the $p_{wCD}(t_{LfD})$ function, with an error of about 7.5% according to **Figure 4.31**. These increased deviations are expected. They are most significant in the time range $10^{-1} \le t_{LfD}/C_{fD} \le 10^{2}$ for when C_{fD} is 1 and diminish rapidly as the value of C_{fD} decreases. Case 2 proves to be an accurate approximation of the actual $p_{wCD}'(t_{LfD})$ solution.

Figure 4.32 shows the behavior of the $q_{wCD}(t_{LfD})$ function and though the slight deviations in the $p_{wCD}(t_{LfD})$ solutions are magnified here, the accuracy of these results is adequate for most reservoir engineering applications. The case 2 approximation is, therefore, a good approximation for fractured well in a homogeneous reservoir problem.

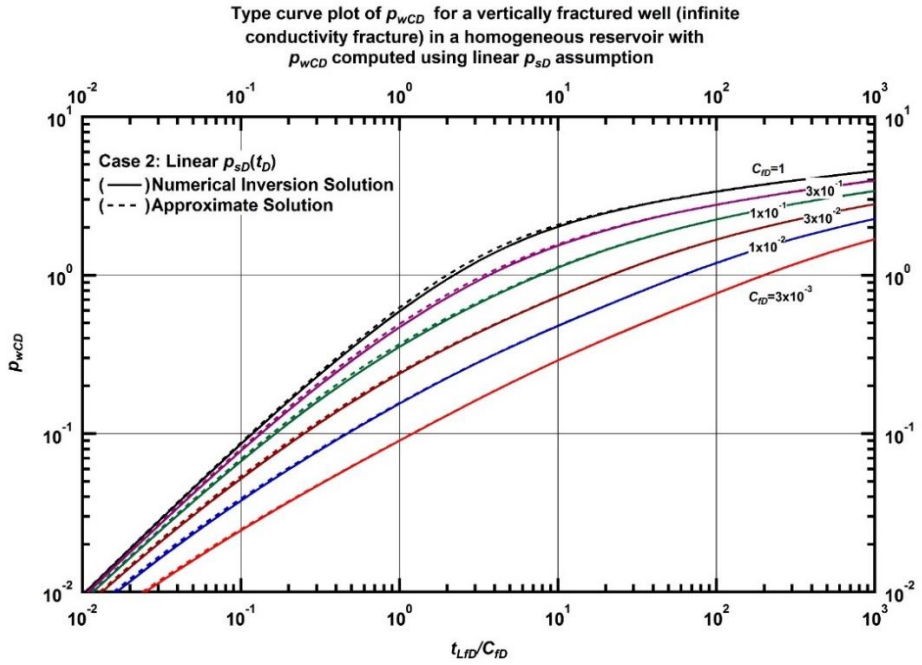

Figure 4.28 — Type curve plot of p_{wCD} for a vertically fractured well (infinite conductivity fracture) in a homogeneous reservoir p_{wCD} computed using linear p_{sD} assumption.

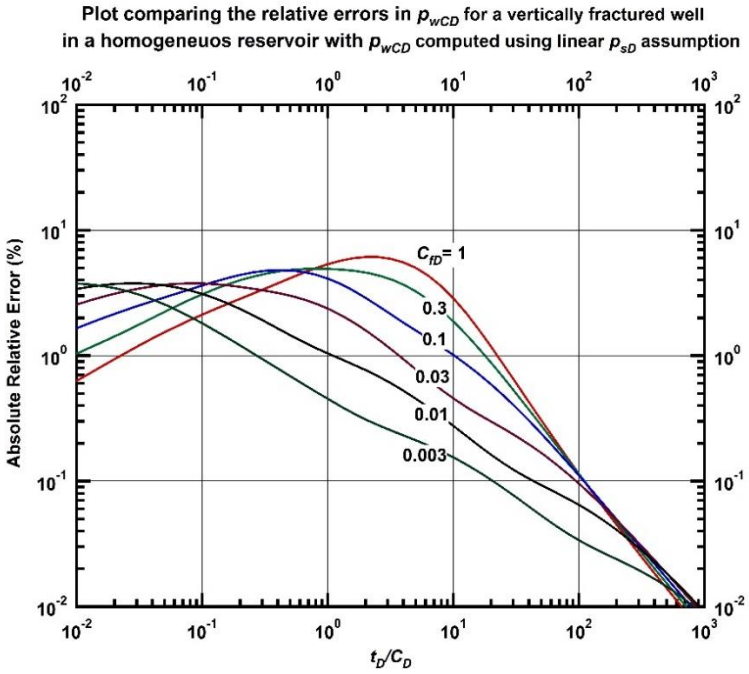

Figure 4.29 — Plot comparing the relative errors in p_{wCD} for a vertically fractured well (infinite conductivity fracture) with p_{wCD} computed using linear p_{sD} assumption.

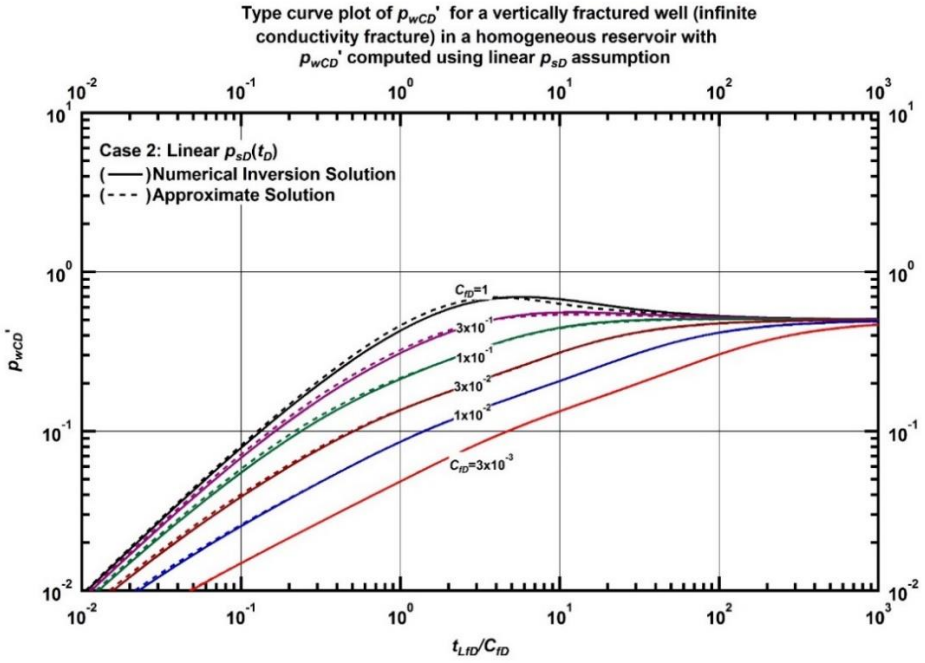

Figure 4.30 — Type curve plot of p_{wCD}' for a vertically fractured well (infinite conductivity fracture) in a homogeneous reservoir p_{wCD}' computed using linear p_{sD} assumption.

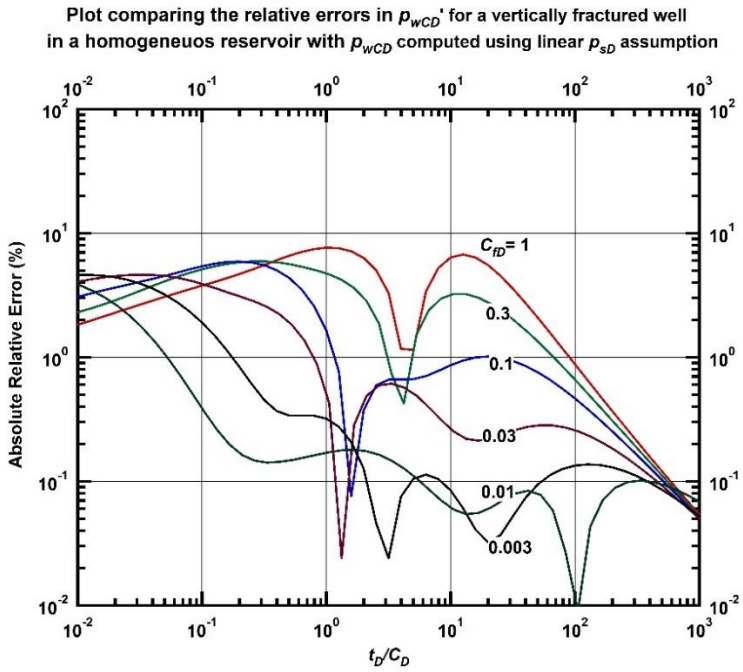

Figure 4.31 — Plot comparing the relative errors in p_{wCD}' for a vertically fractured well (infinite conductivity fracture) with p_{wCD} computed using linear p_{sD} assumption.

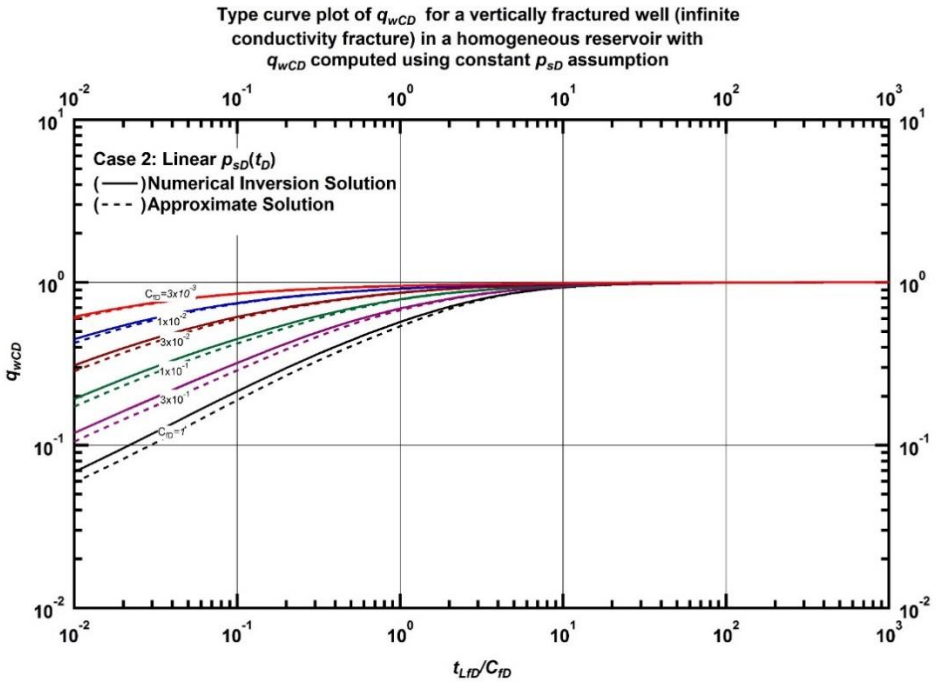

Figure 4.32 — Type curve plot of q_{wCD} for a vertically fractured well (infinite conductivity fracture) in a homogeneous reservoir q_{wCD} computed using linear p_{sD} assumption.

Case 3: $p_{wCD}(t_{LfD})$ Approximation Based on Quadratic $p_{sD}(t_{LfD})$

Figure 4.33 shows the behavior of the $p_{wCD}(t_{LfD})$ function computed according to the procedure given in Appendix D. We note that there is excellent agreement between the actual and approximate $p_{wCD}(t_{LfD})$ results. The maximum deviation is about 5.5% for when C_{fD} is 1 and diminishes as the value of C_{fD} decreases, according to **Figure 4.34**. There is a strong similarity to the results from the case 2 approximation, although it is noted that the case 3 approximation is slightly better approximation. The case 3 approximation is an accurate approximation for the fractured well $p_{wCD}(t_{LfD})$ function.

The same can be said for the the $p_{wCD}'(t_{LfD})$ and $q_{wCD}(t_{LfD})$ functions, as shown in **Figures 4.35 – 4.38**. The case 3 approximation is, therefore, an excellent approximation for fractured well in a homogeneous reservoir problem.

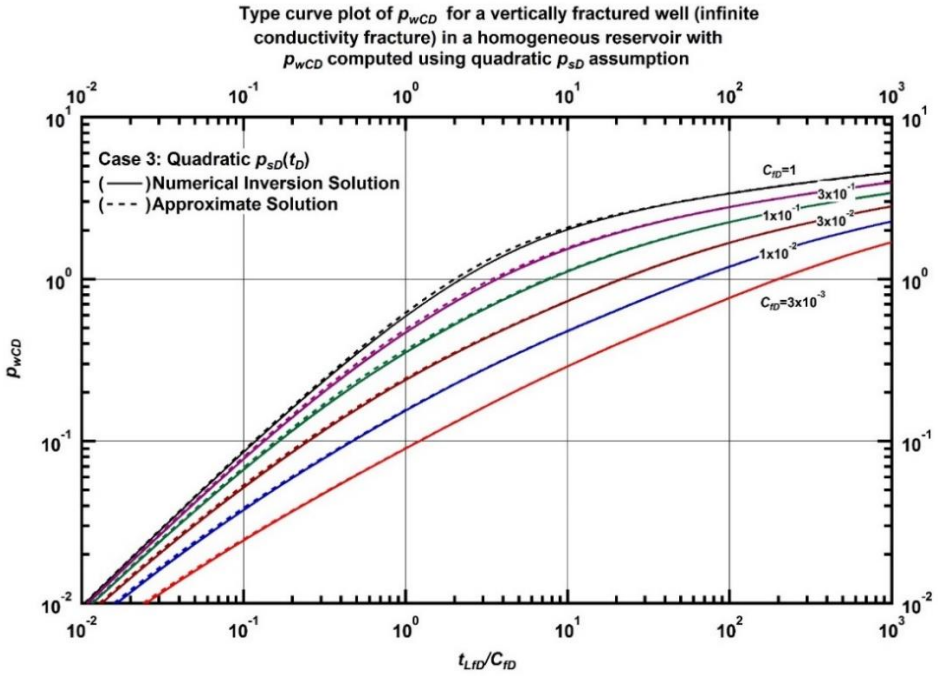

Figure 4.33 — Type curve plot of p_{wCD} for a vertically fractured well (infinite conductivity fracture) in a homogeneous reservoir p_{wCD} computed using quadratic p_{sD} assumption.

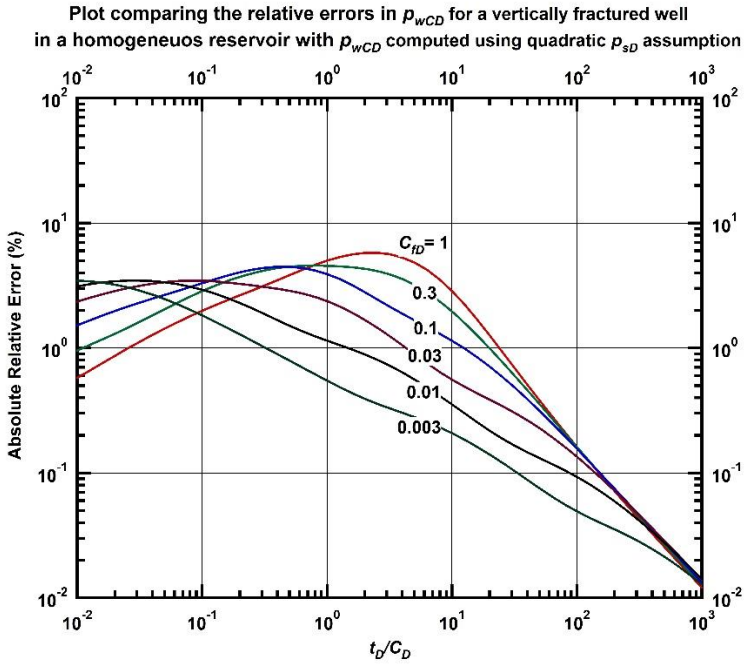

Figure 4.34 — Plot comparing the relative errors in p_{wCD} for a vertically fractured well (infinite conductivity fracture) with p_{wCD} computed using quadratic p_{sD} assumption.

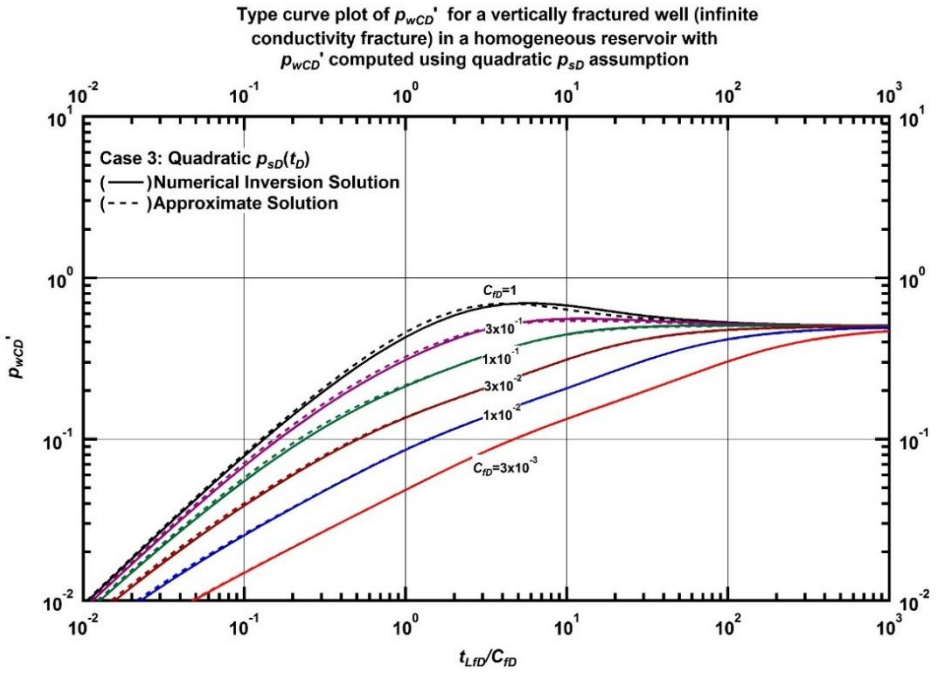

Figure 4.35 — Type curve plot of p_{wCD}' for a vertically fractured well (infinite conductivity fracture) in a homogeneous reservoir p_{wCD}' computed using quadratic p_{sD} assumption.

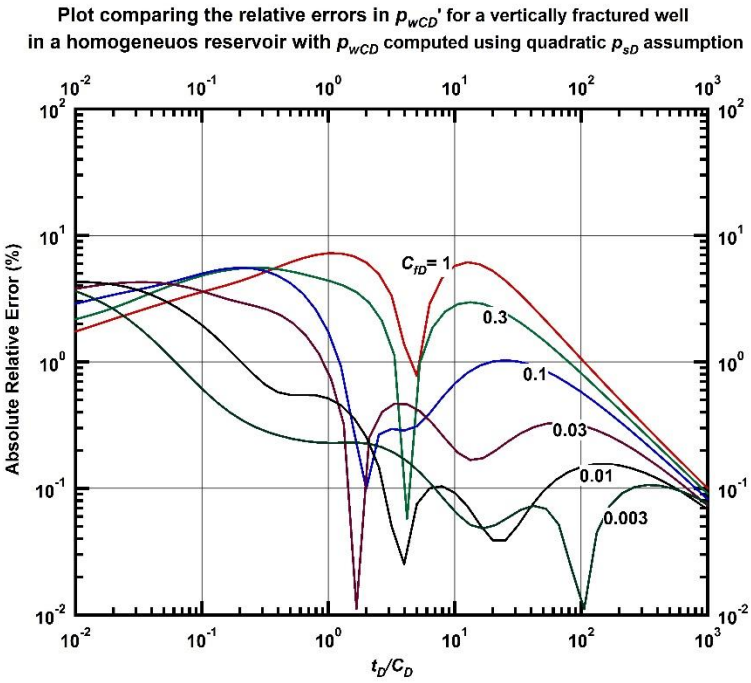

Figure 4.36 — Plot comparing the relative errors in p_{wCD}' for a vertically fractured well (infinite conductivity fracture) with p_{wCD} computed using quadratic p_{sD} assumption.

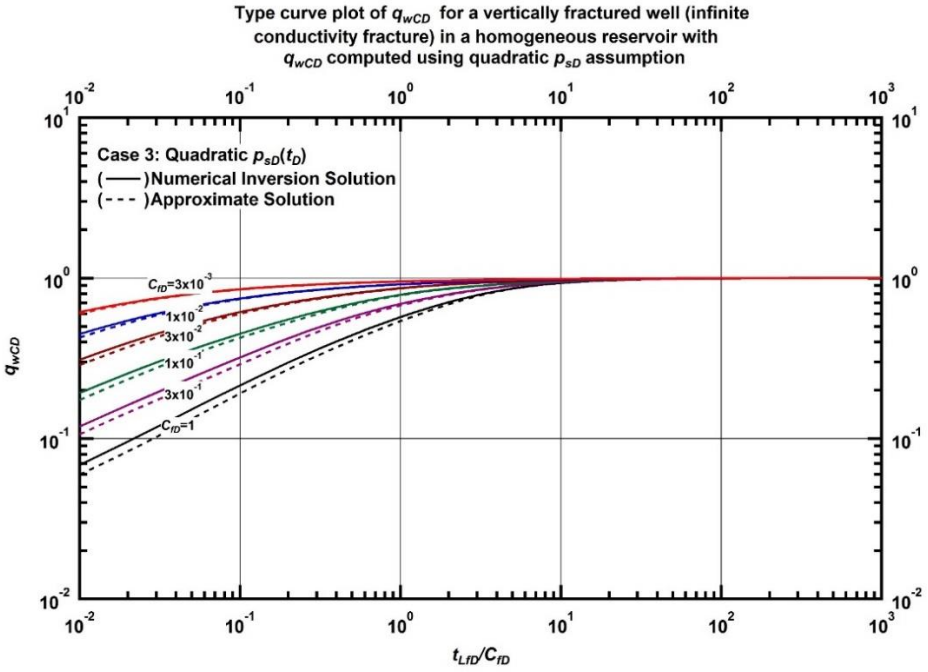

Figure 4.37 — Type curve plot of q_{wCD} for a vertically fractured well (infinite conductivity fracture) in a homogeneous reservoir q_{wCD} computed using quadratic p_{sD} assumption.

We note that the case 1 approximation is poor for the vertically fractured well in a homogeneous reservoir. However, cases 2 and 3 are good approximations, with case 3 having a slightly better accuracy. **Figure 4.38** shows the p_{wCD} and p_{wCD}' responses from the three approximations compared to the numerical responses for C_{fD} = 1. **Figures 4.39** and **4.40** compare the differences in Absolute Relative Error in the approximations for $p_{wCD}(t_D)$ and $p_{wCD}'(t_D)$ respectively, for when C_{fD} is 1. It is noted that there is a significant difference in accuracy between the case 1 approximation and the cases 2 and 3 approximations. The difference between cases 2 and 3 is almost nonexistent, although, case 3 is slightly more accurate. **Figures 4.41** and **4.42** show the same trends for when C_{fD} is 0.3.

Like in the unfractured well in an infinite-acting homogeneous reservoir, SPE 21826, recommended the use of the case 2 approximation due to the fact it is computationally easier than case 3 and they yield similar results. The author agrees with this analysis as there is no difference between the results obtained from these methods in practical terms in this case. It is also important to mention that while the case 1 approximation might be used in for an unfractured well in an infinite-acting homogeneous reservoir, it should not be used for a vertical well in a homogeneous reservoir.

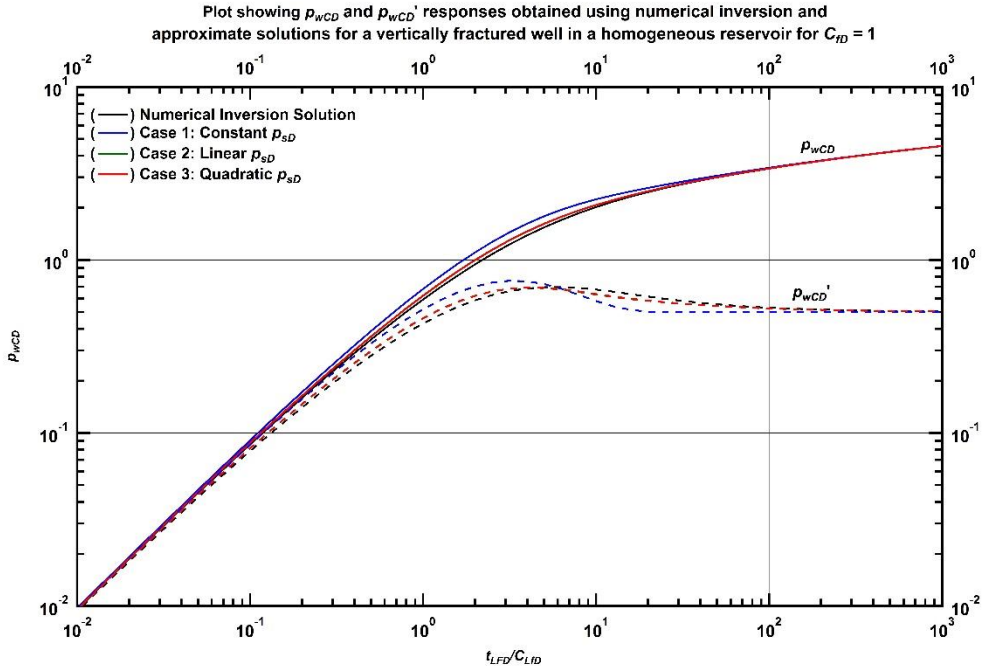

Figure 4.38 — Plot showing p_{wCD} and p_{wCD}' responses obtained using numerical inversion and approximate solutions for a vertically fractured well in a homogeneous reservoir for C_{fD} = 1.

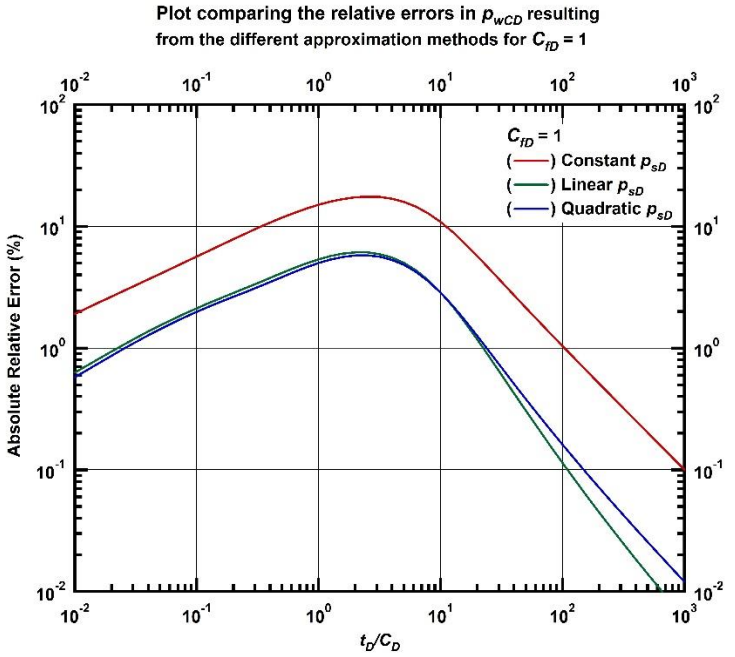

Figure 4.39 — Plot comparing the relative errors in p_{wCD} resulting from the different approximation methods in a vertically fractured well homogeneous reservoir for C_{fD} = 1.

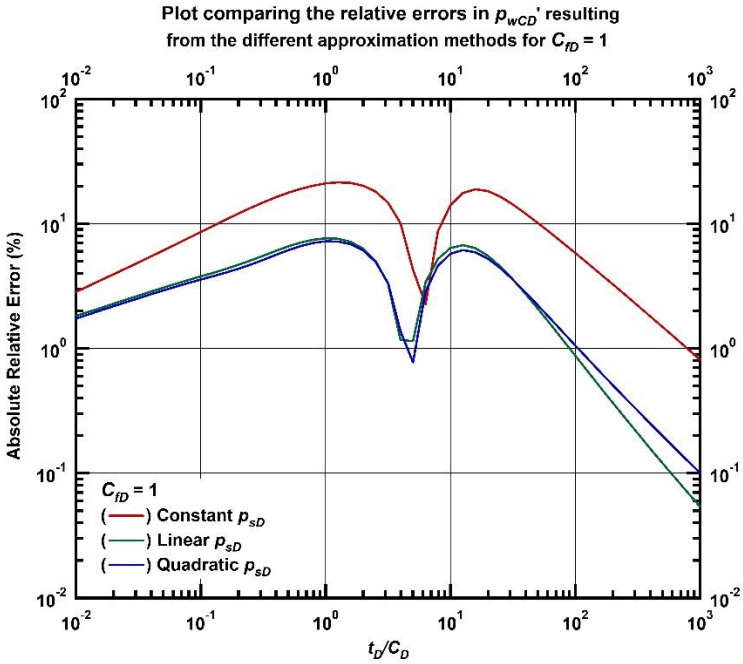

Figure 4.40 — Plot comparing the relative errors in p_{wCD}' resulting from the different approximation methods in a vertically fractured well homogeneous reservoir for C_{fD} = 1.

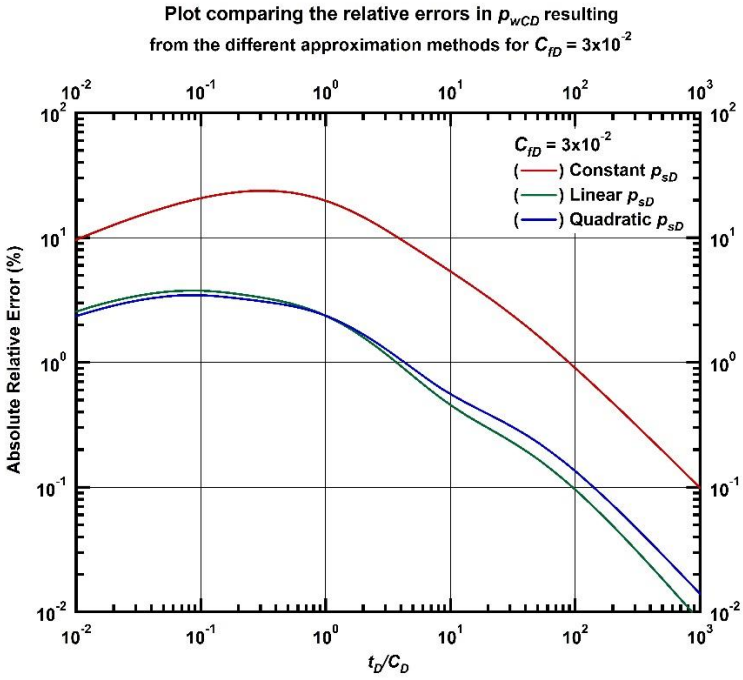

Figure 4.41 — Plot comparing the relative errors in p_{wCD} resulting from the different approximation methods in a vertically fractured well homogeneous reservoir for C_{fD} = 0.03.

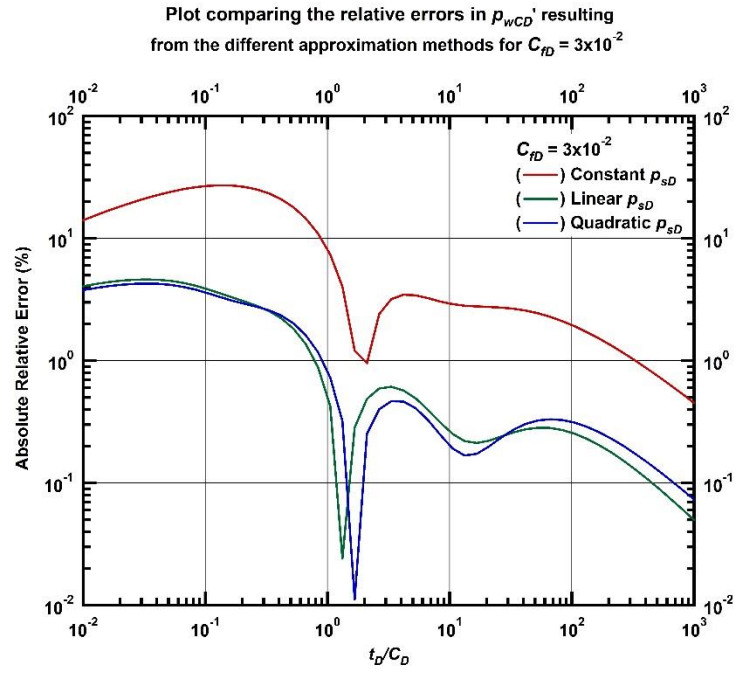

Figure 4.42 — Plot comparing the relative errors in p_{wCD}' resulting from the different approximation methods in a vertically fractured well homogeneous reservoir for C_{fD} = 0.03.

Wells in an Infinite-Acting Naturally Fractured Reservoir

This section considers the application of the explicit relations for wellbore storage and skin effects to a naturally fractured reservoir system. This study considers the pseudosteady-state and transient interporosity flow models. Bourdet and Gringarten (1980) developed a solution for the transient interporosity flow and Warren and Root (1963) developed the pseudosteady-state interporosity flow solution. These solutions were used, in SPE 21826, to generate the actual and approximate $p_{wCD}(t_D)$ solutions. In this work we do the same thing to determine the most accurate and consistent model of the $p_{wCD}(t_D)$ function in the case of an infinite-acting naturally fractured reservoir.

Naturally Fractured Reservoirs: Transient Interporosity Flow Case
(C_D = 1, S = 10, $\lambda = 10^{-6}$, and $\omega = 10^{-3}$)

Figure 4.43 shows the comparison of the three $p_{wCD}(t_D)$ relations to the actual solution obtained by numerical inversion for the transient interporosity flow case. All three cases yield accurate approximations of the $p_{wCD}(t_D)$ function. As was done in SPE 21826, the constant rate solutions, $p_{sD}(t_D)$ and $p_{sD}'(t_D)$ are represented in Figure 4.41 to show the agreement of the $p_{sD}(t_D)$ and $p_{wCD}(t_D)$ and $p_{sD}'(t_D)$ and $p_{wCD}'(t_D)$ solutions once wellbore storage effects have diminished. We note that there is no discernible deviation between the actual and approximate $p_{wCD}(t_D)$ functions and **Figure 4.44** shows that the largest error is less than 2%.

Figure 4.43 shows good agreement with the numerical inversion solution for $p_{wCD}'(t_D)$, for all three cases except in the region $5 \times 10^1 \leq t_{LfD}/C_{fD} \leq 10^3$. However, the cases 2 and 3 approximation for $p_{wCD}'(t_D)$ are closer to the numerical inversion solution than the case 1 approximation, with the case 3 approximation reading slightly higher, while the case 2 approximation reads lower than the numerical inversion solution. Also, from **Figure 4.45**, we can see that the error in some areas is lower for the case 2 approximation than for case 3, while in some other areas, the reverse is the case. This suggests that either the case 2 method or case 3 could be the general explicit model for wellbore storage and skin effects. However, it would be computationally easier to use case 2.

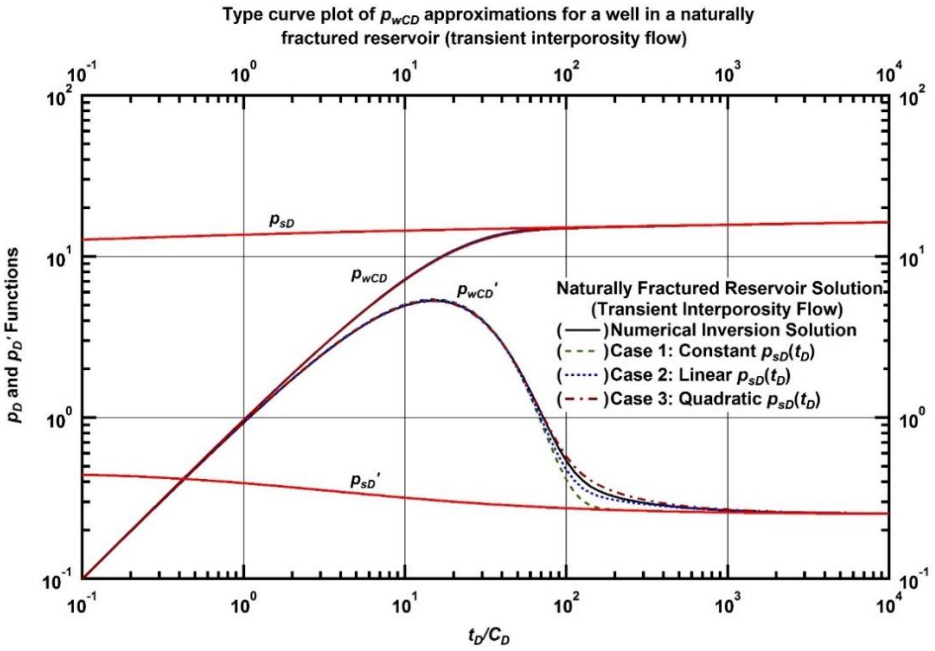

Figure 4.43 — Type curve plot of p_{wCD} approximations for a well in a naturally fractured reservoir (transient interporosity flow, (C_D = 1, s = 10, λ = 1x10^{-6}, and ω = 1x10^{-3}).

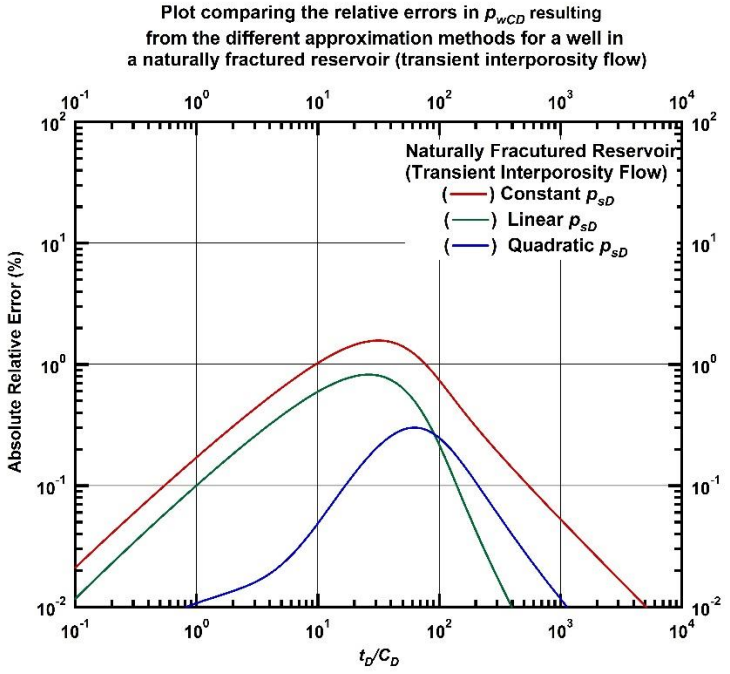

Figure 4.44 — Type curve plot of p_{wCD} approximations for a well in a naturally fractured reservoir (transient interporosity flow, (C_D = 1, s = 10, λ = 1x10^{-6}, and ω = 1x10^{-3}).

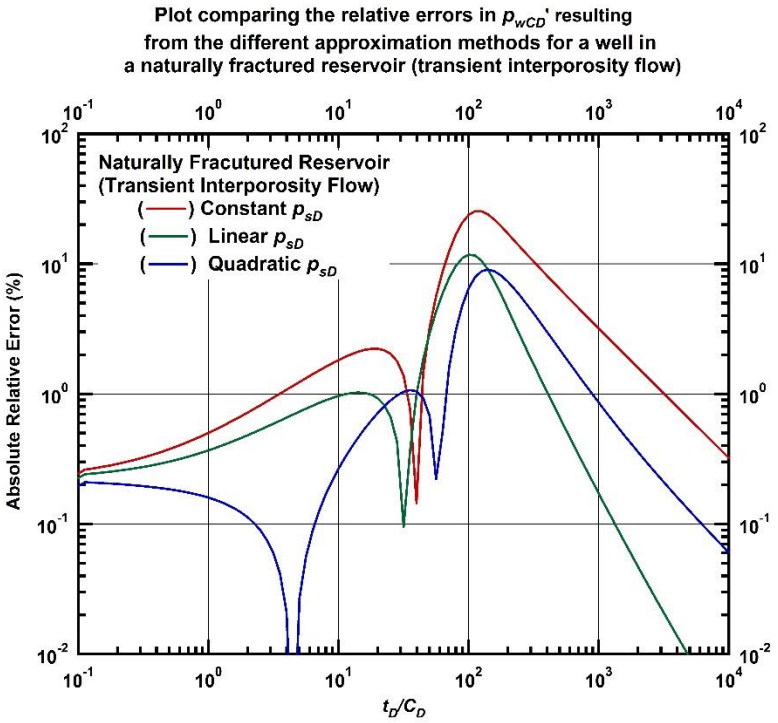

Figure 4.45 — Type curve plot of p_{wCD}' approximations for a well in a naturally fractured reservoir (transient interporosity flow, (C_D = 1, s = 10, λ = 1x10^{-6}, and ω = 1x10^{-3}).

Naturally Fractured Reservoirs: Pseudosteady-State Interporosity Flow Case
(C_D = 1, S = 10, λ = 10^{-6}, and ω = 10^{-3})

Figure 4.46 shows the comparison of the three $p_{wCD}(t_D)$ relations to the actual solution obtained by numerical inversion for the pseudosteady-state interporosity flow case. All three cases yield accurate approximations of the $p_{wCD}(t_D)$ function. As was done in SPE 21826, the constant rate solutions, $p_{sD}(t_D)$ and $p_{sD}'(t_D)$ are represented in Figure 4.41 to show the agreement of the $p_{sD}(t_D)$ and $p_{wCD}(t_D)$ and $p_{sD}'(t_D)$ and $p_{wCD}'(t_D)$ solutions once wellbore storage effects have diminished. We note that there is no discernible deviation between the actual and approximate $p_{wCD}(t_D)$ functions and **Figure 4.47** shows that the largest error is less than 2%.

Figure 4.46 shows good agreement with the numerical inversion solution for $p_{wCD}'(t_D)$, for all three cases except in the region 5 x $10^1 \le t_{LfD}/C_{fD} \le 10^3$. However, transient interporosity flow case, the cases 2 and 3 approximation for $p_{wCD}'(t_{LfD})$ are closer to the numerical inversion solution than the case 1 approximation. Also, from **Figure 4.48**, we can see that the error in some areas is lower for the case 2 approximation than for case 3, while in some other areas, the reverse is the case. This suggests that either the case 2 method or case 3 could be the general explicit model for wellbore storage and skin effects. However, like in the transient interporosity flow case, it would be easier to use the case 2 approximation.

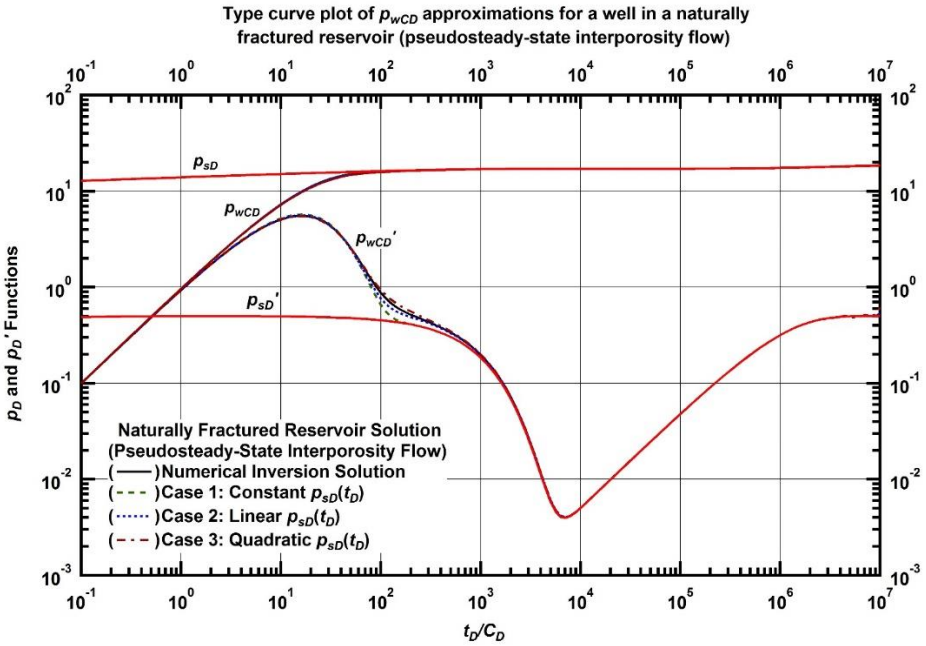

Figure 4.46 — Type curve plot of p_{wCD} approximations for a well in a naturally fractured reservoir (pseudosteady-state interporosity flow, (C_D = 1, s = 10, λ = 1x10^{-6}, and ω = 1x10^{-3}).

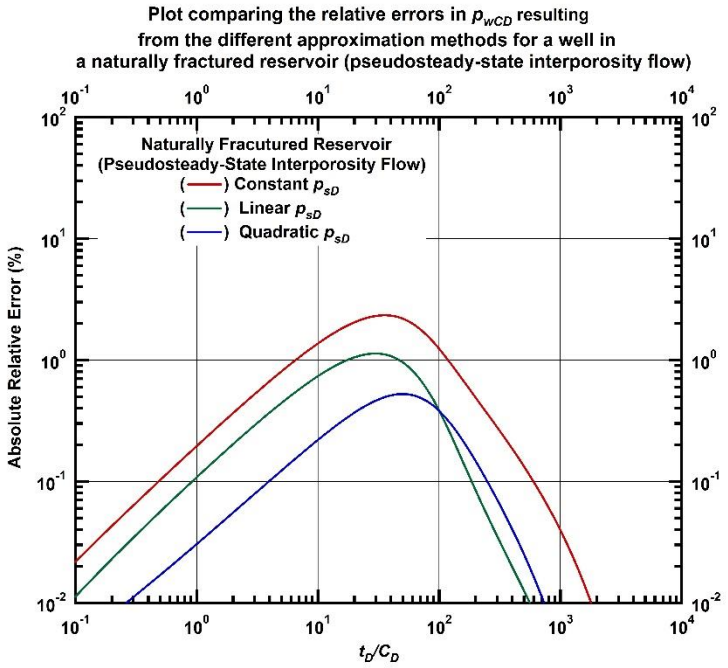

Figure 4.47 — Type curve plot of p_{wCD} approximations for a well in a naturally fractured reservoir (transient interporosity flow, (C_D = 1, s = 10, λ = 1x10^{-6}, and ω = 1x10^{-3}).

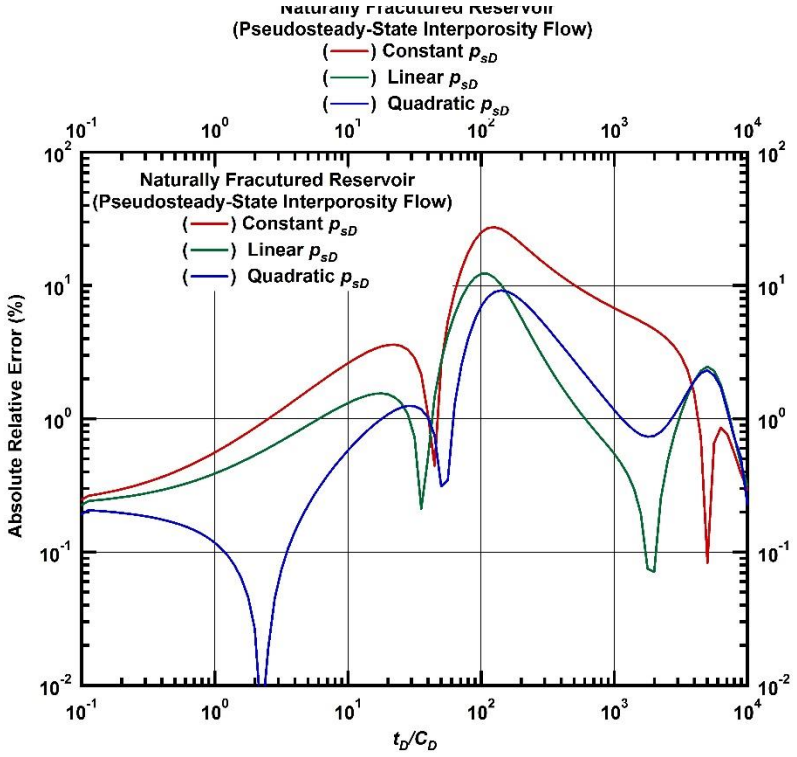

Figure 4.48 — Type curve plot of p_{wCD}' approximations for a well in a naturally fractured reservoir (transient interporosity flow, (C_D = 1, s = 10, λ = 1x10^{-6}, and ω = 1x10^{-3}).

4.2 Validation of Explicit Calculation of the Wellbore Phase Redistribution Dimensionless Pressure, p_{wD}

Figure 4.49 is presented as validation for the formula generated from the explicit calculation of wellbore phase redistribution dimensionless pressure (Eq. 3.3). This plot assumes an unfractured well in an infinite-acting homogeneous reservoir with the properties: $C_D = 10^2$, $C_{\alpha D} = 20$, $C_{\phi D} = 10^2$, and $S = 0$, as was done in SPE 21826. It can be observed that the numerical inversion solution and the explicit computation (Eq. 3.3) yield identical results for the $p_{w\phi D}(t_D)$ function. **Figure 4.50** shows the error in the $p_{wD}(t_D)$ solution is quite low. This result which shows that the total dimensionless pressure, $p_{w\phi D}(t_D)$, can be computed without inversion of Laplace space relations (for $p_{\phi D}(t_D)$, given in explicit form by Eq. 3.4). The advantages of using the explicit calculation also include the prospect for de-coupling of the wellbore storage and wellbore phase redistribution solutions which may lead to a rigorous analysis method for pressure data distorted by wellbore phase redistribution.

Figure 4.49 also shows that the explicit and numerical inversion calculations of the derivative function, $p_{wD}'(t_D)$, agree almost exactly. This agreement of derivatives suggests that for any case of well phase redistribution, the numerical inversion and explicit calculations should agree very well.

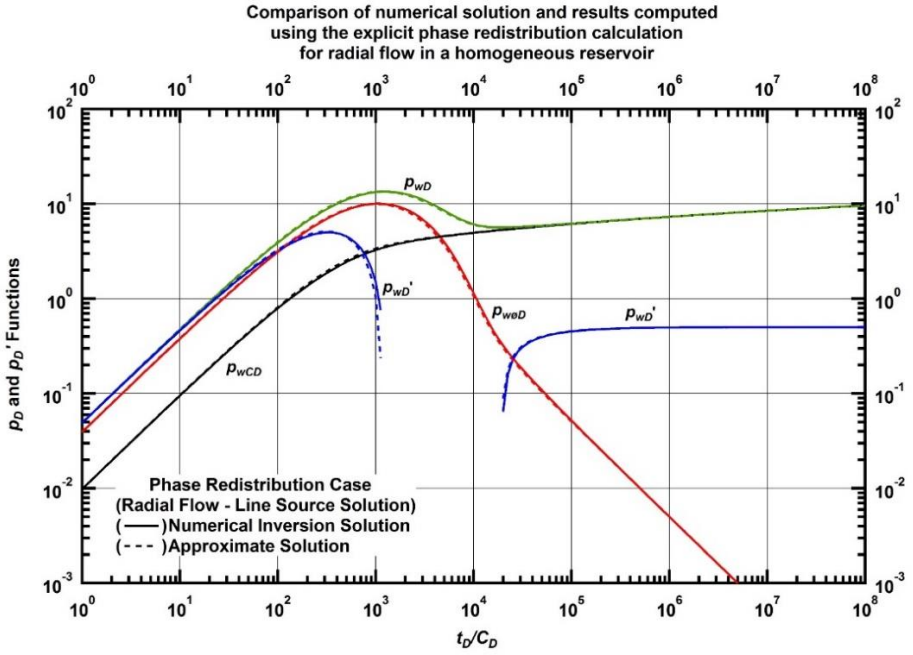

Figure 4.49 — Comparison of numerical inversion solution and results computed using the explicit phase redistribution calculation. Line source (radial flow) solution ($C_D = 10^2$, $C_{aD} = 20$, $C_{\varphi D} = 10^2$, and $s = 0$).

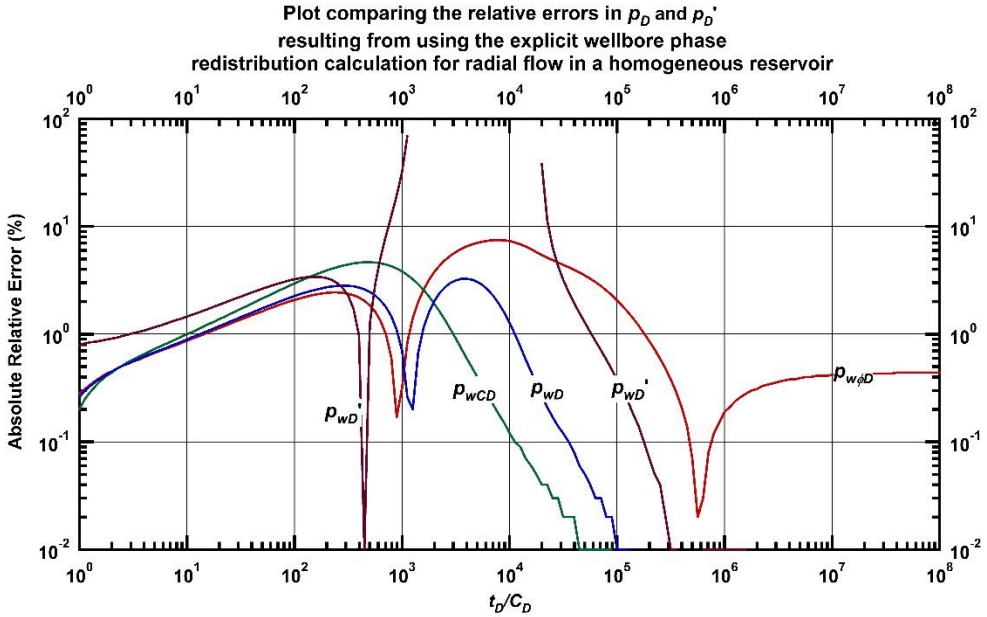

Figure 4.50 — Comparison of numerical inversion solution and results computed using the explicit phase redistribution calculation. Line source (radial flow) solution ($C_D = 10^2$, $C_{aD} = 20$, $C_{\varphi D} = 10^2$, and $s = 0$).

4.3 Validation of Empirical Approximations

The need to reduce the errors in the analytical approximations i.e cases 1, 2 and 3, and make them more accurate necessitated the development of empirical equations. The aim is to obtain $p_{wCD}(t_D)$ functions that are accurate and retain all the properties of the $p_{wCD}(t_D)$ in terms of shape and consistent behavior when used in reservoir engineering calculations.

The correlations that would be validated are the $p_{wCD}(t_D)$ approximations based on constant $p_{sD}(t_D)$ with normal distribution adjustment and modified normal distribution adjustment. They would be validated based on an acceptable level of error between the actual $p_{wCD}(t_D)$ results obtained from numerical inversion and those obtained from the correlation. An $ARE \leq 1.5\%$ is considered acceptable

All validations are done for an infinite-acting homogeneous reservoir. The plots are made for the time period $10^{-1} \leq t_D/C_D \leq 10^4$ for 13 values of C_De^{2S} ranging from 10^1 to 10^{60}.

Validation of Normal Distribution Adjustment Correlation for $p_{wCD}(t_D)$

Figures 4.51 shows the type curve plots of $p_{wCD}(t_D)$ comparing results obtained numerically to those obtained using the Normal Distribution Adjustment Correlation (Eq. 3.12). We note that there is excellent agreement between both sets of solutions, with one almost lying perfectly on top of the other.

Figures 4.52 shows the type curve plots of $p_{wCD}'(t_D)$ comparing results obtained numerically to those obtained using the Normal Distribution Adjustment Correlation and numerical differentiation. We note that there is good agreement between both sets of solutions, with one almost lying perfectly on top of the other in early and late time. It is important to note that the shape of the derivative curve in Figure 4.52 is not as it ought to be, because the transition from wellbore storage and skin effect to radial flow stabilization is not smooth. There is an extra point of inflection as the derivative moves towards radial flow stabilization ($p_{wCD}'(t_D) = 0.5$). **Figures 4.53** and **4.54** show the $p_{wCD}(t_D)$ and $p_{wCD}'(t_D)$ results respectively, obtained from the correlation without the exact $p_{wCD}(t_D)$ and $p_{wCD}'(t_D)$ plotted alongside them and that anomalous inflection can be seen.

Figures 4.55, 4.57 and **4.59** show the errors in the $p_{wCD}(t_D)$ solutions for $C_De^{2s} = 10^1$, 10^6, and, 10^{20} with a maximum error of about 1%. **Figures 4.56, 4.58** and **4.60** also show the errors in the $p_{wCD}'(t_D)$ solutions for the same time period, and the maximum error is about 9%, which is better than the 25.9% obtained from the case 1 approximation. This shows that the correlation has succeeded in improving the case 1 approximation in terms of error.

A noteworthy point is that while this correlation may be useful in certain applications, as it accurately models $p_{wCD}(t_D)$, it is not an accurate representation of $p_{wCD}'(t_D)$.

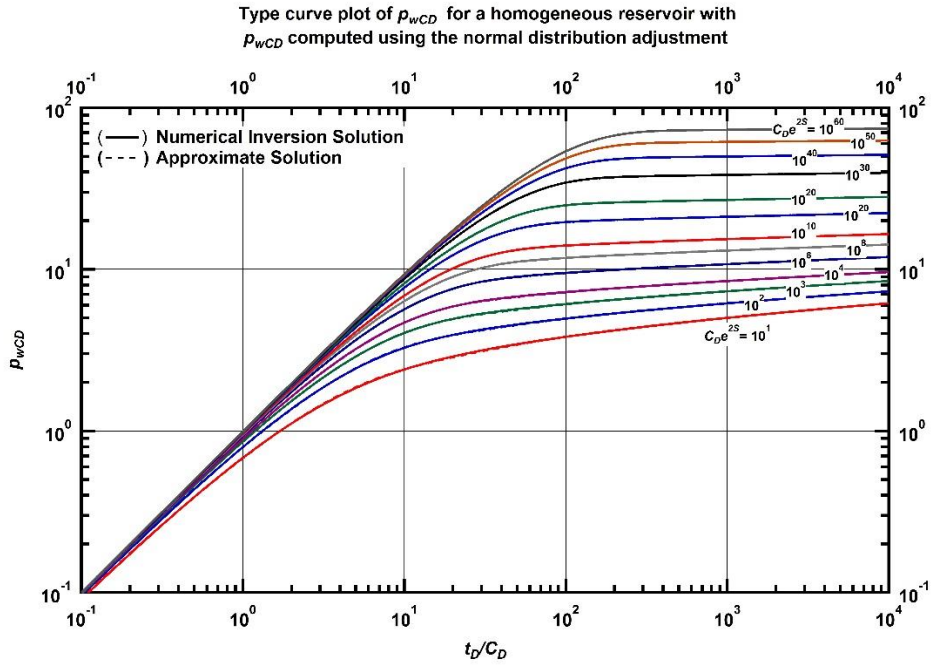

Figure 4.51 — Type curve plot of p_{wCD} for a homogeneous reservoir. p_{wCD} computed using the normal distribution adjustment.

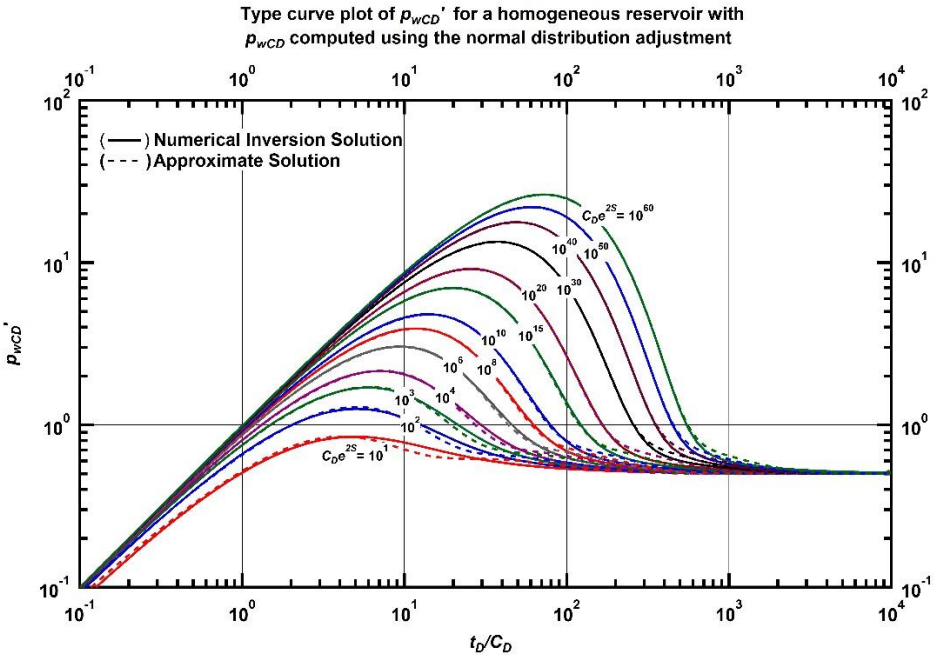

Figure 4.52 — Type curve plot of p_{wCD}' for a homogeneous reservoir. p_{wCD} computed using the normal distribution adjustment.

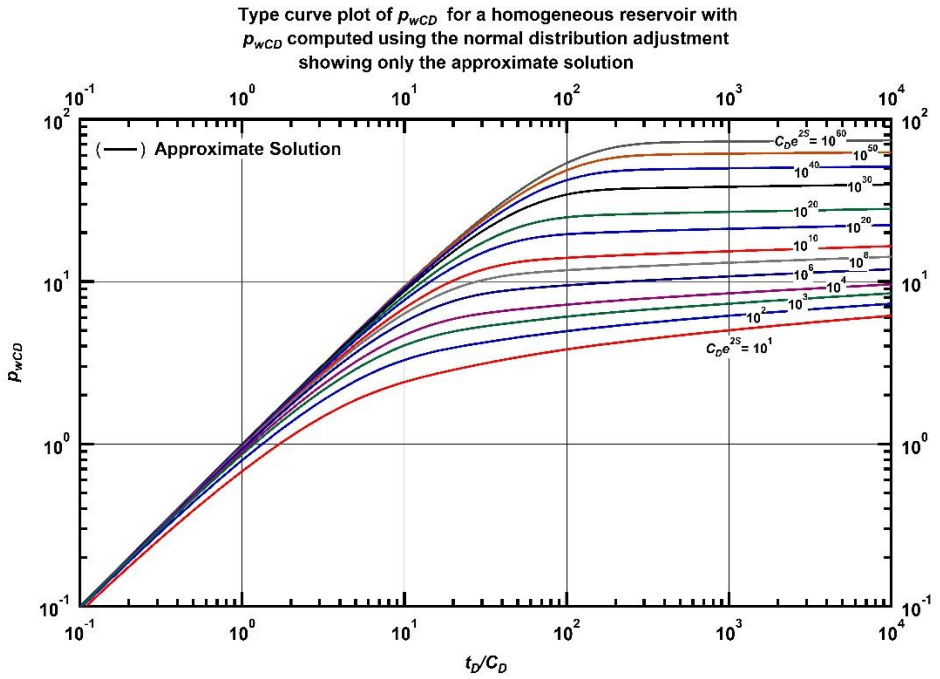

Figure 4.53 — Type curve plot of p_{wCD} for a homogeneous reservoir. p_{wCD} computed using the normal distribution adjustment showing only the approximate solution.

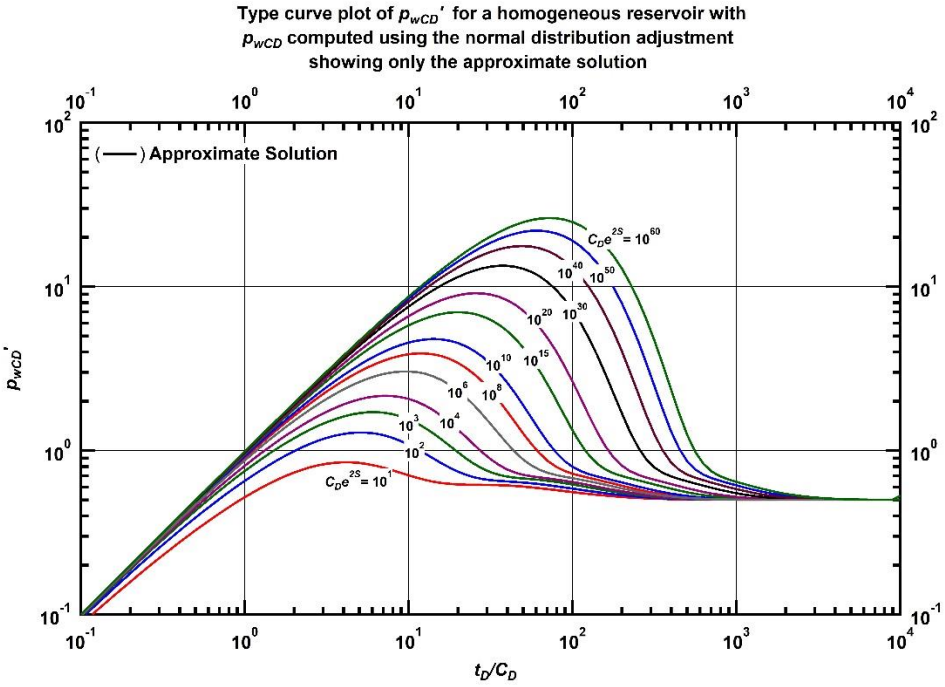

Figure 4.54 — Type curve plot of p_{wCD}' for a homogeneous reservoir. p_{wCD} computed using the normal distribution adjustment showing only the approximate solution.

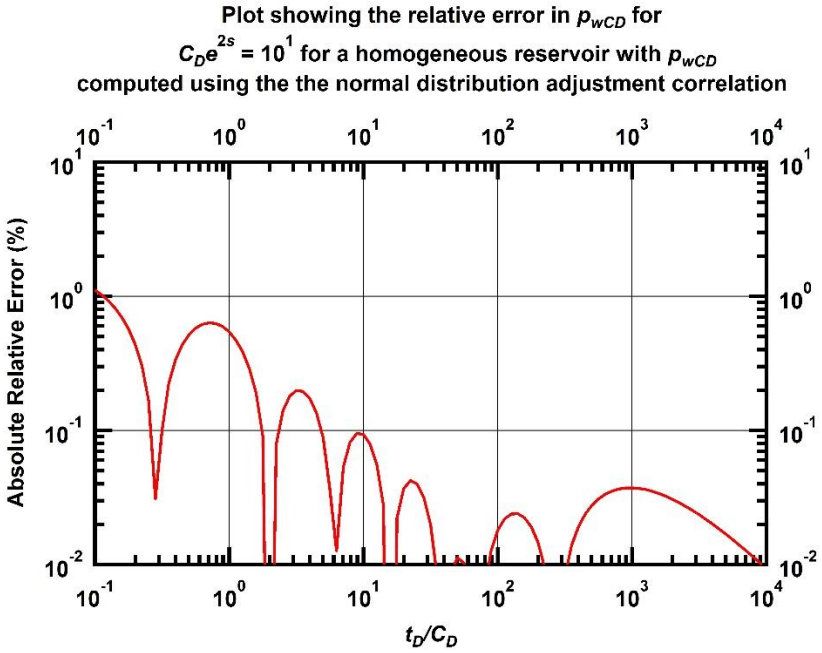

Figure 4.55 — Plot showing the relative error in p_{wCD} for $C_De^{2s} = 10^1$ for a homogeneous reservoir with p_{wCD} computed using the normal distribution adjustment correction.

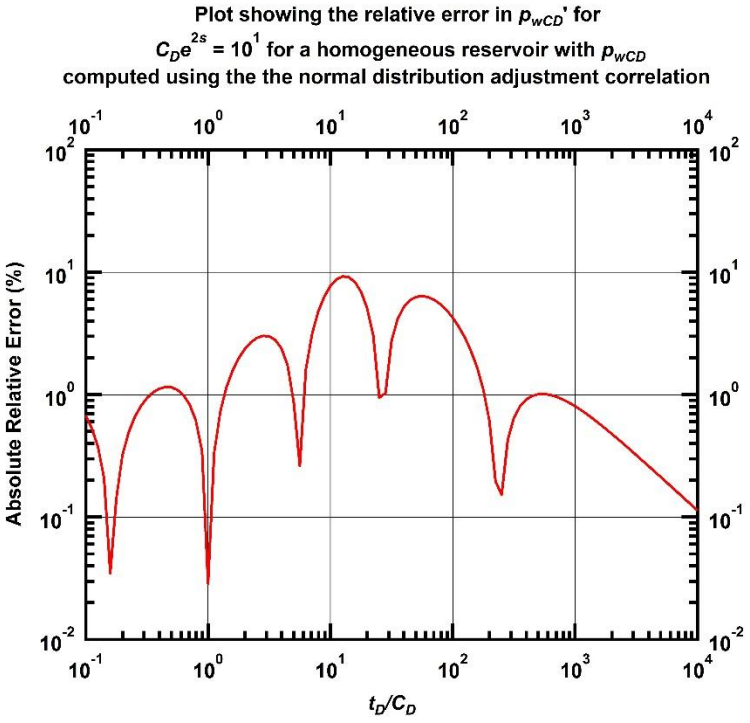

Figure 4.56 — Plot showing the relative error in p_{wCD}' for $C_De^{2s} = 10^1$ for a homogeneous reservoir with p_{wCD} computed using the normal distribution adjustment correction.

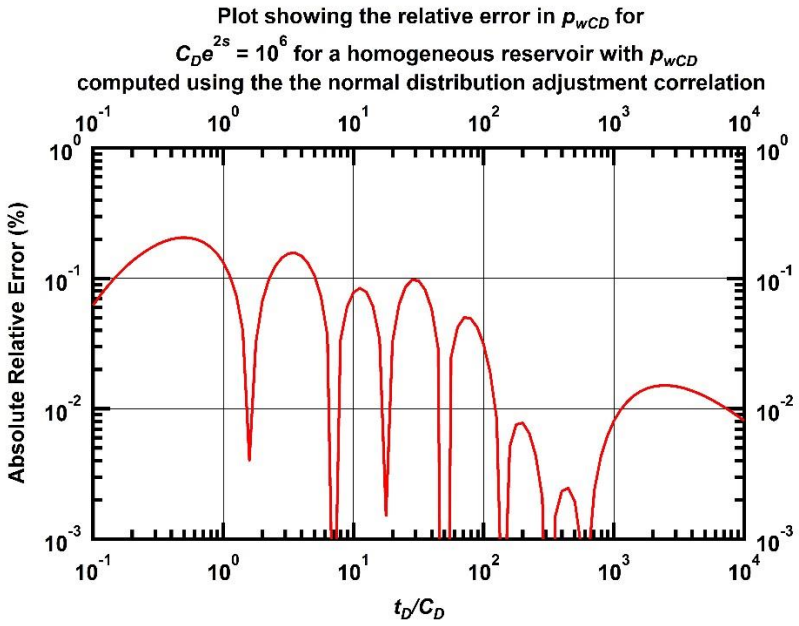

Figure 4.57 — Plot showing the relative error in p_{wCD} for $C_De^{2s} = 10^6$ for a homogeneous reservoir with p_{wCD} computed using the normal distribution adjustment correction.

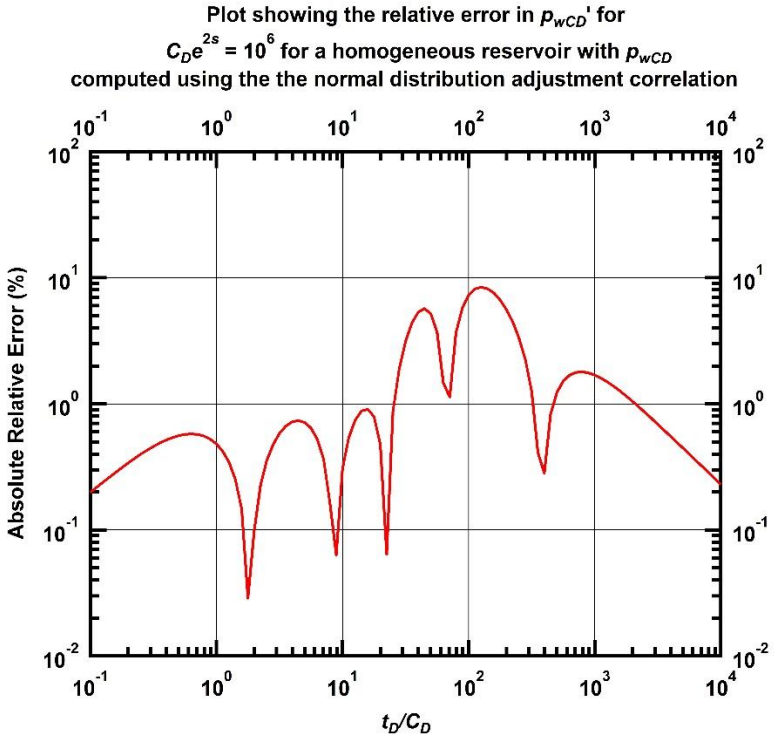

Figure 4.58 — Plot showing the relative error in p_{wCD}' for $C_De^{2s} = 10^6$ for a homogeneous reservoir with p_{wCD} computed using the normal distribution adjustment correction.

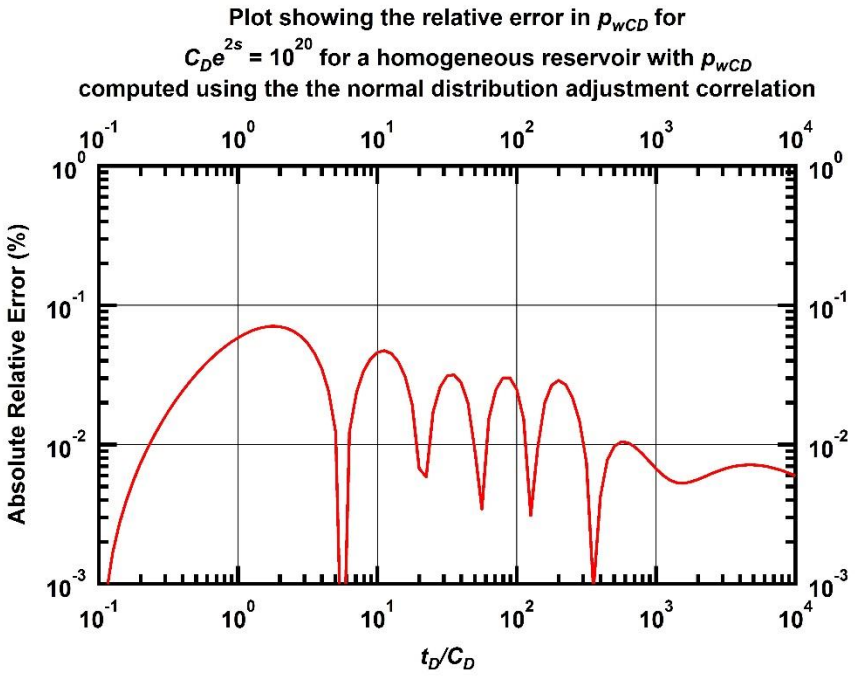

Figure 4.59 — Plot showing the relative error in p_{wCD} for $C_De^{2s} = 10^{20}$ for a homogeneous reservoir with p_{wCD} computed using the normal distribution adjustment correction.

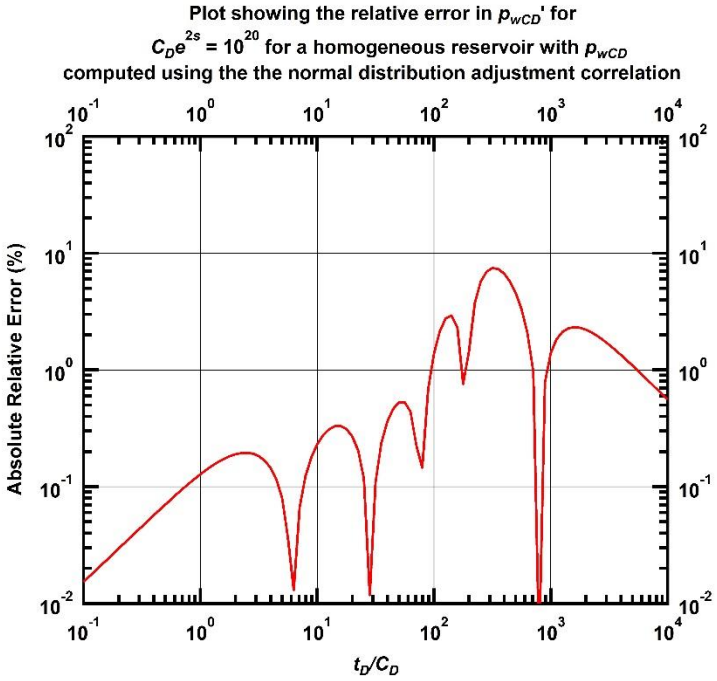

Figure 4.60 — Plot showing the relative error in p_{wCD}' for $C_De^{2s} = 10^{20}$ for a homogeneous reservoir with p_{wCD} computed using the normal distribution adjustment correction.

Validation of Modified Normal Distribution Adjustment Correlation for $p_{wCD}(t_D)$

Figures 4.61 shows the type curve plots of $p_{wCD}(t_D)$ comparing results obtained numerically to those obtained using the Modified Normal Distribution Adjustment Correlation (Eq. 3.18). We note that there is excellent agreement between both sets of solutions, with one almost lying perfectly on top of the other.

Figures 4.62 shows the type curve plots of $p_{wCD}'(t_D)$ comparing results obtained numerically to those obtained using the Normal Distribution Adjustment Correlation and numerical differentiation. We note that there is good agreement between both sets of solutions, with one almost lying perfectly on top of the other from early to late time. It is important to note that the shape of the derivative curve in Figure 4.62 is as it ought to be, with a smooth transition from wellbore storage and skin effect to radial flow stabilization. **Figures 4.63** and **4.64** show the $p_{wCD}(t_D)$ and $p_{wCD}'(t_D)$ results respectively, obtained from the correlation without the exact $p_{wCD}(t_D)$ and $p_{wCD}'(t_D)$ plotted alongside them.

Figures 4.65, 4.67 and **4.69** show the errors in the $p_{wCD}(t_D)$ solutions for C_De^{2s} =10^1, 10^6, and, 10^{20} with a maximum error of about 1%. **Figures 4.66, 4.68** and **4.70** also show the errors in the $p_{wCD}'(t_D)$ solutions for the same time period, and the maximum error is about 9%, which is better than the 25.9% obtained from the case 1 approximation. This shows that the correlation has succeeded in improving the case 1 approximation in terms of error and is better than the Normal Distribution Adjustment Correlation as it models $p_{wCD}'(t_D)$.accurately

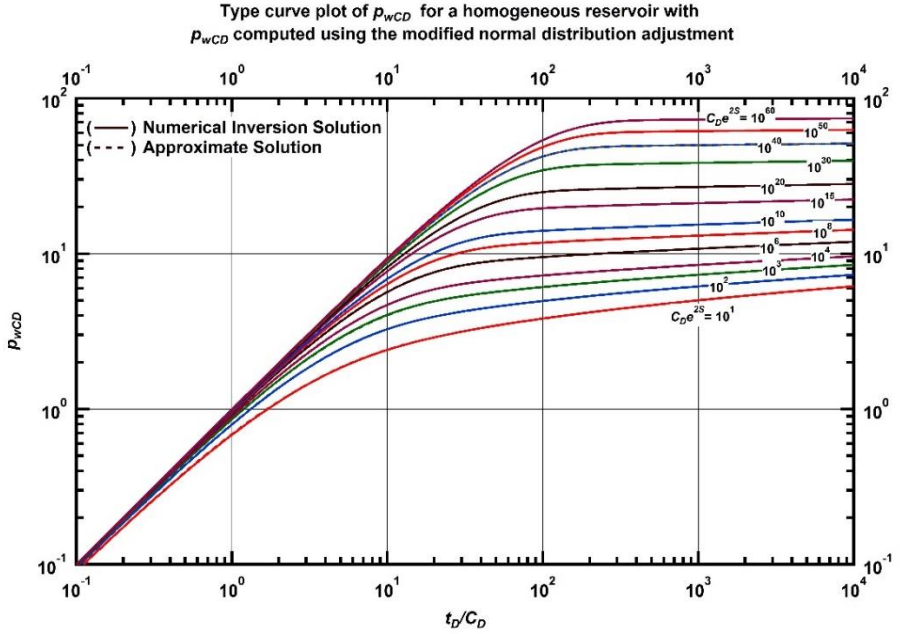

Figure 4.61 — Type curve plot of p_{wCD} for a homogeneous reservoir. p_{wCD} computed using the modified normal distribution adjustment.

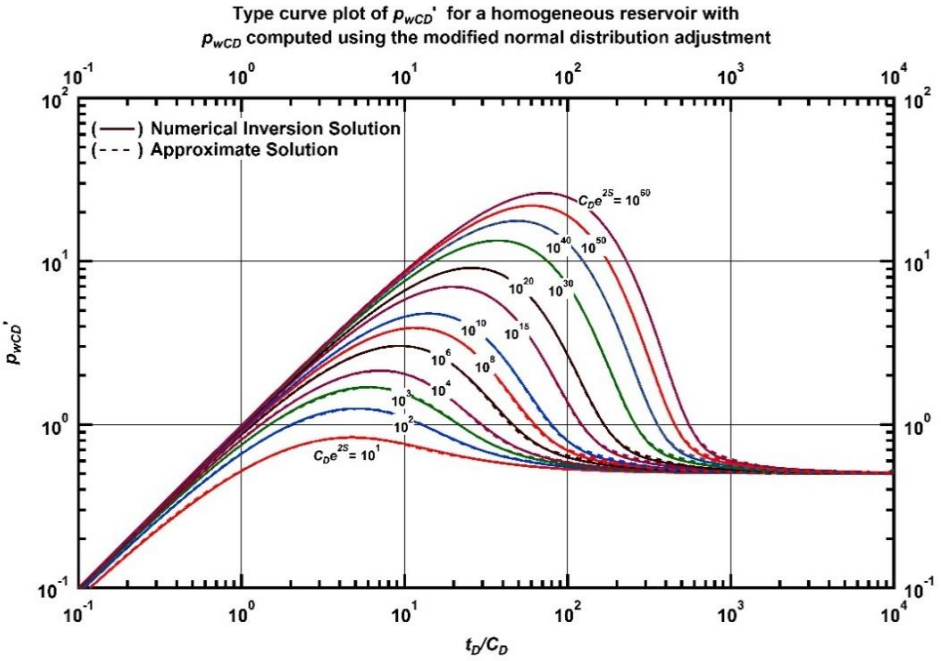

Figure 4.62 — Type curve plot of p_{wCD}' for a homogeneous reservoir. p_{wCD} computed using the modified normal distribution adjustment.

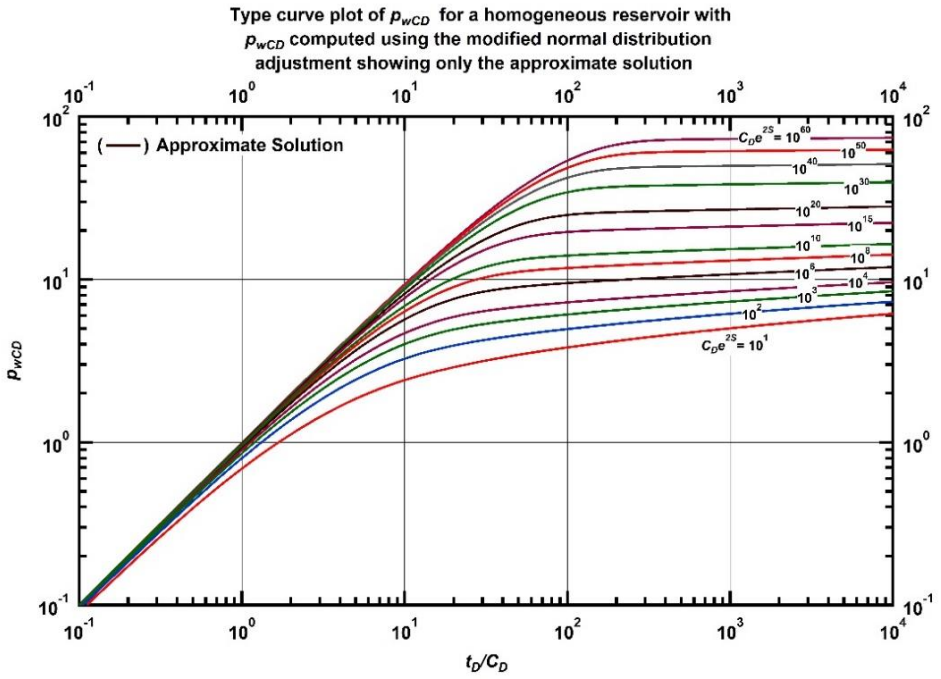

Figure 4.63 — Type curve plot of p_{wCD} for a homogeneous reservoir. p_{wCD} computed using the modified normal distribution adjustment showing only the approximate solution.

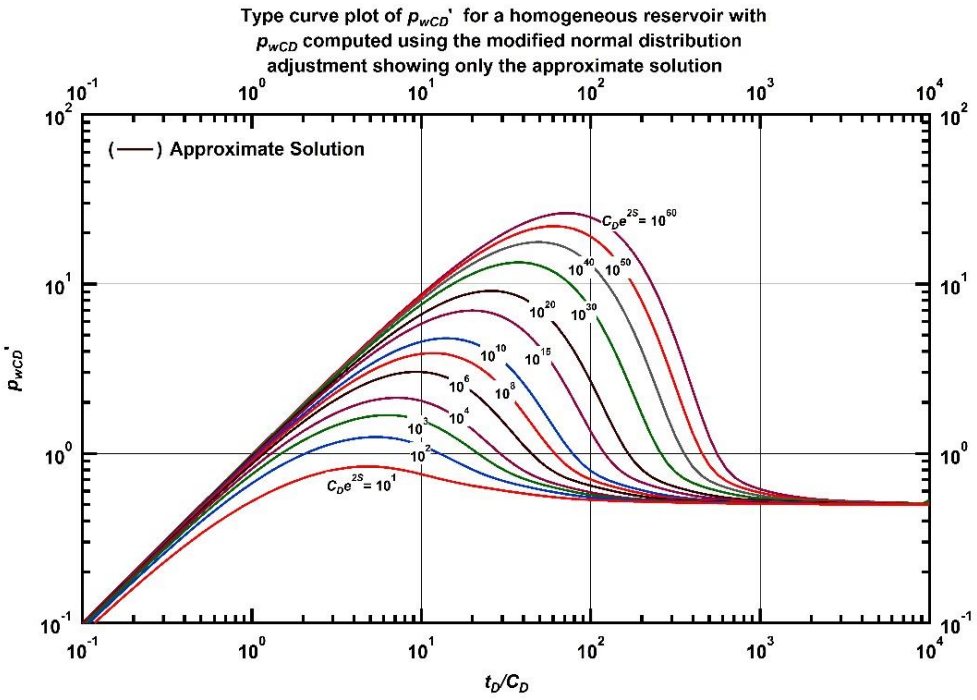

Figure 4.64 — Type curve plot of p_{wCD}' for a homogeneous reservoir. p_{wCD} computed using the modified normal distribution adjustment showing only the approximate solution.

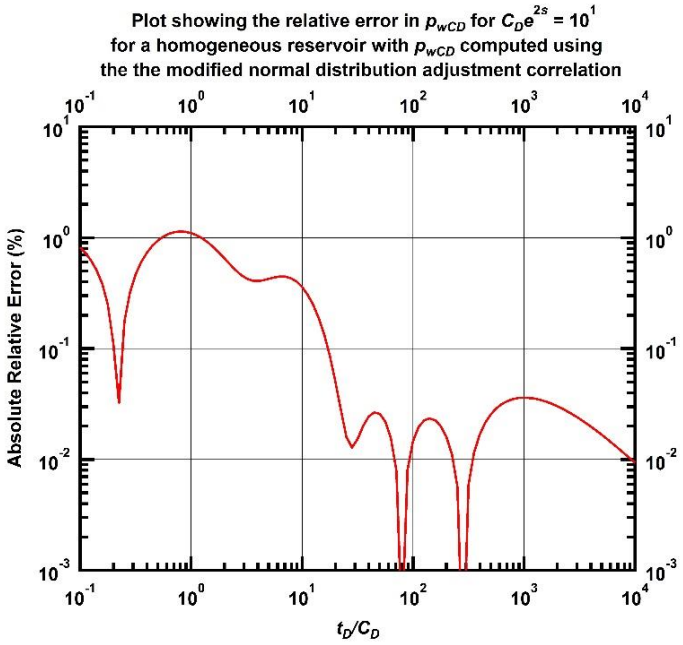

Figure 4.65 — Plot showing the relative error in p_{wCD} for $C_De^{2s} = 10^1$ for a homogeneous reservoir with p_{wCD} computed using the modified normal distribution adjustment correction.

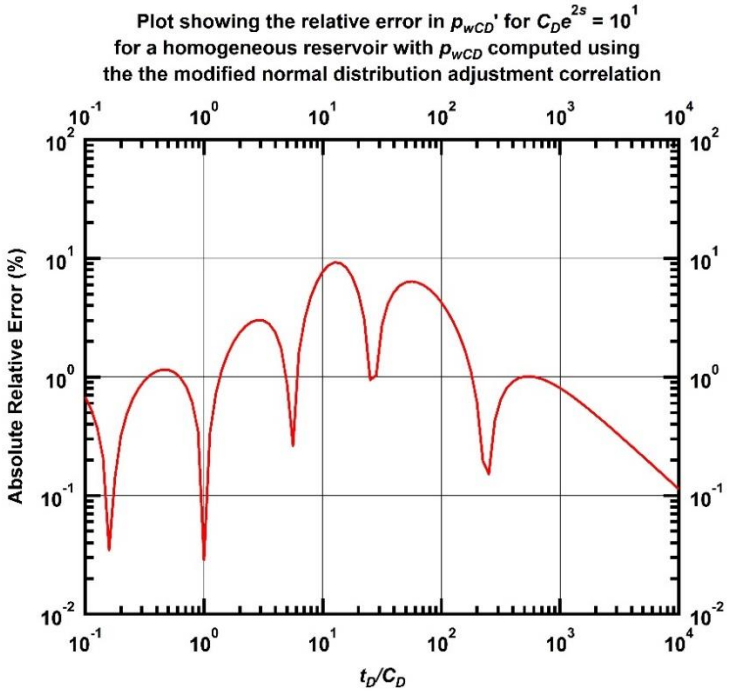

Figure 4.66 — Plot showing the relative error in p_{wCD}' for $C_De^{2s} = 10^1$ for a homogeneous reservoir with p_{wCD} computed using the modified normal distribution adjustment correction.

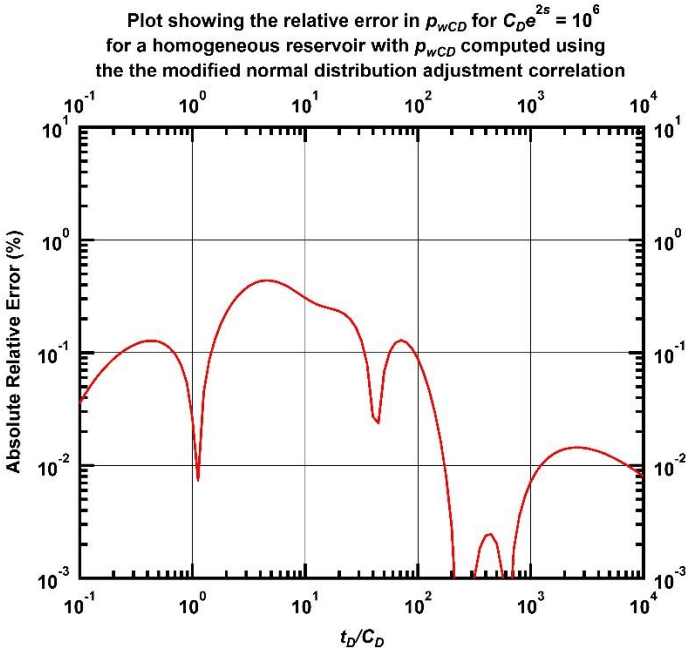

Figure 4.67 — Plot showing the relative error in p_{wCD} for $C_De^{2s} = 10^6$ for a homogeneous reservoir with p_{wCD} computed using the modified normal distribution adjustment correction.

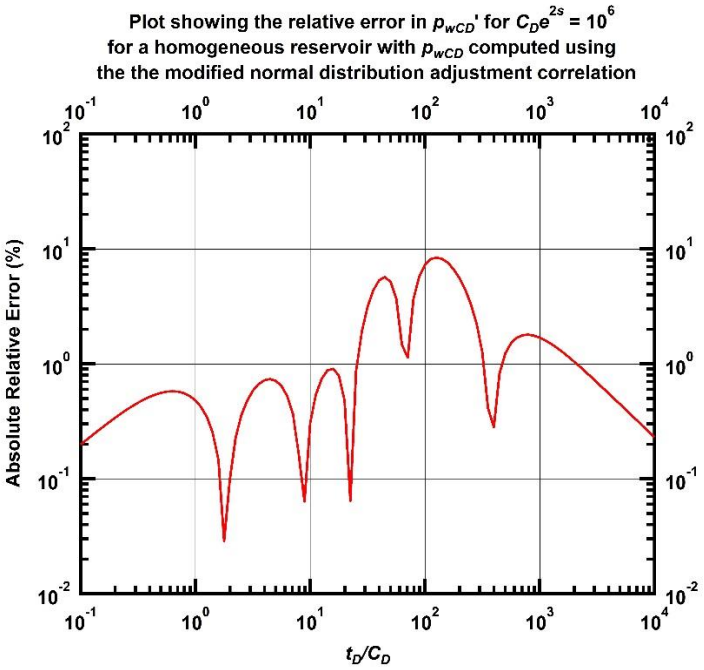

Figure 4.68 — Plot showing the relative error in p_{wCD}' for $C_De^{2s} = 10^6$ for a homogeneous reservoir with p_{wCD} computed using the modified normal distribution adjustment correction.

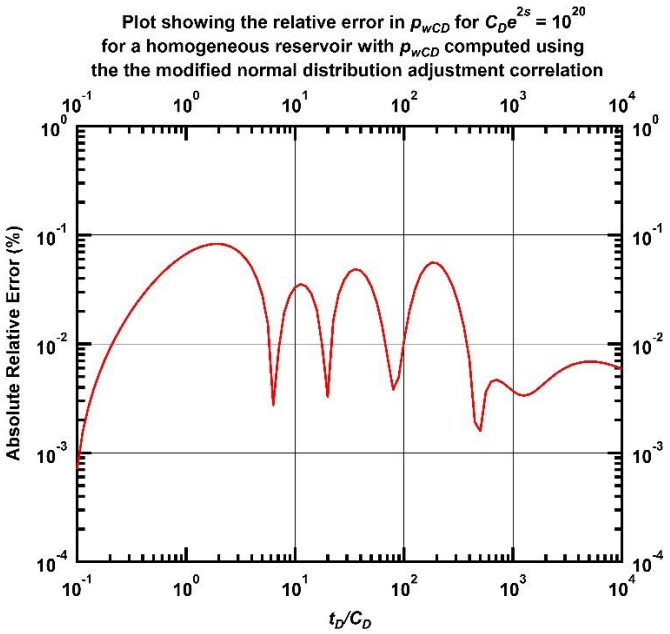

Figure 4.69 — Plot showing the relative error in p_{wCD} for $C_De^{2s} = 10^{20}$ for a homogeneous reservoir with p_{wCD} computed using the modified normal distribution adjustment correction.

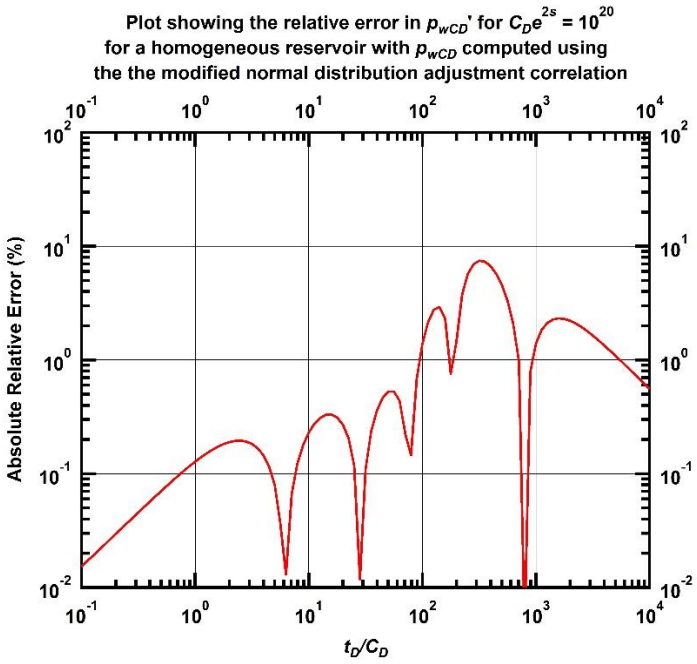

Figure 4.70 — Plot showing the relative error in p_{wCD}' for $C_De^{2s} = 10^{20}$ for a homogeneous reservoir with p_{wCD} computed using the modified normal distribution adjustment correction.

CHAPTER V
DECONVOLUTION

Up to this point, this thesis has dealt with the convolution problem — *i.e.*, attempting to determine $p_{wCD}(t_D)$ from $p_{sD}(t_D)$ for a given C_D. This is a somewhat straightforward problem as we have the convolution integral given in Eq. 3.1 to work with. Deconvolution is the reverse process, where the distortion from wellbore pressure distorted by wellbore storage and skin is reversed or "inverted" to obtain the undistorted constant rate pressure solution. In other words, it is the determination $p_{sD}(t_D)$ from $p_{wCD}(t_D)$ for a given value of C_D. Convolution is an inherently stable mathematical formulation (in its simplest form it is a forward summation). In contrast, deconvolution is inherently unstable as it would be a sort of recursion-type of calculation (as opposed to a forward calculation), as such, any errors/inaccuracies become amplified in a deconvolution process. Our goal is to leverage the approximations and correlations developed in Chapter 3 to attempt a deconvolution process. The aim is to set up the deconvolution as a root-finding problem, since we now have relationships between $p_{sD}(t_D)$ and $p_{wCD}(t_D)$ that are easier to tackle than the convolution integral.

We choose the Modified Normal Distribution Adjustment Correlation and the Linear $p_{sD}(t_D)$ Assumption Approximation (Case 2) for the convolution attempt. The choice of these two approximation methods is because they have accurately modeled the $p_{wCD}(t_D)$ and $p_{wCD}'(t_D)$ functions and can be set up in such a manner as to find $p_{sD}(t_D)$ given $p_{wCD}(t_D)$ and C_D.

5.1 Deconvolution Using the Modified Normal Distribution Adjustment Correlation

Recall that the Modified Normal Distribution Adjustment Correlation is given as

$$p_{wCD}(t_D) = p_{sD}(t_D)\left[\begin{array}{l}\left[1-\exp\left[\dfrac{-t_D}{p_{sD}C_D}\right]\right]-\dfrac{\alpha_1}{\sigma_1\sqrt{2\pi}}\exp\left[-\dfrac{1}{2}\left[\dfrac{\ln\left[\dfrac{t_D}{p_{sD}C_D}\right]-m_1}{\sigma_1}\right]^2\right] \\ +\dfrac{\alpha_2}{\sigma_2\sqrt{2\pi}}\exp\left[-\dfrac{1}{2}\left[\dfrac{\ln\left[\dfrac{t_D}{p_{sD}C_D}\right]-m_2}{\sigma_2}\right]^2\right]\end{array}\right] \quad \text{.....(5.1)}$$

Using actual $p_{wCD}(t_D)$ values for an infinite-acting homogeneous reservoir, obtained from numerical inversion for 13 values of C_De^{2S} ranging from 10^1 to 10^{60} we solve for $p_{sD}(t_D)$ in Eq. 3.8. **Figure 5.1** shows the type curve plot $p_{sD}(t_D)$ solutions obtained for the time period $10^{-1} \le t_D/C_D \le 10^4$ and **Figure 5.2** shows the both actual and calculated $p_{sD}(t_D)$ solutions.. We note that there is a lack of agreement between these

solutions, especially in early times. Also, the shape of the calculated $p_{sD}(t_D)$ curves is not as smooth as the actual and has some "bumps". This is not an accurate deconvolution of $p_{wCD}(t_D)$ function.

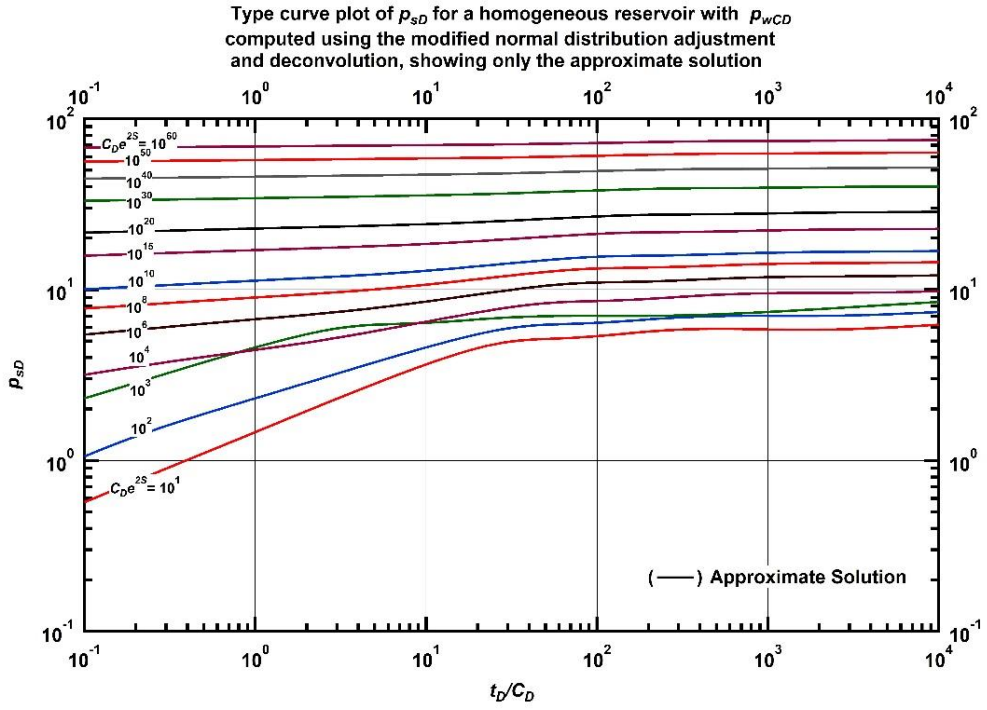

Figure 5.1 — Type curve plot of p_{sD} for a homogeneous reservoir. p_{wCD} computed using the modified normal distribution adjustment and deconvolution, showing only the approximate solution.

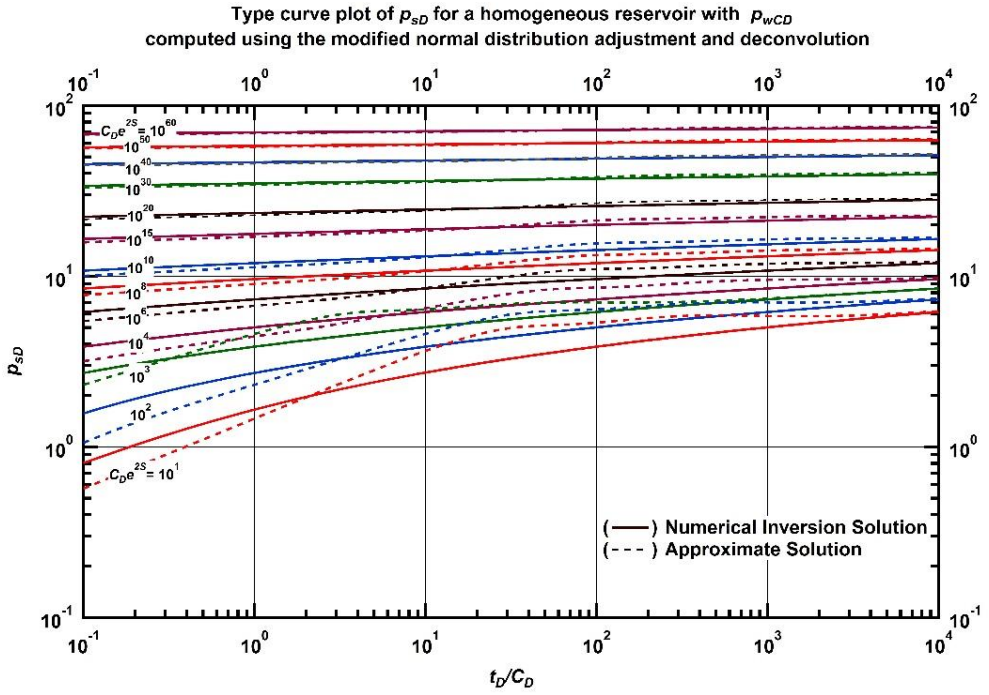

Figure 5.2 — Type curve plot of p_{sD} for a homogeneous reservoir. p_{wCD} computed using the modified normal distribution adjustment and deconvolution.

5.2 Deconvolution Using the Linear $p_{sD}(t_D)$ Assumption Approximation (Case 2)

Recall that the Linear $p_{sD}(t_D)$ Assumption Approximation (Case 2) is given as

$$p_{wCD}(t_D) = \frac{p_{sD}(t_D) + C_D t_D\left[\frac{d}{dt_D}\left[p_{sD}(t_D)\right]\right]^2}{\left[1 + C_D\left[\frac{d}{dt_D}\left[p_{sD}(t_D)\right]\right]\right]^2} + \exp\left[-\frac{t_D + C_D t_D\left[\frac{d}{dt_D}\left[p_{sD}(t_D)\right]\right]}{C_D\left[p_{sD}(t_D) - t_D\frac{d}{dt_D}\left[p_{sD}(t_D)\right]\right]}\right]\left[\frac{t_D\frac{d}{dt_D}\left[p_{sD}(t_D)\right] - p_{sD}(t_D)}{\left[1 + C_D\left[\frac{d}{dt_D}\left[p_{sD}(t_D)\right]\right]\right]^2}\right] \quad \text{.....(5.2)}$$

We note that it is impossible to solve this equation for $p_{sD}(t_D)$ without specifying a value for or an expression of the derivative of $p_{sD}(t_D)$ with respect to t_D. For the purpose of this work, we use utilize the log approximation solution to the diffusivity equation for the unfractured well in a homogeneous reservoir. Appendix G shows the details of this calculation.

Figure 5.3 shows the type curve plot of $p_{sD}(t_D)$ comparing results obtained from the numerical Laplace transform inversion and the solution of the calculated results. There is disagreement between the results in the region $t_D/C_D \leq 10^1$. **Figures 5.4** and **5.5** show the $p_{sD}'(t_D)$ functions obtained by numerical Laplace transform inversion and our calculations respectively. It is clear that these two plots do not match each other.

This shows that we have been unable to successfully carry out deconvolution for a vertical well in an infinitely-acting homogeneous reservoir using the Linear $p_{sD}(t_D)$ Assumption Approximation.

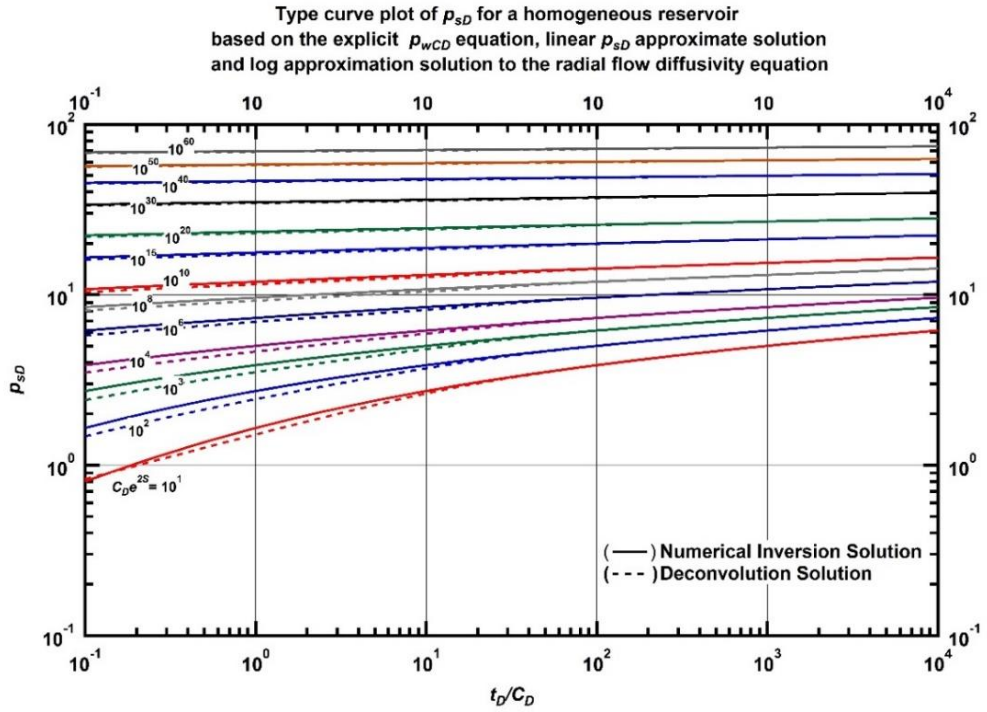

Figure 5.3 — Type curve plot of p_{sD} for a homogeneous reservoir comparing p_{sD} computed using the explicit p_{wCD} equation, the linear p_{sD} approximate solution and the log approximation solution to that computed using numerical laplace transform inversion.

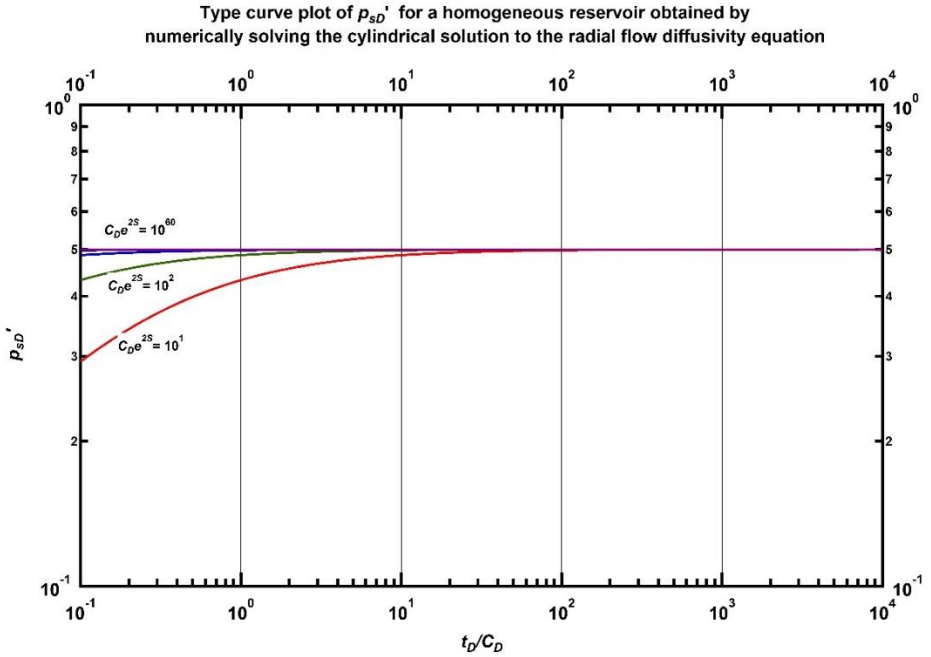

Figure 5.4 — Type curve plot of p_{sD}' for a homogeneous reservoir, computed using numerical Laplace transform inversion.

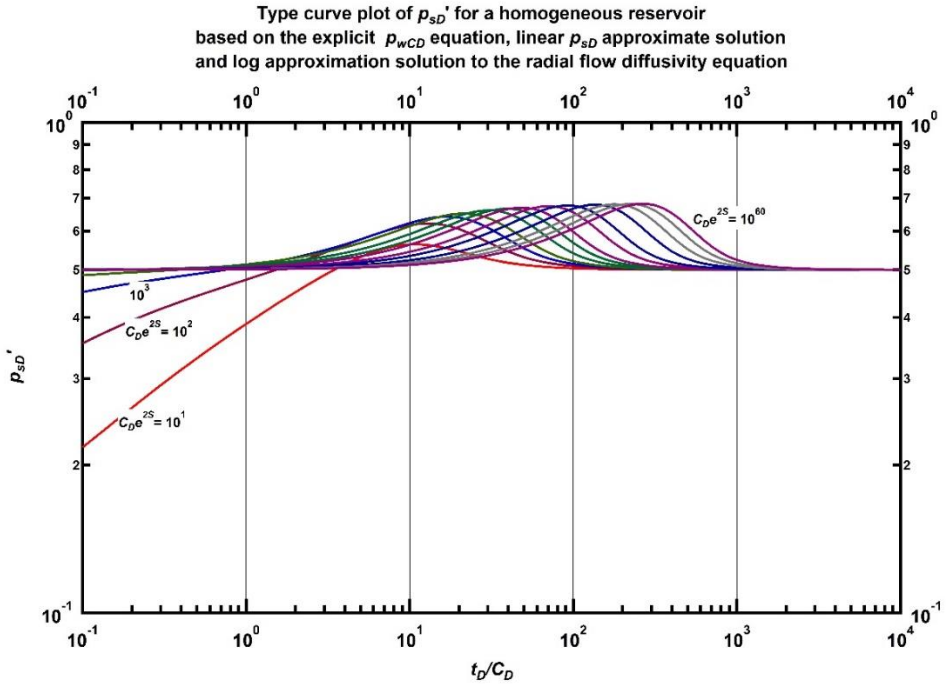

Figure 5.5 — Type curve plot of p_{sD}' for a homogeneous reservoir, computed using the explicit p_{wCD} equation, the linear p_{sD} approximate solution and the log approximation solution

CHAPTER VI
SUMMARY, CONCLUSIONS AND FUTURE WORK

6.1 Summary

In an effort to validate and extend prior work to create explicit solutions for the computation of the effects of wellbore storage and phase redistribution, we have derived three approximate solutions. These approximations are based on "imposing" a particular behavior in time on between the undistorted constant rate pressure function, $p_{sD}(t_D)$. These behaviors include:

- The "constant" $p_{sD}(t_D)$ case which considers: $p_{sD}(t_D) = a$
- The "linear" $p_{sD}(t_D)$ case which considers: $p_{sD}(t_D) = a + bt_D$
- The "quadratic" $p_{sD}(t_D)$ case which considers: $p_{sD}(t_D) = a_0 + a_1 t_D + a_2^* t_D^2$

With these simplifying assumptions, the Laplace domain forms of the convolution integral were solved and inverted into real space to obtain closed-form expressions for pressure that is affected by wellbore storage distortions, $p_{wCD}(t_D)$.

The approximations were validated by applying them to different reservoir systems and comparing the results to the actual solutions both qualitatively, by visual inspection, and quantitatively, by computation of the error between the results. Of the three approximate solutions, the case which assumes that the constant rate $p_{sD}(t_D)$ is quadratic in time gives the most accurate. However, the linear case is very close to the quadratic in accuracy and consistency, and is significantly easier to implement, even on a spreadsheet application.

From the quantitative validation done on the approximate solutions, it was clear that further work could be done to improve them. In that light, two correlations were developed to reduce the errors in the approximate solutions, thereby increasing their accuracy. These correlations tried to improve the constant case by modeling the error and "adding" that error to the approximate solution. The correlations developed were:

- The normal distribution adjustment correlation.
- The modified normal distribution adjustment correlation.

Validation of these correlations was done in the manner as the analytical approximate solutions i.e. qualitatively and quantitatively. The normal distribution adjustment correlation accurately modeled the $p_{wCD}(t_D)$ function but failed to do the same for the derivative, $p_{wCD}'(t_D)$. The modified normal distribution adjustment correlation accurately modeled both the $p_{wCD}(t_D)$ and $p_{wCD}'(t_D)$ functions, achieving the aim of improving the approximate solutions. Also, both of these correlations are easy to implement in a direct computer solution or spreadsheet calculation.

For the special case of the wellbore storage problem, the total wellbore dimensionless pressure with distortion effects was derived such that the wellbore storage effect and wellbore phase redistribution effect were de-coupled. This means that explicit relations can be written for the total wellbore dimensionless pressure, $p_{wD}(t_D)$, which includes the effects of wellbore storage, skin and wellbore phase redistribution effects. Validation, similar to that done for the approximate solutions and correlations, was done on these explicit relations for $p_{wD}(t_D)$. The results show that these explicit expressions are accurate and compare very well with the numerical inversion solutions.

Finally, using the approximate solutions and correlations developed, attempts are made to derive the $p_{sD}(t_D)$ function from the $p_{wCD}(t_D)$. Two attempts were made using the linear $p_{sD}(t_D)$ approximate solution and the modified normal distribution adjustment correlation. While these deconvolution attempts ultimately proved unsuccessful, they give some insight into what might be done to produce a better outcome in the future.

6.2 Conclusions

- Three closed-form expressions were analytically developed for the computation of the dimensionless wellbore pressure with wellbore storage and skin effects, $p_{wCD}(t_D)$.
- These approximate solutions were validated for fractured and unfractured wells in homogeneous reservoirs and for unfractured wells in naturally fractured (dual porosity) reservoirs.
- The linear and quadratic $p_{sD}(t_D)$ approximate solutions show good accuracy and consistency and could be used for any of the well and reservoir scenarios for which they are validated, but the linear $p_{sD}(t_D)$ approximate solution is (much) easier to implement.
- Two correlations were developed for the improvement of the analytical approximate solutions.
- These solutions were validated for an unfractured well in an infinite-acting homogeneous reservoir.
- The normal distribution adjustment correlation showed good accuracy in modeling the $p_{wCD}(t_D)$ function, but this correlation did not yield accurate results for the $p_{wCD}'(t_D)$ function.
- The modified normal distribution adjustment correlation excellently modeled both the $p_{wCD}(t_D)$ and $p_{wCD}'(t_D)$ functions, and showed significantly better accuracy than the approximate solutions.
- The explicit relations developed for the computation of the dimensionless wellbore pressure which includes wellbore storage, skin effects, and the effect of wellbore phase redistribution ($p_{wD}(t_D)$) have been verified to be on the same order of accuracy as the Laplace transform numerical inversion solutions for this problem.
- Deconvolution using the linear $p_{sD}(t_D)$ approximate solution and the modified normal distribution adjustment correlation for an infinite-acting homogeneous reservoir were attempted, but ultimately these solutions are not viable in terms of accuracy or form, and are provided only as a "proof-of-concept" for the deconvolution of the $p_{wCD}(t_D)$ function.

6.3 Recommendations

- Develop and validate correlations that cover well and reservoir types other than the vertical well in an infinite-acting homogeneous reservoir.
- Develop an improved $p_{wCD}(t_D)$ correlation that provides accuracy, consistency in results and is of such simple formulation that it gives stable $p_{sD}(t_D)$ results in the "root-finding" deconvolution calculations.

REFERENCES

Agarwal, R.G., Al-Hussainy, R., and Ramey Jr, H. 1970. An Investigation of Wellbore Storage and Skin Effect in Unsteady Liquid Flow: I. Analytical Treatment. Society of Petroleum Engineers Journal 10 (03): 279-290. https://doi.org/10.2118/2466-PA

Blasingame, T.A. 1994. Development and Application of Concepts in Wellbore Storage Distortion, *Class Notes PETE 620*, College Station, TX, Texas A&M University. http://www.pe.tamu.edu/blasingame/data/z_zCourse_Archive/P620_15C/P620_15C_Lectures_(base)/P620_Lec_27_Mod4_ResFlw_08_WellboreStrg.pdf

Blasingame, T., Johnston, J., Lee, W. et al. 1991. Advances in the Use of Convolution Methods in Well Test Analysis. paper SPE 21826: 15-17.

Bourdet, D. and Gringarten, A.C. 1980. Determination of Fissure Volume and Block Size in Fractured Reservoirs by Type-Curve Analysis. In SPE Annual Technical Conference and Exhibition: Society of Petroleum Engineers.ISBN 1555636934. https://doi.org/10.2118/9293-MS

Economides, M. J., Hill, A. D., Ehlig-Economides, C., Zhu., D., 2013. *Petroleum Production Systems.* 2nd Edition. Chapter 1, pp. 1-18. Uper Saddle River, New Jersey, USA. Pearson Education, Inc.

Fair Jr, W.B. 1981. Pressure Buildup Analysis with Wellbore Phase Redistribution. Society of Petroleum Engineers Journal 21 (02): 259-270. http://dx.doi.org/10.2118/8206-PA

Gringarten, A.C., Bourdet, D.P., Landel, P.A. et al. 1979. A Comparison between Different Skin and Wellbore Storage Type-Curves for Early-Time Transient Analysis. In SPE Annual Technical Conference and Exhibition: Society of Petroleum Engineers. ISBN 155563706X. https://doi.org/10.2118/8205-MS

Joseph, J., Homoky, S., Davidson, R. et al. 1985. Automated Analysis of Pressure and Flow Data. In 2nd Annual Computer Technology Symposium, Texas Technical University, Lubbock, Texas.

Lee, J. Rollins, J.B., & Spivey, J.P., 2003. *Pressure Transient Testing*, Richardson, TX: Society of Petroleum Engineers.

McKinley, R. 1971. Wellbore Transmissibility from Afterflow-Dominated Pressure Buildup Data. Journal of Petroleum Technology 23 (07): 863-872. https://doi.org/10.2118/2416-PA

Ozkan, E. and Raghavan, R. 1988. Some New Solutions to Solve Problems in Well Test Analysis: Part 2-Computational Considerations and Applications. Society of Petroleum Engineers. SPE-18616.

Ramey Jr, H. 1965. Non-Darcy Flow and Wellbore Storage Effects in Pressure Build-up and Drawdown of Gas Wells. Journal of Petroleum Technology 17 (02): 223-233. https://doi.org/10.2118/1058-PA

Stegemeier, G. L., & Matthews, C. S., 1958. A Study of Anomalous Pressure Build-Up Behavior. *Petroleum Transactions,* AIME. **213** (1958): 44-50. SPE-927G. http://dx.doi.org/10.2118/SPE-927-G.

Stehfest, H. 1970. Algorithm 368: Numerical Inversion of Laplace Transforms [D5]. Communications of the ACM 13 (1): 47-49.

Valkó, P. P., and Abate, J. Comparison of sequence accelerators for the Gaver method of numerical Laplace transform inversion. Computers & Mathematics with Applications 48, no. 3 (2004): 629-636.

Van Everdingen, A. 1953. The Skin Effect and Its Influence on the Productive Capacity of a Well. Journal of Petroleum Technology 5 (06): 171-176. https://doi.org/10.2118/203-G

Van Everdingen, A. and Hurst, W. 1949. The Application of the Laplace Transformation to Flow Problems in Reservoirs. Journal of Petroleum Technology 1 (12): 305-324. https://doi.org/10.2118/949305-G

Warren, J. and Root, P.J. 1963. The Behavior of Naturally Fractured Reservoirs. Society of Petroleum Engineers Journal 3 (03): 245-255. https://doi.org/10.2118/426-PA

Wattenbarger, R.A. and Ramey Jr, H. 1970. An Investigation of Wellbore Storage and Skin Effect in Unsteady Liquid Flow: II. Finite Difference Treatment. Society of Petroleum Engineers Journal 10 (03): 291-297. https://doi.org/10.2118/2467-PA

Wiewiorowski, N.E., 2016. *Characterization of Early-Time Performance of a Well with a Vertical Fracture Producing at a Constant Pressure* (Master's thesis, Texas A&M University). http://hdl.handle.net/1969.1/158132

Wolfram Mathematica 10, 2007. https://www.wolfram.com/mathematica/

NOMENCLATURE

Dimensionless Variables

$C_{\alpha D}$ = Dimensionless "apparent" wellbore storage coefficient for wellbore phase redistribution model

C_D = Dimensionless wellbore storage coefficient

C_{LfD} = Dimensionless wellbore storage coefficient based on fracture half-length

$C_{\phi D}$ = Dimensionless coefficient for wellbore phase redistribution model

p_D = Dimensionless pressure

p_{sD} = Dimensionless pressure with skin effects

p_{wD} = Total dimensionless pressure with wellbore storage, skin and wellbore phase redistribution effects

p_{wCD} = Dimensionless pressure with wellbore storage and skin effects

$p_{w\phi D}$ = Dimensionless pressure with wellbore storage, skin and wellbore phase redistribution effects

$p_{\phi D}$ = Dimensionless pressure with wellbore phase redistribution effects

p_D' = Dimensionless pressure derivative function

q_{wCD} = Dimensionless sandface flowrate with wellbore storage and skin effects

$q_{w\phi D}$ = Dimensionless sandface flowrate with wellbore storage, skin and wellbore phase redistribution effects

S = Dimensionless skin factor

t_D = Dimensionless time based on wellbore radius

t_{LfD} = Dimensionless time based on fracture half-length

u = Laplace transformation variable

$\alpha_{\phi D}$ = Dimensionless parameter for wellbore phase redistribution model

Field Variables (Pressure Functions)

p_i = Initial reservoir pressure, psia

p_{wf} = Flowing bottomhole pressure, psia

p_{ws} = Shut-in bottomhole pressure, psia

Δp = Pressure drop, psi

Field Variables (Formation and Fluid Properties)

B = Formation volume factor, RB/STB

C = Wellbore storage coefficient, BBL/psi

c_t = Total compressibility, $psia^{-1}$

h = Total formation thickness, ft

k = Permeability, md

L_f = Fracture half-length, ft

p_i = Initial reservoir pressure, psia

p_{wf} = Flowing bottomhole pressure, psia

p_{ws} = Shut-in bottomhole pressure, psia

q = Flowrate, STB/D

r_w = Wellbore radius, ft

$\alpha_{\phi D}$ = Porosity, fraction

ϕ = Porosity, fraction

λ = Interporosity flow coefficient (natural fracture system parameter)

μ = Viscosity, cp

ω = Storativity ratio (natural fracture system parameter)

Dimensionless Correlation Variables

ARE = Absolute relative error, percent

α = Normal distribution scaling parameter

ε = Discrepancy parameter

m = Normal distribution mean parameter

σ = Normal distribution standard deviation parameter

c_t = Flowing bottomhole pressure, psia

APPENDIX A
DERIVATION OF LAPLACE TRANSFORM IDENTITIES FOR WELLBORE STORAGE DISTORTION

It has been shown that the constant rate bottomhole pressure affected by wellbore storage and skin effects can be written as a convolution integral given by

$$p_{wCD}(t_D) = \int_0^{t_D} \frac{d}{d\tau}\left[q_{wCD}(\tau)\right] p_{sD}(t_D - \tau)\, d\tau \,, \quad \text{(A.1)}$$

where

$$q_{wCD}(t_D) = 1 - C_D \frac{d}{dt_D}\left[p_{wCD}(t_D)\right] \quad \text{(A.2)}$$

and

$$p_{sD}(t_D) = p_D(t_D) + s \,. \quad \text{(A.3)}$$

Taking the Laplace transforms of Eqs. A.1 and A.2 gives

$$\bar{p}_{wCD}(u) = u\,\bar{q}_{wCD}(u)\,\bar{p}_{sD}(u) \quad \text{(A.4)}$$

and

$$\bar{q}_{wCD}(u) = \frac{1}{u} - C_D u\,\bar{p}_{wCD}(u) \quad \text{(A.5)}$$

Combining Eqs. A.4 and A.5 and solving for $p_{wCD}(u)$ gives

$$p_{wCD}(u) = \frac{1}{\left[\dfrac{1}{\bar{p}_{sD}(u)} + C_D u^2\right]} \,, \quad \text{(A.6)}$$

or alternatively

$$p_{wCD}(u) = \left[\frac{\bar{p}_{sD}(u)}{1 + C_D u^2 \bar{p}_{sD}(u)}\right]. \quad \text{(A.7)}$$

Eqs. A.6 and A.7 are mathematically equivalent. More importantly, they convenient simplifications when used with certain relations of $\bar{p}_{sD}(u)$. These relations will be discussed as they arise in the subsequent derivations.

APPENDIX B

DERIVATION OF APPROXIMATIONS FOR $p_{wCD}(t_D)$ BASED ON CONSTANT $p_{sD}(t_D)$

The assumption in this method is not that $p_{sD}(t_D)$ is constant for all t_D. It is that $p_{sD}(t_D)$ can be approximated as being constant near a particular time of interest. Proceeding along this theme

$$p_{sD}(t_D) = a \,. \quad \text{(B.1)}$$

Taking the Laplace transform of Eq. B.1 gives

$$\bar{p}_{sD}(u) = \frac{a}{u} \quad \text{(B.2)}$$

The Laplace transform identity for bottomhole pressure with wellbore storage and skin effects is given as

$$p_{wCD}(u) = \frac{1}{\left[\frac{1}{\bar{p}_{sD}(u)} + C_D u^2\right]} \quad \text{(B.3)}$$

Substituting Eq. B.2 into Eq. B.3 gives

$$\bar{p}_{wCD}(u) = \frac{1}{\left[\frac{u}{a} + C_D u^2\right]} \quad \text{(B.4)}$$

Factoring the denominator of Eq. B.4 and rearranging gives

$$\bar{p}_{wCD}(u) = \frac{1}{C_D} \frac{1}{u\left[u + \frac{1}{a C_D}\right]}$$

or

$$\bar{p}_{wCD}(u) = \frac{x}{u[u + y]} \quad \text{(B.5)}$$

where

$$x = \frac{1}{C_D} \quad \text{(B.6)}$$

and

$$y = \frac{1}{a\,C_D} \quad \text{(B.7)}$$

The inverse Laplace transform of Eq. B.5 is

$$p_{wCD}(t_D) = \frac{x}{y}\left[1 - \exp(-y t_D)\right] \quad \text{(B.8)}$$

Substituting Eqs. B.6 and B.7 into B.8, we obtain

$$p_{wCD}(t_D) = a\left[1 - \exp\left[\frac{-t_D}{a\,C_D}\right]\right] \quad \text{(B.9)}$$

Recall Eq. B.1

$$p_{sD}(t_D) = a \quad \text{(B.1)}$$

Combining Eqs. B.1 and B.9 gives

$$p_{wCD}(t_D) = p_{sD}(t_D)\left[1 - \exp\left[\frac{-t_D}{p_{sD}(t_D)\,C_D}\right]\right]. \quad \text{(B.10)}$$

We differentiate Eq. B.10 with respect to t_D. We have two options. First, we will "blindly" differentiate Eq. B.10 assuming that $p_{sD}(t_D)$ is constant. This gives

$$\frac{d}{dt_D}\left[p_{wCD}(t_D)\right] = \left[1 - \exp\left[\frac{-t_D}{p_{sD}(t_D)\,C_D}\right]\right] \quad \text{(B.11)}$$

Second, assuming

$$p_{sD}(t_D) = f(t_D),$$

we differentiate Eq. B.10. This gives

$$\frac{d}{dt_D}\left[p_{wCD}(t_D)\right] = \left[1 - \exp\left[\frac{-t_D}{p_{sD}(t_D)\,C_D}\right]\right]\frac{d}{dt_D}\left[p_{sD}(t_D)\right] + \frac{1}{p_{sD}(t_D)\,C_D}\left[p_{sD}(t_D) - t_D\frac{d}{dt_D}\left[p_{sD}(t_D)\right]\right]\exp\left[\frac{-t_D}{p_{sD}(t_D)\,C_D}\right] \quad \text{(B.12)}$$

Rearranging Eq. B.11 gives

$$\exp\left[\frac{-t_D}{p_{sD}(t_D)\,C_D}\right] = 1 - \frac{p_{wCD}(t_D)}{p_{sD}(t_D)}. \quad \text{(B.13)}$$

Combining Eqs. B.11 and B.13 gives

$$\frac{d}{dt_D}\left[p_{wCD}(t_D)\right]=\frac{1}{C_D}\left[1-\frac{p_{wCD}(t_D)}{p_{sD}(t_D)}\right] \quad \text{(B.14)}$$

Combining Eqs. B.10, B.12 and B.13 gives

$$\frac{d}{dt_D}\left[p_{wCD}(t_D)\right]=\frac{p_{wCD}(t_D)}{p_{sD}(t_D)}\frac{d}{dt_D}\left[p_{sD}(t_D)\right]+ \frac{1}{C_D}\left[1-\frac{t_D}{p_{sD}(t_D)}\frac{d}{dt_D}\left[p_{sD}(t_D)\right]\right]\left[1-\frac{p_{wCD}(t_D)}{p_{sD}(t_D)}\right] \quad \text{(B.15)}$$

The purpose of obtaining the derivative function is to generate plotting functions for type curve analysis and for use in the computation of dimensionless sandface flow rates, q_{wCD}, as given by

$$q_{wCD}(t_D)=1-C_D\frac{d}{dt_D}\left[p_{wCD}(t_D)\right] \quad \text{(B.16)}$$

Combining Eqs. B.10 and B.16 gives

$$q_{wCD}(t_D)=1-\exp\left[\frac{-t_D}{p_{sD}(t_D)C_D}\right], \quad \text{(B.17)}$$

which is of the form

$$q_{wCD}(t_D)=1-\exp\left[-\beta_{vED}\,t_D\right] \quad \text{(B.18)}$$

where

$$\beta_{vED}=\frac{1}{p_{sD}(t_D)C_D} \quad \text{(B.19)}$$

Eq. B.17 was proposed originally by van Everdingen, and used by Ramey for well test analysis. van Everdingen proposed Eq. B.17 based on empirical observations of field data. In this work, however, Eq. B.17 is proposed based on analytical considerations. The significance of the derivation done here is not that it proves van Everdingen's observations, rather it shows that the form of Eq. B.17 can be developed rigorously. The applicability of Eq. B.17 must be determined via comparison of Eqs. B.16 and B.18 using simulated data.

Similar results for q_{wCD} could be obtained by combining Eqs. B.16 and B.12 (or B.15). However, for the purposes of the present discussion, we only wished to verify the van Everdingen model for q_{wCD}.

APPENDIX C

DERIVATION OF APPROXIMATIONS FOR $p_{wCD}(t_D)$ BASED ON LINEAR $p_{sD}(t_D)$

The assumption in this method is not that $p_{sD}(t_D)$ is linear for all t_D. It is that $p_{sD}(t_D)$ can be approximated as being linear near a particular time of interest. Proceeding along this theme,

$$p_{sD}(t_D) = a + bt_D \quad \text{(C.1)}$$

Taking the Laplace transform of Eq. C.1 gives

$$\bar{p}_{sD}(u) = \frac{a}{u} + \frac{b}{u^2} \quad \text{(C.2)}$$

The Laplace transform identity for bottomhole pressure with wellbore storage and skin effects is given as

$$p_{wCD}(u) = \left[\frac{\bar{p}_{sD}(u)}{1 + C_D u^2 \bar{p}_{sD}(u)}\right] \quad \text{(C.3)}$$

Substituting Eq. C.2 into Eq. C.3 gives

$$\bar{p}_{wCD}(u) = \frac{\left[\frac{a}{u} + \frac{b}{u^2}\right]}{1 + C_D u^2 \left[\frac{a}{u} + \frac{b}{u^2}\right]} \quad \text{(C.4)}$$

Expanding and simplifying gives

$$\bar{p}_{wCD}(u) = \frac{a}{u + C_D a u^2 + C_D b u} + \frac{b}{u^2 + C_D a u^3 + C_D b u^2}$$

$$\bar{p}_{wCD}(u) = \frac{a}{u(C_D a u + 1 + C_D b)} + \frac{b}{u^2 (C_D a u + 1 + C_D b u)}$$

$$\bar{p}_{wCD}(u) = \frac{1}{C_D} \frac{1}{u\left[u + \frac{1 + C_D b}{C_D a}\right]} + \frac{b}{a C_D} \frac{1}{u^2 \left[u + \frac{1 + C_D b}{C_D a}\right]}$$

$$\bar{p}_{wCD}(u) = y \frac{1}{u[u + x]} + z \frac{1}{u^2 [u + x]} \quad \text{(C.5)}$$

where

$$x = \frac{1 + C_D b}{C_D a}, \quad \text{(C.6)}$$

$$y = \frac{1}{C_D}, \quad \text{(C.7)}$$

$$z = \frac{b}{a C_D}. \quad \text{(C.8)}$$

The inverse Laplace transform of Eq. C.5 is

$$p_{wCD}(t_D) = \frac{y}{x}\left[1 - \exp(-xt_D)\right] + \frac{z}{x^2}\left[\exp(-xt_D) + xt_D - 1\right] \quad \text{(C.9)}$$

For convenience, we leave our result in the form given by Eq. C.9. Now we must consider a scheme to determine the coefficients *a* and *b* in the $p_{sD}(t_D)$ model. Recall Eq. C.1

$$p_{sD}(t_D) = a + bt_D \quad \text{(C.1)}$$

Differentiating Eq. C.1 with respect to t_D gives

$$\frac{d}{dt_D}\left[p_{sD}(t_D)\right] = b \quad \text{(C.10)}$$

Combining Eqs. C.1 and C.10 and solving for the *a* coefficient gives

$$a = p_{sD}(t_D) - t_D \frac{d}{dt_D}\left[p_{sD}(t_D)\right] \quad \text{(C.11)}$$

In conclusion, we have developed Eq. C.9 based on the assumption of $p_{sD}(t_D)$ behaving in a linear fashion, at least locally. Although a closed form derivative of Eq. 40 could be developed, this expression is so complex (recall *x*, *y* and *z* are functions of time) that numerical differentiation would be more efficient.

APPENDIX D

DERIVATION OF APPROXIMATIONS FOR $p_{wCD}(t_D)$ BASED ON QUADRATIC $p_{sD}(t_D)$

The assumption in this method is not that $p_{sD}(t_D)$ is quadratic for all t_D. It is that $p_{sD}(t_D)$ can be approximated as being quadratic near a particular time of interest. Proceeding along this theme,

Starting with the quadratic model

$$p_{sD}(t_D) = a_0 + a_1 t_D + a_2^* {t_D}^2 \quad \text{(D.1)}$$

Taking the Laplace transform of Eq. D.1 gives

$$\bar{p}_{sD}(u) = \frac{a_0}{u} + \frac{a_1}{u^2} + \frac{2a_2^*}{u^3}, \quad \text{(D.2)}$$

which can be expressed as

$$\bar{p}_{sD}(u) = \frac{a_0}{u} + \frac{a_1}{u^2} + \frac{2a_2}{u^3}, \quad \text{(D.3)}$$

where

$$a_2 = 2a_2^* \quad \text{(D.4)}$$

The Laplace transform identity for bottomhole pressure with wellbore storage and skin effects is given as

$$p_{wCD}(u) = \frac{\bar{p}_{sD}(u)}{\left[1 + C_D u^2 \bar{p}_{sD}(u)\right]} \quad \text{(D.5)}$$

Substituting Eq. D.3 into Eq. D.5 gives

$$\bar{p}_{wCD}(u) = \frac{\left[\frac{a_0}{u} + \frac{a_1}{u^2} + \frac{a_2}{u^3}\right]}{1 + C_D u^2 \left[\frac{a_0}{u} + \frac{a_1}{u^2} + \frac{a_2}{u^3}\right]}. \quad \text{(D.6)}$$

Rearranging Eq. D.6 gives

$$\bar{p}_{wCD}(u) = \frac{c_0}{\left[u^2 + xu + y\right]} + \frac{c_0}{u\left[u^2 + xu + y\right]} + \frac{c_0}{u^2\left[u^2 + xu + y\right]}, \quad \text{(D.7)}$$

where

$$c_0 = a_0 / b_1$$

$$c_1 = a_1 / b_1$$

$$c_2 = a_2 / b_1$$

$$b_0 = 1 + C_D a_1$$

$$b_1 = C_D a_0$$

$$b_2 = 1 + C_D a_2$$

and

$$x = b_0 / b_1$$

$$y = b_2 / b_1$$

For the purpose of mathematical convenience, the terms *v* and *w* are defined as

$$v = \sqrt{\frac{x^2}{4} - y}$$

$$w = x / 2 .$$

And finally,

$$A = \frac{1}{2v}$$

$$B = w - v$$

$$C = w + v$$

Taking the inverse Laplace transform of Eq. D.7 gives

$$p_{wCD}(t_D) = c_0 f_0(t_D) + c_1 f_1(t_D) + c_2 f_2(t_D) \quad \text{(D.8)}$$

where

$$f_0(t_D) = A[\exp(-Bt_D) -]\exp(-Ct_D) \quad \text{(D.9)}$$

$$f_1(t_D) = A\left[\frac{1}{B}[1 - \exp(-Bt_D)] - \frac{1}{C}1 - \exp(-Ct_D)\right] \quad \text{(D.10)}$$

$$f_2(t_D) = A\left[\left[\frac{1}{B} - \frac{1}{C}\right]t_D - \left[\frac{1}{B^2} - \frac{1}{C^2}\right] + \frac{1}{B^2}\exp(-Bt_D) - \frac{1}{C^2}\exp(-Ct_D)\right] \quad \text{(D.11)}$$

Although Eq. D.8 is a bit tedious for hand calculations, it should be relatively easy to program into a calculator or spreadsheet application software package. We are, however, left with the problem of determining the coefficients of Eq. D.8. We recommend the use of a quadratic collocation polynomial over a 3-point grid. The computational procedure is initiated by calculating the collocation coefficients. For a 3-point grid, collocation coefficients are

$$y_0 = p_{sD}(t_{D0})$$

$$y_1 = \frac{p_{sD}(t_{D1}) - p_{sD}(t_{D0})}{t_{D1} - t_{D0}}$$

$$y_2 = \frac{p_{sD}(t_{D2}) - y_0 - y_1(t_{D2} - t_{D0})}{2(t_{D2} - t_{D0})(t_{D2} - t_{D1})}$$

And the *a* coefficients are

$$a_0 = y_0 - y_1 t_{D0} + y_2 t_{D0} t_{D1}$$

$$a_1 = y_1 - y_2(t_{D0} + t_{D1})$$

$$a_2^* = y_2$$

APPENDIX E

DERIVATION OF EXPLICIT FORMULAE FOR THE COMPUTATION OF WELLBORE PHASE REDISTRIBUTION EFFECTS

The purpose of this derivation is to provide explicit means to compute wellbore phase redistribution effects. Previously, the effects have only been computed using Laplace space solutions. This appendix provides a rigorous derivation of convolution identities which use the dimensionless wellbore storage pressure, $p_{wCD}(t_D)$ and the dimensionless phase redistribution pressure, $p_{\phi D}(t_D)$.

The dimensionless sandface flow rate, $q_{w\phi D}(t_D)$ for this case is given by Fair (1981) as

$$q_{w\phi D}(t_D) = 1 - C_D \left[\frac{d}{dt_D}\left[p_{wCD}(t_D)\right] - \frac{d}{dt_D}\left[p_{\phi D}(t_D)\right] \right] \quad \text{.....(E.1)}$$

The convolution integral for this case is

$$p_{wD}(t_D) = \int_0^{t_D} \frac{d}{dt_D}\left[q_{w\phi D}(\tau)\right] p_{sD}(t_D - \tau)\, d\tau \ . \quad \text{.....(E.2)}$$

The Laplace transform of Eq. E.1 is

$$\bar{p}_{wD}(u) = u\, \bar{q}_{w\phi D}(u)\, \bar{p}_{sD}(u) \ . \quad \text{.....(E.3)}$$

Taking the Laplace transform of Eq. E.2, we have

$$\bar{q}_{w\phi D}(u) = \frac{1}{u} - uC_D\left[\bar{p}_{sD}(u) - \bar{p}_{\phi D}(u)\right]. \quad \text{.....(E.4)}$$

Rearranging Eq. E.3 gives

$$\frac{\bar{p}_{wD}(u)}{\bar{p}_{sD}(u)} = u\, \bar{q}_{w\phi D}(u) \quad \text{.....(E.5)}$$

Rearranging Eq. E.4 gives

$$u\, \bar{q}_{w\phi D}(u) = 1 - u^2 C_D\left[\bar{p}_{wD}(u) - \bar{p}_{\phi wD}(u)\right] \quad \text{.....(E.6)}$$

Equating Eqs. E.5 and E.6 gives

$$\frac{\bar{p}_{wD}(u)}{\bar{p}_{sD}(u)} = 1 - u^2 C_D\left[\bar{p}_{wD}(u) - \bar{p}_{\phi wD}(u)\right] \quad \text{.....(E.7)}$$

Rearranging

$$\bar{p}_{wD}(u) = \frac{1}{\left[\frac{1}{\bar{p}_{sD}(u)} + u^2 C_D\right]} + u^2 C_D \bar{p}_{\phi D}(u)\left[\frac{1}{\bar{p}_{sD}(u)} + u^2 C_D\right] \quad \text{.....(E.8)}$$

or

$$\bar{p}_{wD}(u) = \bar{p}_{wCD}(u) + u^2 C_D \bar{p}_{\phi D}(u)\, \bar{p}_{wCD}(u) \quad \text{.....(E.9)}$$

where

$$\bar{p}_{wCD}(u) = \left[\frac{1}{\bar{p}_{sD}(u)} + u^2 C_D\right] \quad \text{.....(E.10)}$$

We recognize that Eq. E.10 is the relation for wellbore storage that was derived in Appendix A.

Eq. E.9 can be rewritten as

$$\bar{p}_{wD}(u) = \bar{p}_{wCD}(u) + \bar{p}_{w\phi D}(u) \quad \text{.....(E.11)}$$

where

$$\bar{p}_{w\phi D}(t_D) = u^2 C_D \bar{p}_{\phi D}(u)\, \bar{p}_{wCD}(u) \quad \text{.....(E.12)}$$

The inverse Laplace transform of Eq. E.11 is given as

$$p_{wD}(t_D) = p_{wCD}(t_D) + p_{w\phi D}(t_D) \quad \text{.....(E.13)}$$

E.13 suggests that we can express the effect of distortion due to wellbore phase redistribution as a component term added to the existing wellbore storage solution. The application of this method will depend on our ability to obtain the inverse Laplace transform of Eq. E.12.

Taking the inverse Laplace transform, we obtain the following using the convolution identity

$$p_{w\phi D}(t_D) = C_D \int_0^{t_D} \frac{d^2}{d\tau^2}\left[p_{\phi D}(\tau)\right] p_{wCD}(t_D - \tau)\, d\tau\,, \quad \text{.....(E.14)}$$

or alternatively

$$p_{w\phi D}(t_D) = C_D \int_0^{t_D} \frac{d^2}{d\tau^2}\left[p_{wCD}(\tau)\right] p_{\phi D}(t_D - \tau)\, d\tau \quad \text{.....(E.15)}$$

Recalling that the convolution integral for wellbore storage is given as

$$p_{wCD}(t_D) = C_D \int_0^{t_D} \frac{d}{d\tau}\left[q_{wCD}(\tau)\right] p_{sD}(t_D - \tau)\, d\tau \quad \text{.....(E.16)}$$

van Everdingen and Hurst (1949) give the discretized form of Eq. E.16 as

$$p_{wCD}(t_D) = C_D \sum_{i=1}^{n} \left[q_{wCD}(t_{D,i}) - q_{wCD}(t_{D,i-1})\right] p_{sD}(t_D - t_{D,i-1}) \quad \text{.....(E.17)}$$

By analogy of Eqs. E.14, E.15, E.16and E.17, we obtain

$$p_{w\phi D}(t_D) = C_D \sum_{i=1}^{n} \left[\frac{d}{dt_D}\left[p_{\phi D}(t_{D,i})\right] - \frac{d}{dt_D}\left[p_{\phi D}(t_{D,i-1})\right] \right] p_{wCD}(t_D - t_{D,i-1}) \quad \text{.....(E.18)}$$

and

$$p_{w\phi D}(t_D) = C_D \sum_{i=1}^{n} \left[\frac{d}{dt_D}\left[p_{wCD}(t_{D,i})\right] - \frac{d}{dt_D}\left[p_{wCD}(t_{D,i-1})\right] \right] p_{\phi D}(t_D - t_{D,i-1}) \quad \text{.....(E.19)}$$

We note that Eqs. E.18 and E.19 are general in nature and only require knowledge of the dimensionless wellbore storage coefficient, C_D, the dimensionless wellbore storage pressure, $p_{wCD}(t_D)$, and the dimensionless phase redistribution pressure, $p_{\phi D}(t_D)$.

Citing physical observations, Fair (1981) proposed the following model for the dimensionless phase redistribution pressure, $p_{\phi D}(t_D)$.

$$p_{\phi D}(t_D) = C_{\phi D}\left[1 - \exp\left(\frac{-t}{\alpha_{\phi D}}\right)\right] \quad \text{.....(E.20)}$$

Taking the first derivative of Eq. E.20 with respect to t_D we obtain

$$\frac{d}{dt_D}\left[p_{\phi D}(t_{D,i})\right] = \frac{C_{\phi D}}{\alpha_{\phi D}} \exp\left(\frac{-t}{\alpha_{\phi D}}\right) \quad \text{.....(E.21)}$$

In practice, the $\alpha_{\phi D}$ parameter is rarely used. More commonly, the "apparent" wellbore storage coefficient, $C_{\alpha D}$, is specified. The relationship of $\alpha_{\phi D}$ and the variables C_D, $C_{\alpha D}$ and $C_{\phi D}$, is

$$\alpha_{\phi D} = \frac{C_{\phi D}}{\left(\frac{1}{C_{\alpha D}} - \frac{1}{C_D}\right)} \quad \text{.....(E.22)}$$

Our computations suggest that, when using the model of $p_{\phi D}(t_D)$ given by Eq. E.20, Eq. E.19 and E.20 will yield the most accurate results for $p_{w\phi D}(t_D)$ relative to the numerical inversion of Eq. E.12, as opposed to using Eqs. E.18 and E.21. However, further investigation is recommended.

APPENDIX F

DERIVATION OF DECONVOLUTION APPROXIMATION FOR $p_{sD}(t_D)$ BASED ON $p_{wCD}(t_D)$ DERIVED USING THE CONSTANT $p_{sD}(t_D)$ ASSUMPTION

It has been shown that the constant rate bottomhole pressure affected by wellbore storage and skin effects can be written as a convolution integral given by

$$p_{wCD}(t_D) = \int_0^{t_D} \frac{d}{d\tau}\left[q_{wCD}(\tau)\right] p_{sD}(t_D - \tau)\, d\tau \,, \quad \text{(F.1)}$$

where

$$q_{wCD}(t_D) = 1 - C_D \frac{d}{dt_D}\left[p_{wCD}(t_D)\right], \quad \text{(F.2)}$$

and

$$p_{sD}(t_D) = p_D(t_D) + s\,. \quad \text{(F.3)}$$

Eq. F.1 can be approximated as

$$p_{wCD}(t_D) = p_{sD}(t_D)\left[1 - \exp\left[\frac{-t_D}{p_{sD}(t_D)\, C_D}\right]\right], \quad \text{(F.4)}$$

where $p_{sD}(t_D)$ is the constant rate bottom hole pressure with only skin effects.

A comparison of $p_{wCD}(t_D)$ values obtained using Eqs. F.1 and F.4 shows a difference, $\Delta p_D(t_D)$, between them. Actual $p_{wCD}(t_D)$ can therefore be modeled as

$$p_{wCD}(t_D) = p_{sD}(t_D)\left[1 - \exp\left[\frac{-t_D}{p_{sD}(t_D)\, C_D}\right]\right] - \Delta p_D(t_D) \quad \text{(F.5)}$$

where $p_{wCD}(t_D)$ is obtained by convolution and the numerical inversion of the cylindrical source solution and $\Delta p_D(t_D)$ is the difference between the actual and approximate $p_{wCD}(t_D)$.

Eq. F.5 can also be rewritten as

$$p_{wCD}(t_D) = p_{sD}(t_D)\left[\left[1 - \exp\left[\frac{-t_D}{p_{sD}\, C_D}\right]\right] - \varepsilon\left[\frac{t_D}{p_{sD}\, C_D}\right]\right], \quad \text{(F.6)}$$

where

$$\Delta p_D(t_D) = p_{sD}(t_D)\left[\varepsilon\left[\frac{t_D}{p_{sD}C_D}\right]\right] \quad \text{.....(F.7)}$$

Rearranging Eq. F.6, we obtain

$$\varepsilon\left[\frac{t_D}{p_{sD}C_D}\right] = \left[1-\exp\left[\frac{-t_D}{p_{sD}C_D}\right]\right] - \frac{p_{wCD}(t_D)}{p_{sD}(t_D)} \quad \text{.....(F.8)}$$

A semilog plot of $\varepsilon[t_D/(p_{sD}\,C_D)]$ vs. $t_D/(p_{sD}\,C_D)$ for C_De^{2s} values of 10^1, 10^2, 10^3, 10^4 and 10^{10} is shown in **Figure F.1**. All other values of C_De^{2s} show a similar shape. This plot suggests that $\varepsilon[t_D/(p_{sD}\,C_D)]$ is either normally distributed (Gaussian distribution) or distributed in a fashion that is similar in shape to the normal distribution. This implies that a mathematical equation describing the normal distribution or one that describes a shape such as this could accurately model $\varepsilon[t_D/(p_{sD}\,C_D)]$. There are several equations of varying mathematical complexity that could describe a function shaped like this.

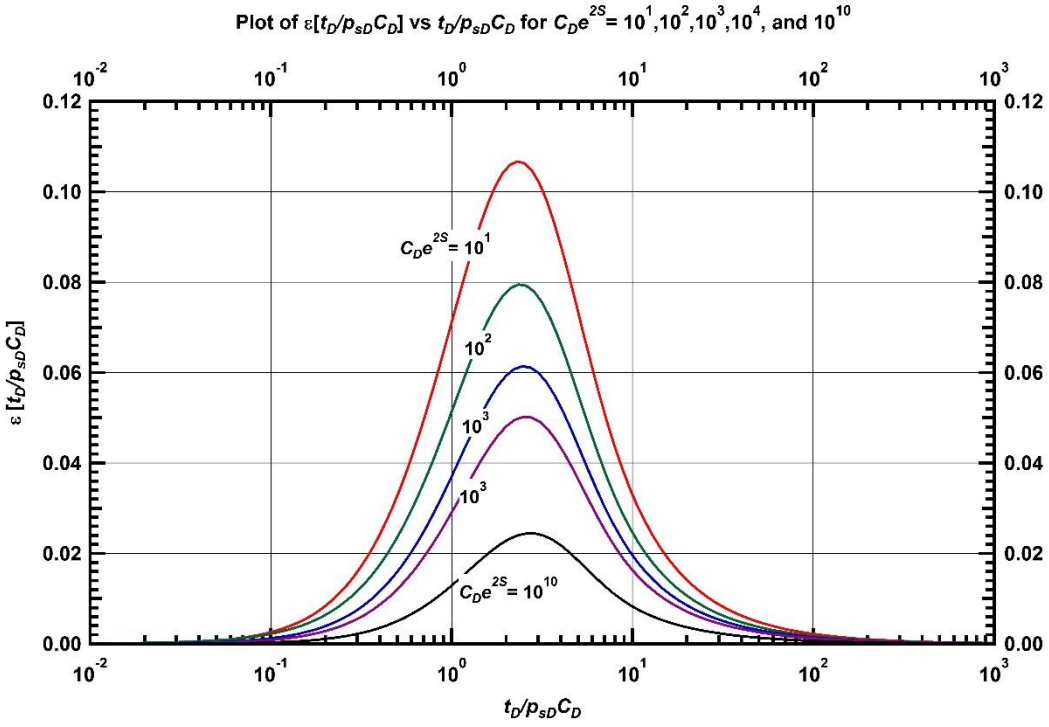

Figure F.1 — Plot showing ε vs. $t_D/(p_{sD}\,C_D)$for C_De^{2s} values of 10^1, 10^2, 10^3, 10^4 and 10^{10}

F.1 Deconvolution with Normal Distribution adjustment

The normal distribution is given by Abramowitz and Stegun (1972) as

$$p = \frac{\alpha}{\sigma\sqrt{2\pi}} \exp\left[-\frac{1}{2}\left[\frac{x-m}{\sigma} \right]^2 \right] . \quad \text{.....(F.9)}$$

Where p is the probability distribution function, α is a scaling factor, m is the mean of the distribution, σ is the variance of the distribution and x is value of the data point.

In our case, the normal distribution equation describing $\varepsilon[t_D/(p_{sD}\, C_D)]$ would be

$$\varepsilon\left[\frac{t_D}{p_{sD} C_D} \right] = \frac{\alpha}{\sigma\sqrt{2\pi}} e^{-\frac{1}{2}\left[\frac{\ln\left[\frac{t_D}{p_{sD} C_D} \right] - m}{\sigma} \right]^2} , \quad \text{.....(F.10)}$$

where the values of α, m, and, σ vary based on C_D.

An improved approximation of $p_{wCD}(t_D)$ obtained from combining Eqs. F.6 and F.10 can, therefore, be written as

$$p_{wCD}(t_D) = p_{sD}(t_D)\left[\left[1 - \exp\left[\frac{-t_D}{p_{sD} C_D} \right] \right] - \frac{\alpha}{\sigma\sqrt{2\pi}} e^{-\frac{1}{2}\left[\frac{\ln\left[\frac{t_D}{p_{sD} C_D} \right] - m}{\sigma} \right]^2} \right] \quad \text{.....(F.11)}$$

While the choice of the normal distribution equation is based on the shape of $\varepsilon[t_D/(p_{sD}\, C_D)]$, the parameters of the normal distribution equation that provide a good fit for a particular value of C_D are determined by

- A good visual match of a plot that compares $\varepsilon[t_D/(p_{sD}\, C_D)]$ obtained from Eq. F.8 and $\varepsilon[t_D/(p_{sD}\, C_D)]$ obtained from the normal distribution equation (Eq. F.10), and
- An acceptable level of error between $\varepsilon[t_D/(p_{sD}\, C_D)]$ obtained from Eq. F.8 and $\varepsilon[t_D/(p_{sD}\, C_D)]$ obtained from the normal distribution equation (Eq. F.10).

For the determination of error, we introduce the term Absolute Relative Error (*ARE*), in percent, which is the absolute value of the difference between $p_{wCD}(t_D)$ obtained from solving Eq. F.1 using numerical methods and $p_{wCD}(t_D)$ obtained using Eq. F.6. It is given as,

$$ARE = \frac{\left| p_{wCD_{Actual}} - p_{wCD_{Approximate}} \right|}{p_{wCD_{Actual}}} \times 100 \quad \text{.....(F.12)}$$

An acceptable level of error would be one with an $ARE \leq 1.5\%$.

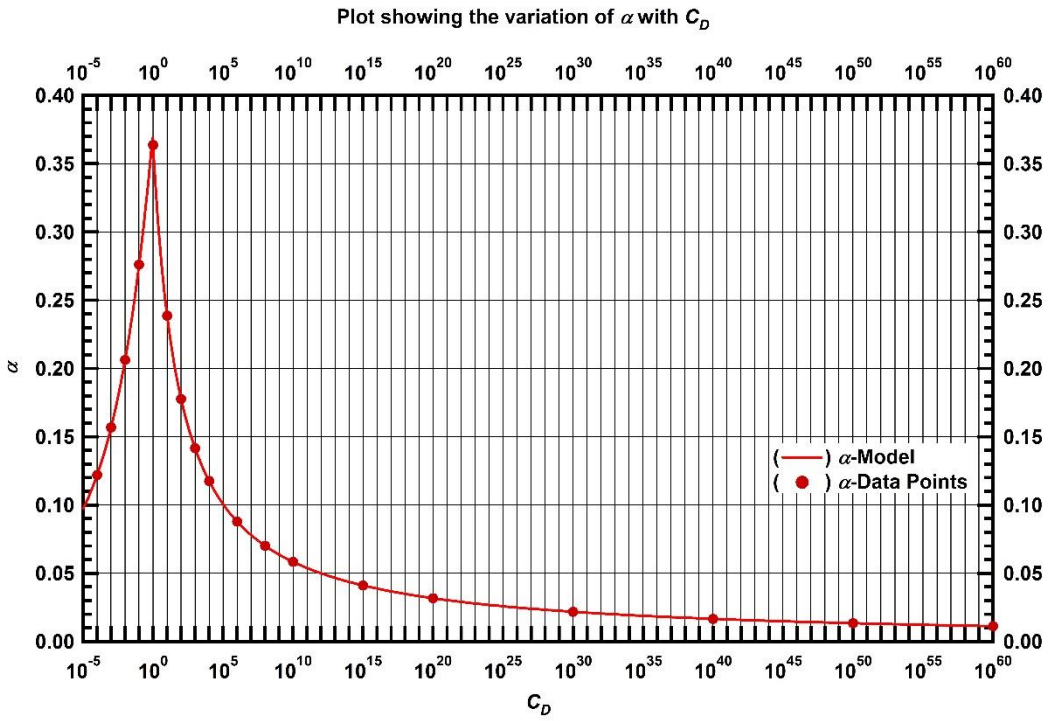

Figure F.2 — Plot showing the variation of α with C_D.

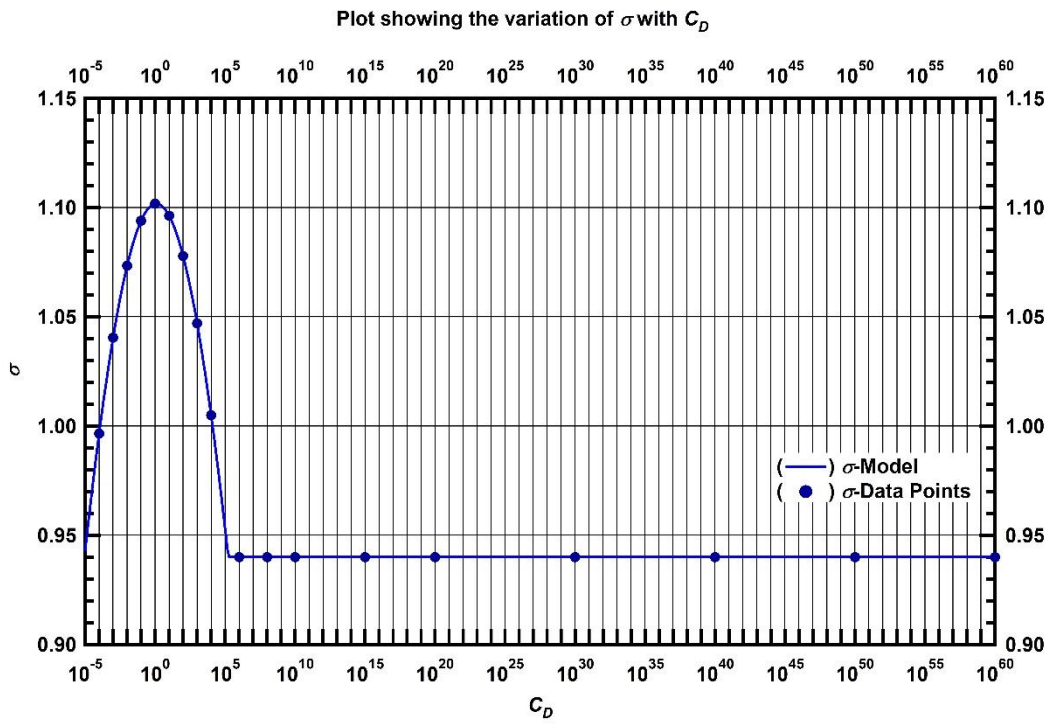

Figure F.3 — Plot showing the variation of m with C_D.

Figures F.4 – F.11 show match plots and *ARE* plots for selected values of $C_D e^{2s}$. These plots show good fits and acceptable *ARE*. By this process of matching and error determination, relationships between the parameters α, m, and, σ and C_D, were determined empirically to be given as

$$\alpha = \frac{26}{77.1579}\exp\left[-\frac{\left|1.43087\ln C_D + 1\right|}{9.50843}\right] + 0.03772, \text{for } C_D < 1, \quad \text{(F.13a)}$$

$$\alpha = \frac{1.6}{\ln C_D + 4.4}, \quad \text{(F.13b)}$$

$$m = 0.90, \text{for } C_D < 10^3, \quad \text{(F.14a)}$$

$$m = 1.00, \text{for } C_D \geq 10^3, \quad \text{(F.14b)}$$

$$\sigma = \frac{58}{21\sqrt{2\pi}} e^{-\frac{1}{2}\left[\frac{\ln C_D - 1}{21}\right]^2}, \text{for } C_D < 10^6, \quad \text{(F.15a)}$$

$$\sigma = 0.94, \text{for } C_D \geq 10^6 \quad \text{(F.15b)}$$

Table F.1 shows the empirical values of α, m, and, σ for various values of C_D.

Table F.1— Empirical values of α, m, and, σ for various values of C_D.

C_D	a	m	s
10^{-4}	0.1200	0.90	1.000
10^{-3}	0.1550	0.90	1.020
10^{-2}	0.2020	0.90	1.075
10^{-1}	0.2800	0.90	1.095
10^{0}	0.3680	0.90	1.100
10^{1}	0.2700	0.90	1.100
10^{2}	0.2000	0.90	1.090
10^{3}	0.1560	1.00	1.040
10^{4}	0.1270	1.00	1.020
10^{6}	0.0900	1.00	0.940
10^{8}	0.0685	1.00	0.940
10^{10}	0.0570	1.00	0.940
10^{15}	0.0401	1.00	0.940
10^{20}	0.0310	1.00	0.940
10^{30}	0.0215	1.00	0.940
10^{40}	0.0165	1.00	0.940
10^{50}	0.0133	1.00	0.940
10^{60}	0.0112	1.00	0.940

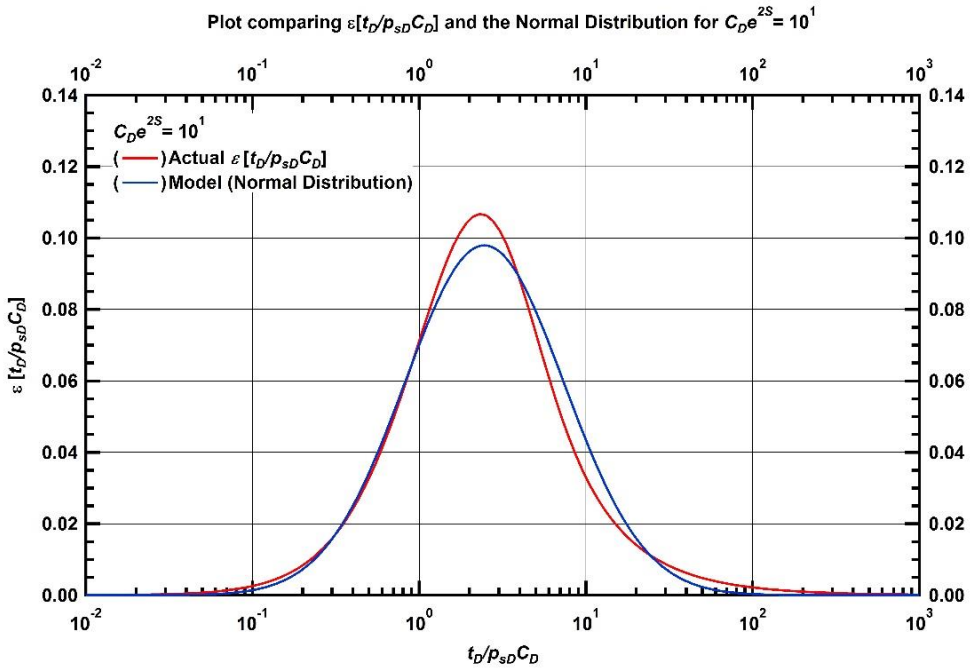

Figure F.4 — Plot comparing $\varepsilon[t_D/(p_{sD}\, C_D)]$ and the Normal Distribution for $C_De^{2s} = 10^1$.

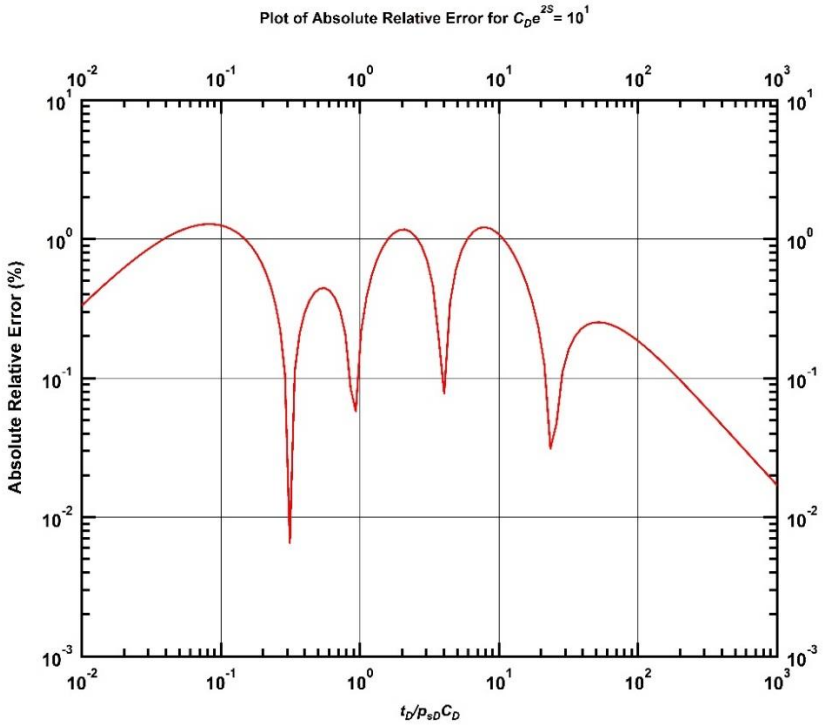

Figure F.5 — Absolute Relative Error Plot for $C_De^{2s} = 10^1$.

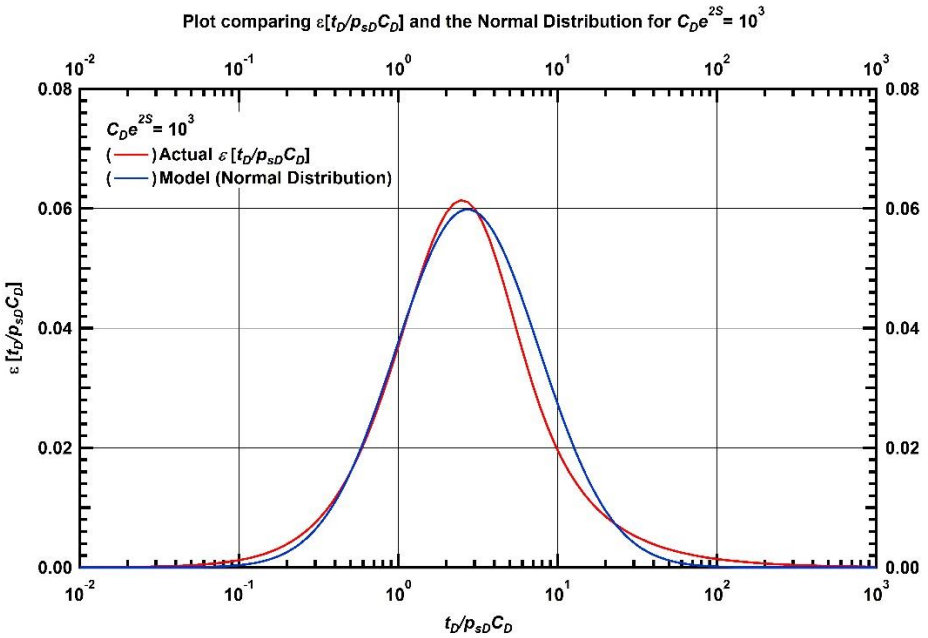

Figure F.6 — Plot comparing $\varepsilon[t_D/(p_{sD}\, C_D)]$ and the Normal Distribution for $C_De^{2s} = 10^3$.

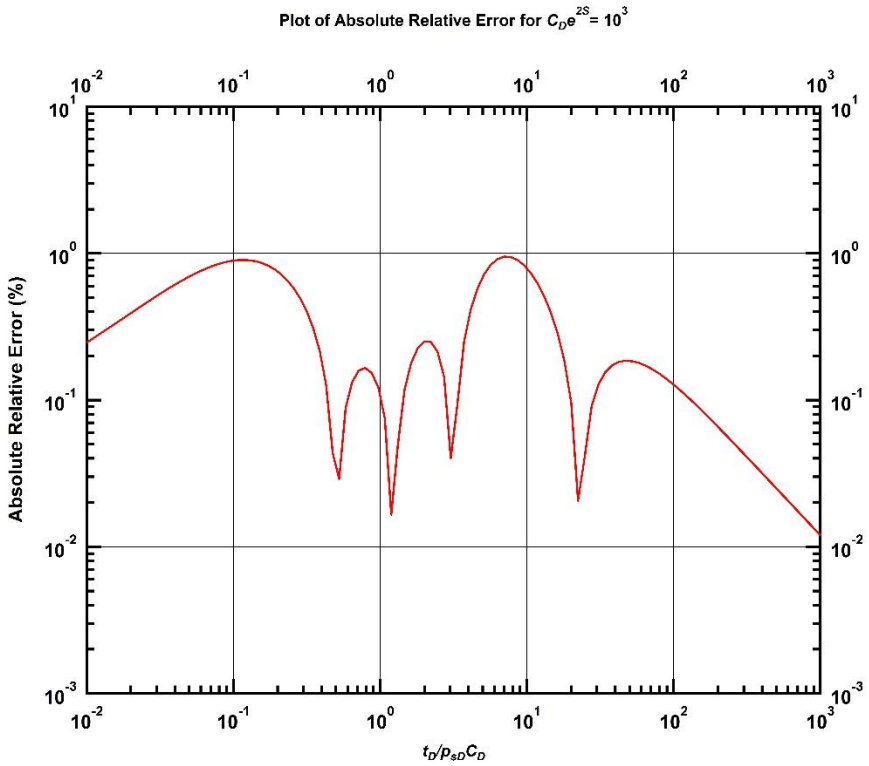

Figure F.7 — Absolute Relative Error Plot for $C_De^{2s} = 10^3$.

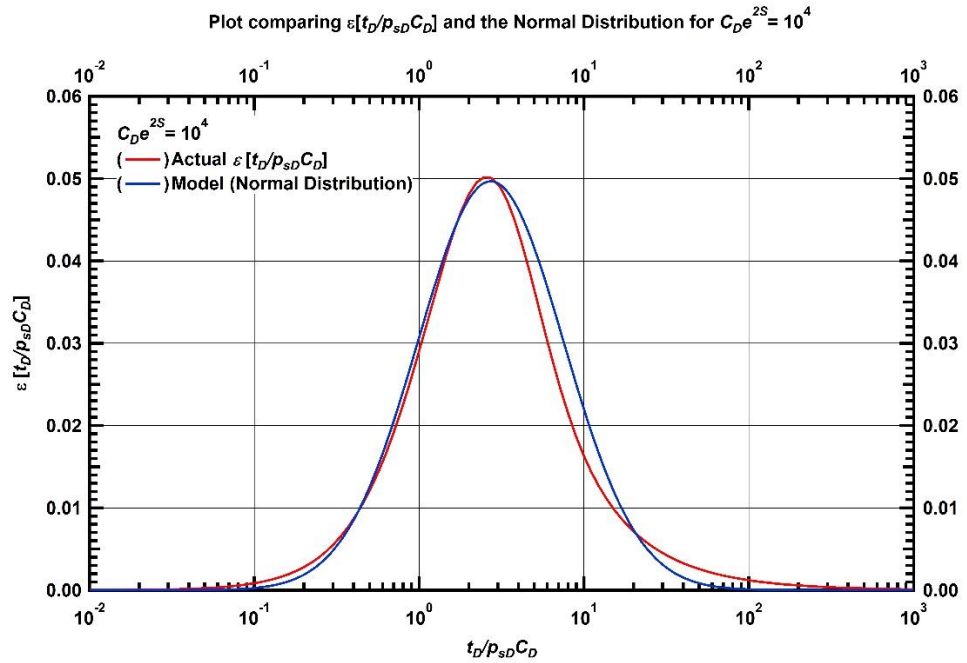

Figure F.8 — Plot comparing $\varepsilon[t_D/(p_{sD}\,C_D)]$ and the Normal Distribution for $C_De^{2s} = 10^4$.

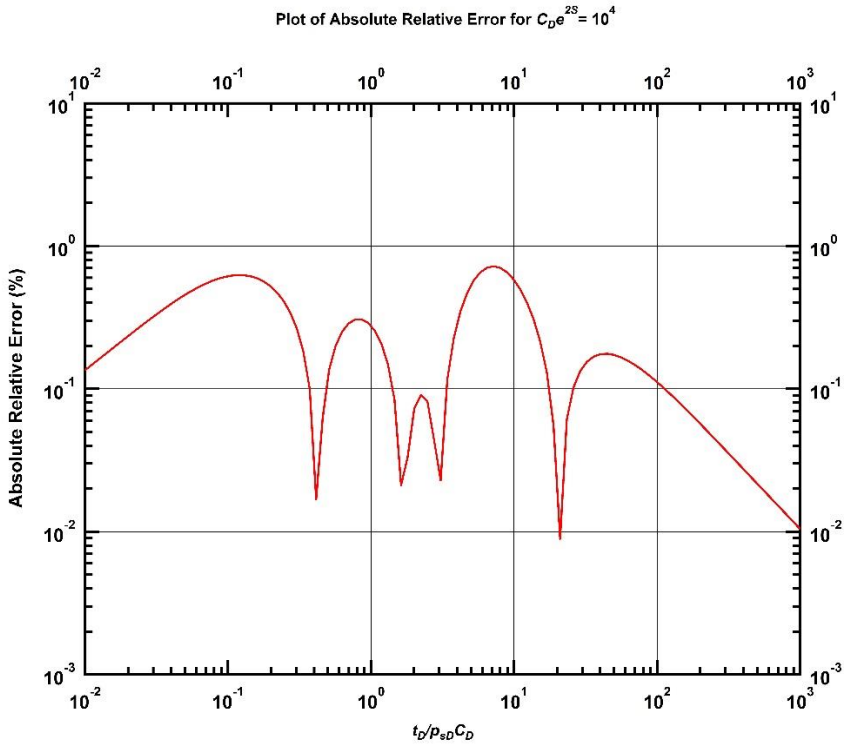

Figure F.9 — Absolute Relative Error Plot for $C_De^{2s} = 10^4$.

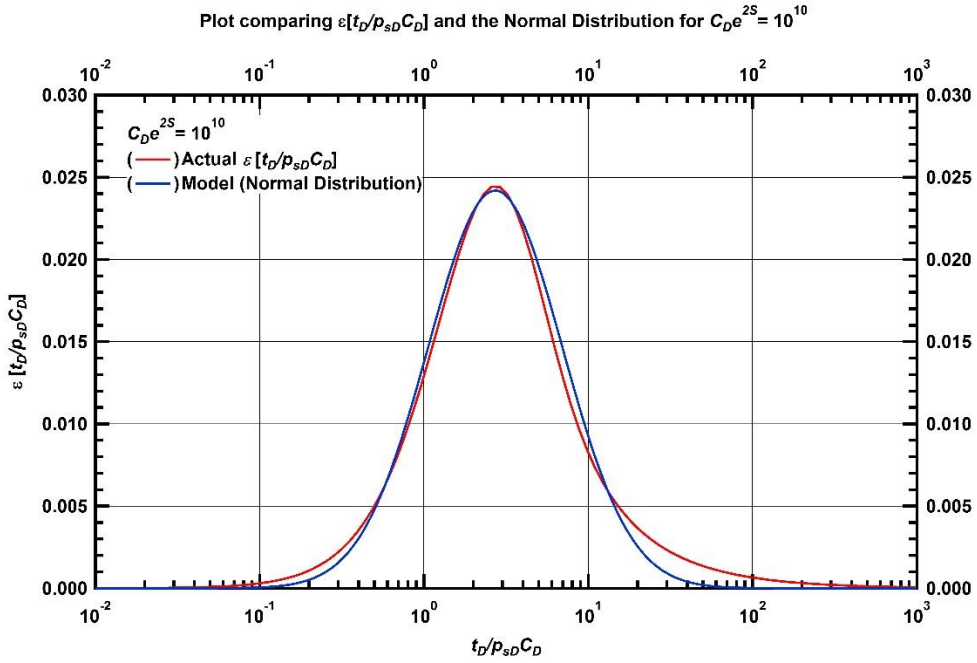

Figure F.10 — Plot comparing $\varepsilon[t_D/(p_{sD}\,C_D)]$ and the Normal Distribution for $C_De^{2s} = 10^{10}$.

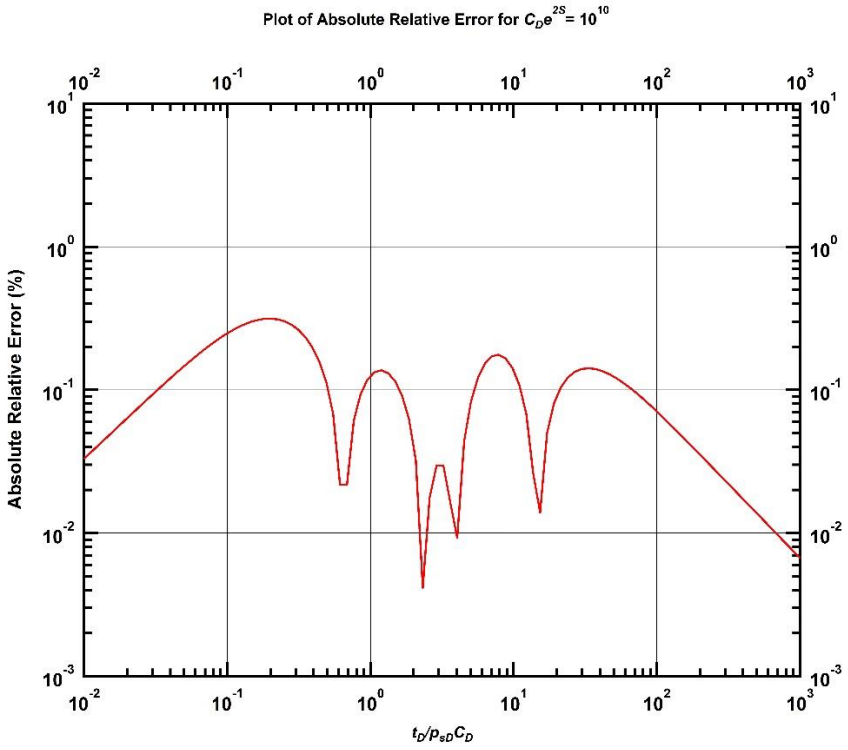

Figure F.11 — Absolute Relative Error Plot for $C_De^{2s} = 10^{10}$.

Figures F.12 and **F.13**show type curve plots of $p_{wCD}(t_D)$. While Figure F.12 shows a type curve plot of $p_{wCD}(t_D)$ obtained numerically compared with that obtained from Eq. F.13, Figure F.13 shows a type curve plot of $p_{wCD}(t_D)$ obtained from Eq. F.13. It can be observed that the match is good, as corresponding C_De^{2s} curves lie on top of each other almost perfectly.

Figures F.14 and **F.15** show type curve plots of $p_{wCD}'(t_D)$. While Figure F.14 shows a type curve plot of $p_{wCD}(t_D)$ obtained numerically compared with that obtained from the numerical differentiation of the $p_{wCD}(t_D)$ in Eq. F.13, Figure F.15 shows a type curve plot of $p_{wCD}(t_D)$ obtained from Eq. F.13. It can be observed that the shape of the derivative curve in Figure F.15 is not as it ought to be. There is an extra point of inflection as the derivative moves towards radial flow stabilization ($p_{wCD}'(t_D) = 0.5$).

This implies that this approximation is not an accurate representation of $p_{wCD}(t_D)$. Attempting to carry out a deconvolution calculation aimed at determining $p_{sD}(t_D)$ from this flawed $p_{wCD}(t_D)$ cannot yield accurate results.

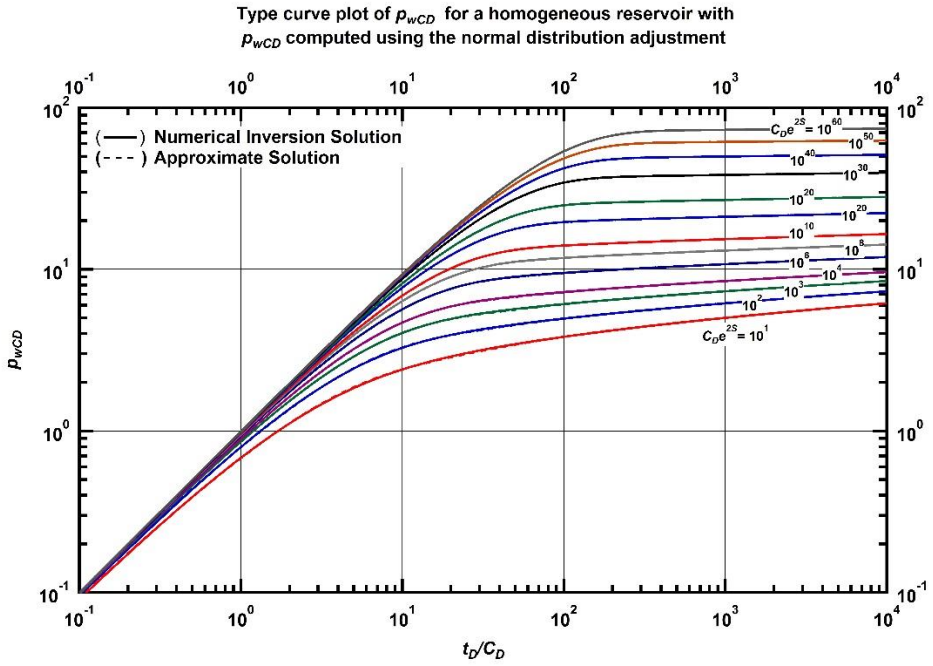

Figure F.12 — Type curve plot of p_{wCD} for a homogeneous reservoir. p_{wCD} computed using the normal distribution adjustment.

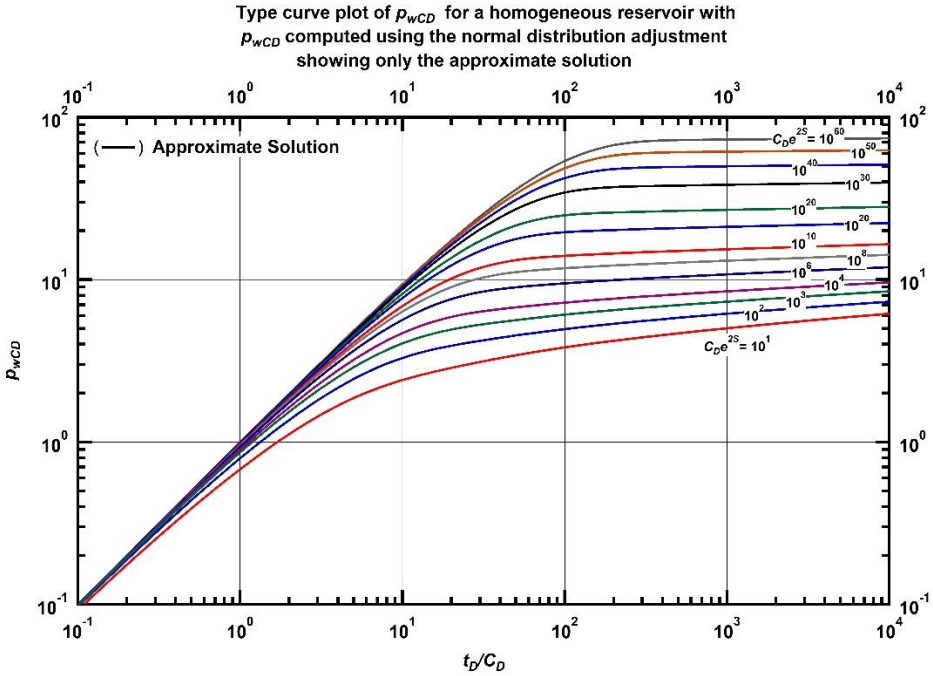

Figure F.13 — Type curve plot of p_{wCD} for a homogeneous reservoir. p_{wCD} computed using the normal distribution adjustment showing only the approximate solution.

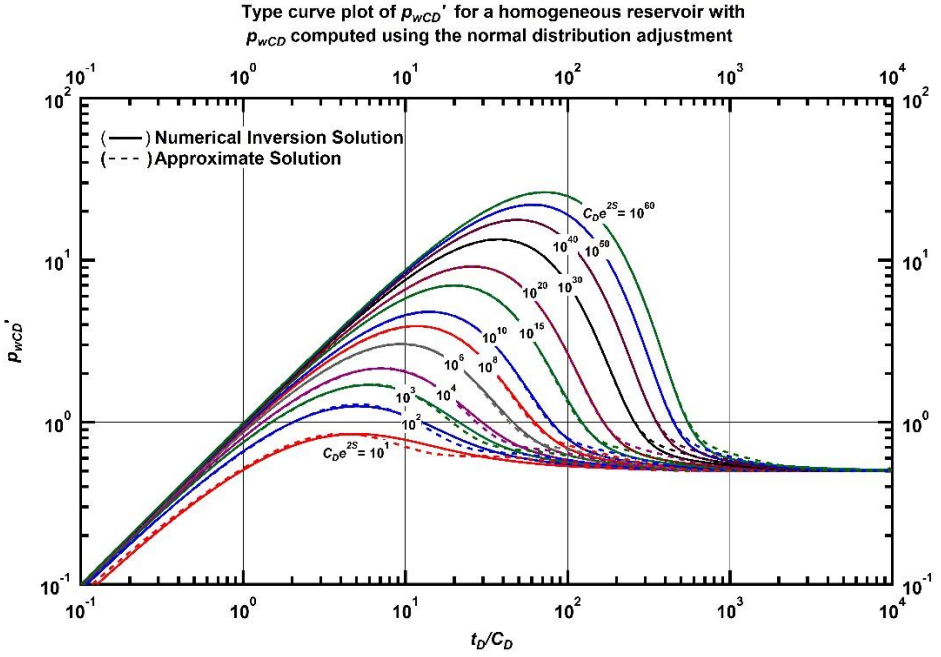

Figure F.14 — Type curve plot of p_{wCD}' for a homogeneous reservoir. p_{wCD} computed using the normal distribution adjustment.

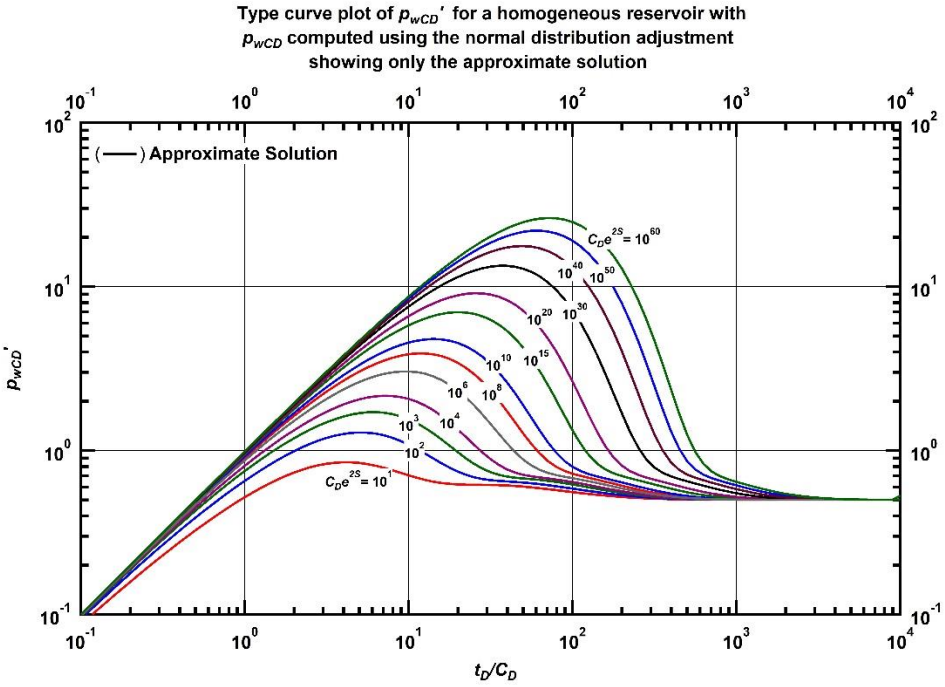

Figure F.15 — Type curve plot of p_{wCD}' for a homogeneous reservoir. p_{wCD} computed using the normal distribution adjustment showing only the approximate solution.

F.2 Deconvolution with Modified Normal Distribution adjustment

The modification of the normal distribution could be written as

$$p = \frac{\alpha_1}{\sigma_1\sqrt{2\pi}}\exp\left[-\frac{1}{2}\left[\frac{x-m_1}{\sigma_1}\right]^2\right] + \frac{\alpha_2}{\sigma_2\sqrt{2\pi}}\exp\left[-\frac{1}{2}\left[\frac{x-m_2}{\sigma_2}\right]^2\right] \quad \text{.....(F.16)}$$

This is essentially the addition to two normal distribution equations, where p is the probability distribution function, α_1 and α_2 are the scaling factors, m_1 and m_2 are the means of the distributions, σ_1 and σ_2 are the variances of the distributions and x is value of the data point.

In our case, the normal distribution equation describing $\varepsilon[t_D/(p_{sD}\,C_D)]$ would be

$$\varepsilon\left[\frac{t_D}{p_{sD}C_D}\right] = \frac{\alpha_1}{\sigma_1\sqrt{2\pi}}\exp\left[-\frac{1}{2}\left[\frac{\ln\left[\frac{t_D}{p_{sD}C_D}\right]-m_1}{\sigma_1}\right]^2\right] + \frac{\alpha_2}{\sigma_2\sqrt{2\pi}}\exp\left[-\frac{1}{2}\left[\frac{\ln\left[\frac{t_D}{p_{sD}C_D}\right]-m_2}{\sigma_2}\right]^2\right]$$

.....(F.17)

where the values of α_1, α_2, m_1, m_2, σ_1, and σ_2 vary based on C_D.

An improved approximation of $p_{wCD}(t_D)$ obtained from combining Eqs. F.6 and F.10 can, therefore, be written as

$$p_{wCD}(t_D) = p_{sD}(t_D)\left[\begin{array}{l}\left[1-\exp\left[\frac{-t_D}{p_{sD}C_D}\right]\right] - \frac{\alpha_1}{\sigma_1\sqrt{2\pi}}\exp\left[-\frac{1}{2}\left[\frac{\ln\left[\frac{t_D}{p_{sD}C_D}\right]-m_1}{\sigma_1}\right]^2\right] \\ + \frac{\alpha_2}{\sigma_2\sqrt{2\pi}}\exp\left[-\frac{1}{2}\left[\frac{\ln\left[\frac{t_D}{p_{sD}C_D}\right]-m_2}{\sigma_2}\right]^2\right]\end{array}\right] \quad \text{.....(F.18)}$$

While the choice of the modified normal distribution equation is based on the shape of $\varepsilon[t_D/(p_{sD}\,C_D)]$, the parameters of the normal distribution equation that provide a good fit for a particular value of C_D are determined by

- A good visual match of a plot that compares $\varepsilon[t_D/(p_{sD}\,C_D)]$ obtained from Eq. F.8 and $\varepsilon[t_D/(p_{sD}\,C_D)]$ obtained from the modified normal distribution equation (Eq. F.17), and

- An acceptable level of error between $\varepsilon[t_D/(p_{sD}\, C_D)]$ obtained from Eq. F.8 and $\varepsilon[t_D/(p_{sD}\, C_D)]$ obtained from the modified normal distribution equation (Eq. F.17) i.e. an Absolute Relative Error (*ARE*) ≤ 1.5%.

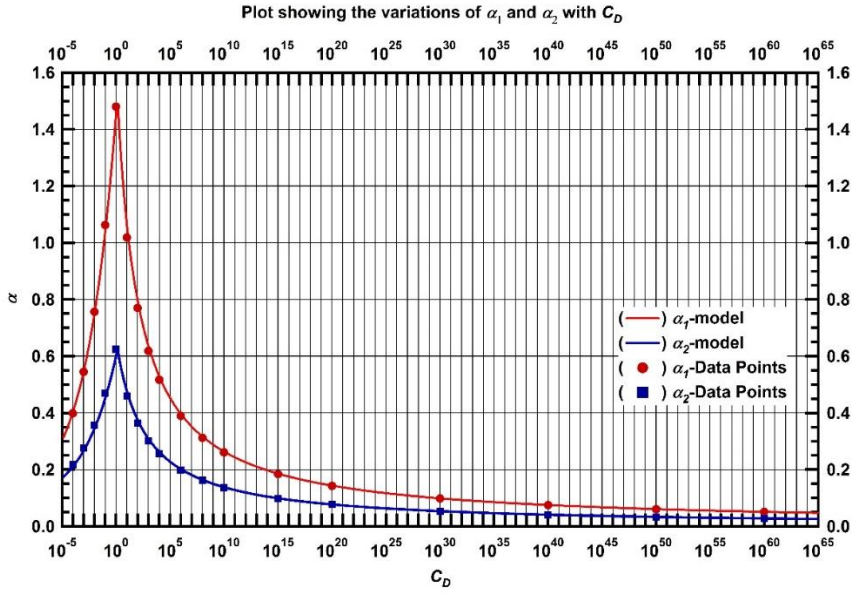

Figure F.16 — Plot showing the variation of α_1 and α_2 with C_D.

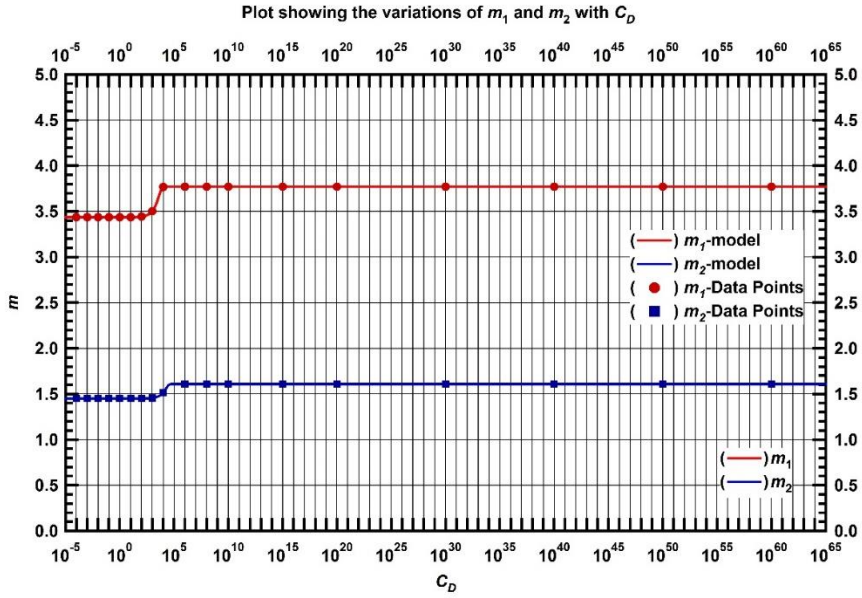

Figure F.17 — Plot showing the variation of m_1 and m_2 with C_D.

Figures F.18 – F.25 show match plots and *ARE* plots for selected values of C_De^{2s}. These plots show good fits and acceptable *ARE*. By this process of matching and error determination, relationships between the parameters α_1, α_2, m_1, m_2, σ_1, σ_2 and C_D, were determined empirically to be given as

$$\alpha_1 = \frac{67}{46.79328048}\exp\left[-\frac{|0.17712654\ln C_D|}{6.491984578}\right] + 0.06176, \text{for } C_D < 1, \quad \text{(F.19a)}$$

$$\alpha_1 = \frac{7.25627685}{\ln C_D + 4.82070369}, \text{ for } C_D \geq 1, \quad \text{(F.19b)}$$

$$\alpha_2 = \frac{67}{46.79328048}\exp\left[-\frac{|0.17712654\ln C_D|}{6.491984578}\right] + 0.06176, \text{for } C_D < 1, \quad \text{(F.20a)}$$

$$\alpha_2 = \frac{4.02500168}{\ln C_D + 6.45174628}, \text{ for } C_D \geq 1, \quad \text{(F.20b)}$$

$$m_1 = 0.33475819\,\text{erf}(0.00017879C_D) + 3.43607917, \quad \text{(F.21)}$$

$$m_2 = 0.16\,\text{erf}(0.000038895C_D) + 1.44896298, \quad \text{(F.22)}$$

$$\sigma_1 = 1.58, \quad \text{(F.23)}$$

$$\sigma_2 = 0.79. \quad \text{(F.24)}$$

Table F.2 shows the empirical values of α, m, and, σ for various values of C_D.

Table F.2— Empirical values of α, m, and, σ for various values of C_D.

C_D	a_1	m_1	s_1	a_2	m_2	s_2
10^{-4}	0.989677	3.436079	1.58	0.612319	1.448963	0.79
10^{-3}	1.096792	3.436079	1.58	0.613858	1.448963	0.79
10^{-2}	1.216340	3.436080	1.58	0.615751	1.448963	0.79
10^{-1}	1.349764	3.436086	1.58	0.618231	1.448964	0.79
10^{0}	1.505232	3.436147	1.58	0.623862	1.448970	0.79
10^{1}	1.018669	3.436755	1.58	0.459773	1.449033	0.79
10^{2}	0.769825	3.442832	1.58	0.364026	1.449665	0.79
10^{3}	0.618690	3.502901	1.58	0.301284	1.455982	0.79
10^{4}	0.517159	3.767002	1.58	0.25699	1.515799	0.79
10^{6}	0.389364	3.770837	1.58	0.198596	1.608963	0.79
10^{8}	0.312214	3.770837	1.58	0.161826	1.608963	0.79
10^{10}	0.260581	3.770837	1.58	0.136544	1.608963	0.79
10^{15}	0.184359	3.770837	1.58	0.098193	1.608963	0.79
10^{20}	0.142637	3.770837	1.58	0.076662	1.608963	0.79
10^{30}	0.098193	3.770837	1.58	0.053291	1.608963	0.79
10^{40}	0.074866	3.770837	1.58	0.04084	1.608963	0.79
10^{50}	0.060494	3.770837	1.58	0.033106	1.608963	0.79
10^{60}	0.050752	3.770837	1.58	0.027834	1.608963	0.79

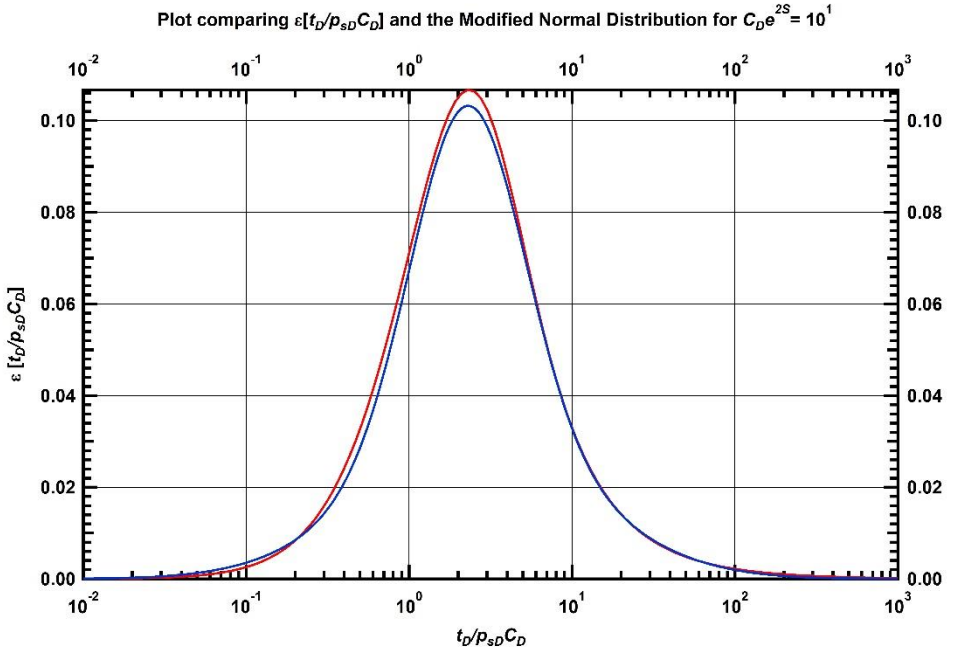

Figure F.18 — Plot comparing $\varepsilon[t_D/(p_{sD}\, C_D)]$ and the Modified Normal Distribution for $C_De^{2s} = 10^1$.

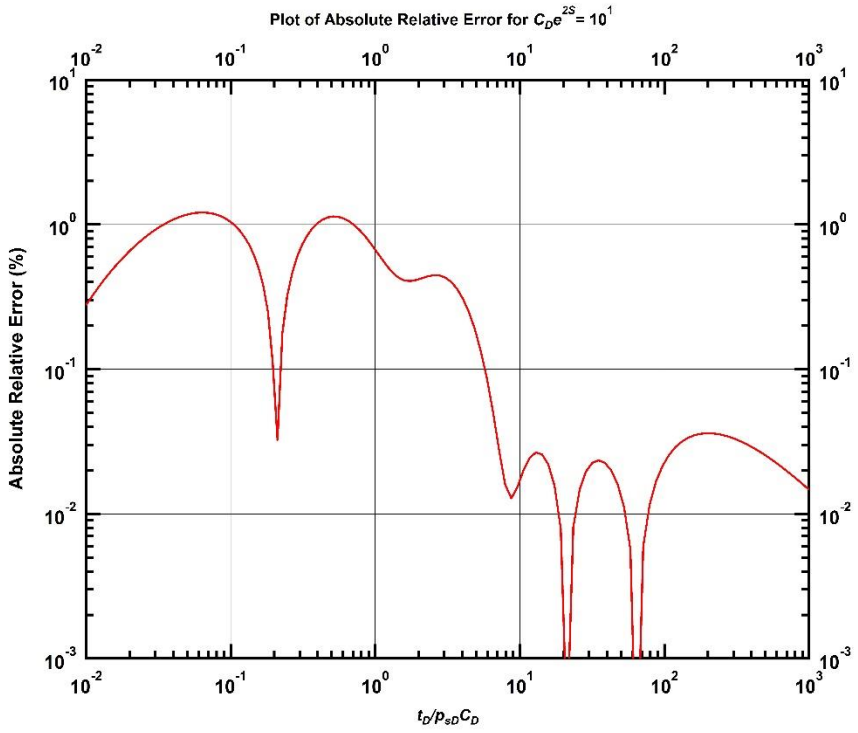

Figure F.19 — Absolute Relative Error Plot for $C_De^{2s} = 10^1$ (Modified Normal Distribution).

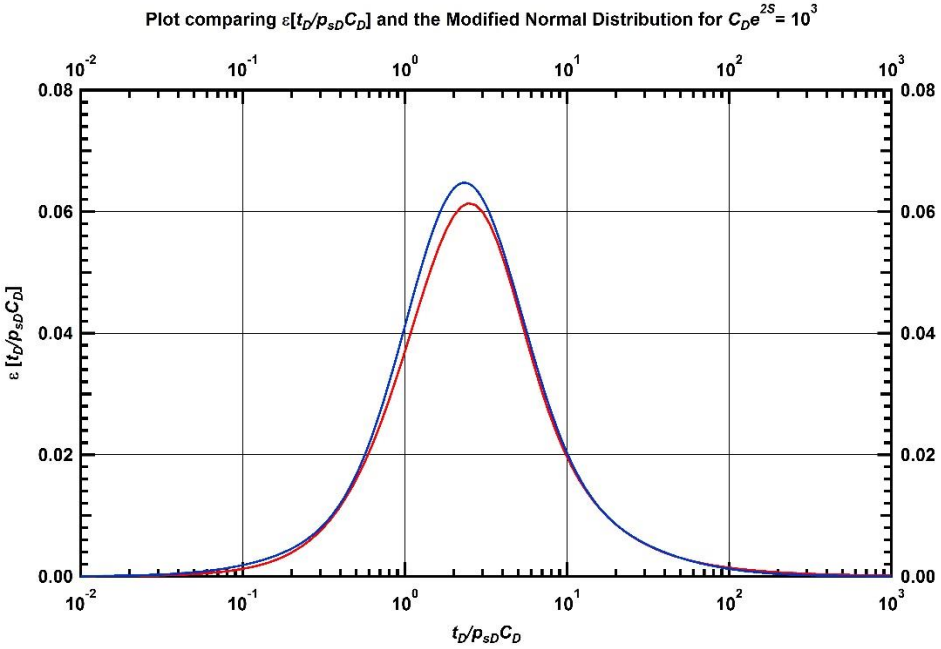

Figure F.20 — Plot comparing $\varepsilon[t_D/(p_{sD}\, C_D)]$ and the Modified Normal Distribution for $C_De^{2s} = 10^3$.

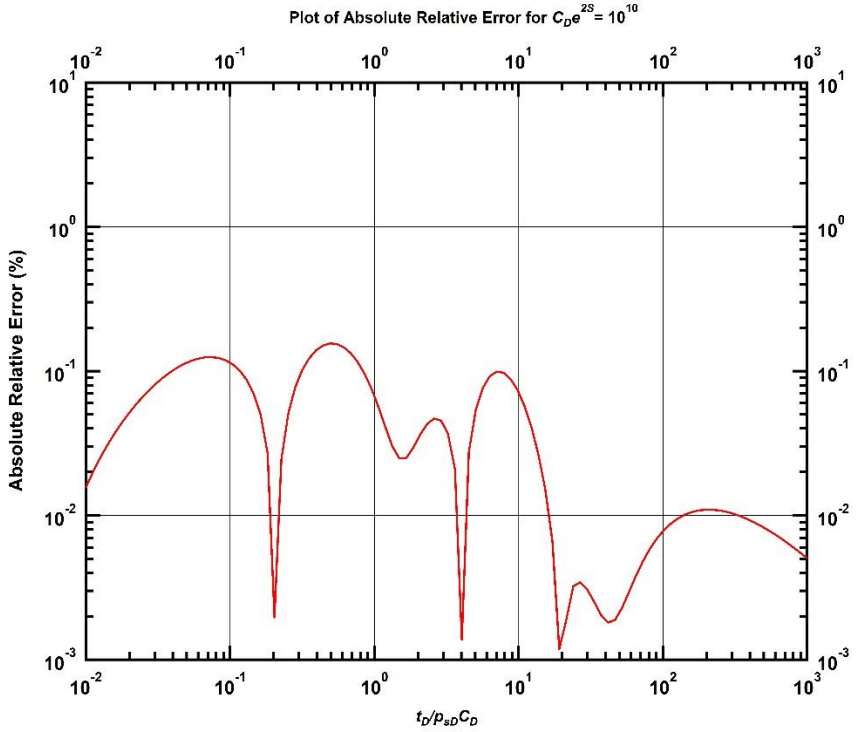

Figure F.21 — Absolute Relative Error Plot for $C_De^{2s} = 10^3$ (Modified Normal Distribution).

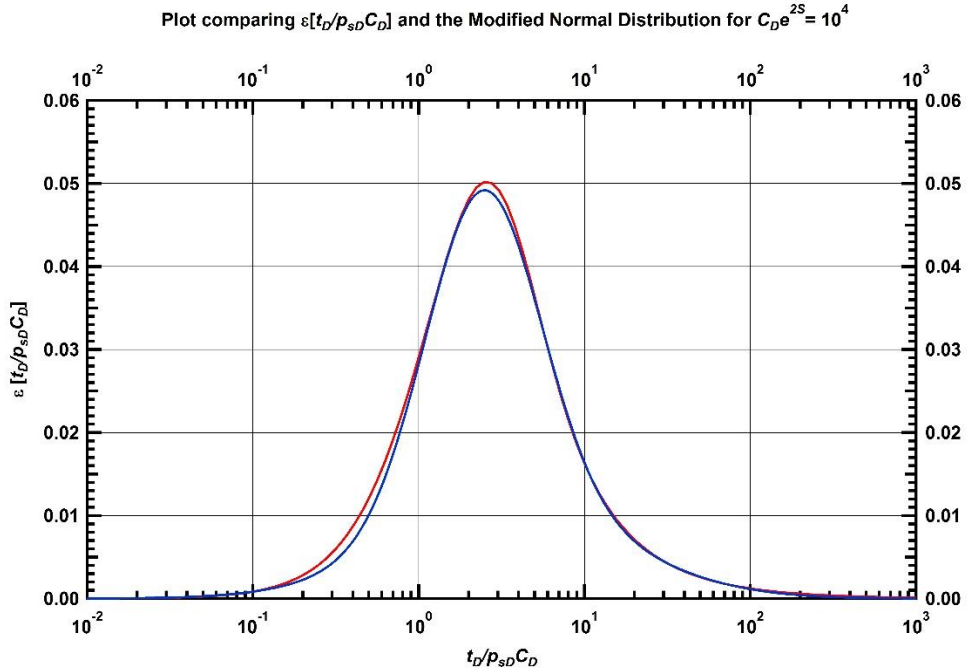

Figure F.22 — Plot comparing $\varepsilon[t_D/(p_{sD}\, C_D)]$ and the Modified Normal Distribution for $C_De^{2s} = 10^4$.

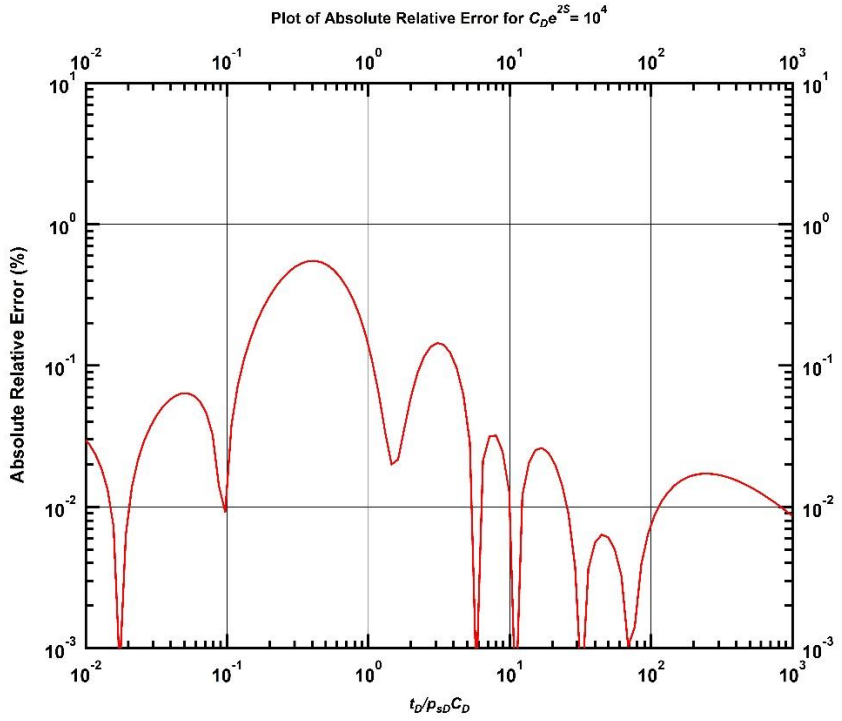

Figure F.23 — Absolute Relative Error Plot for $C_De^{2s} = 10^4$ (Modified Normal Distribution).

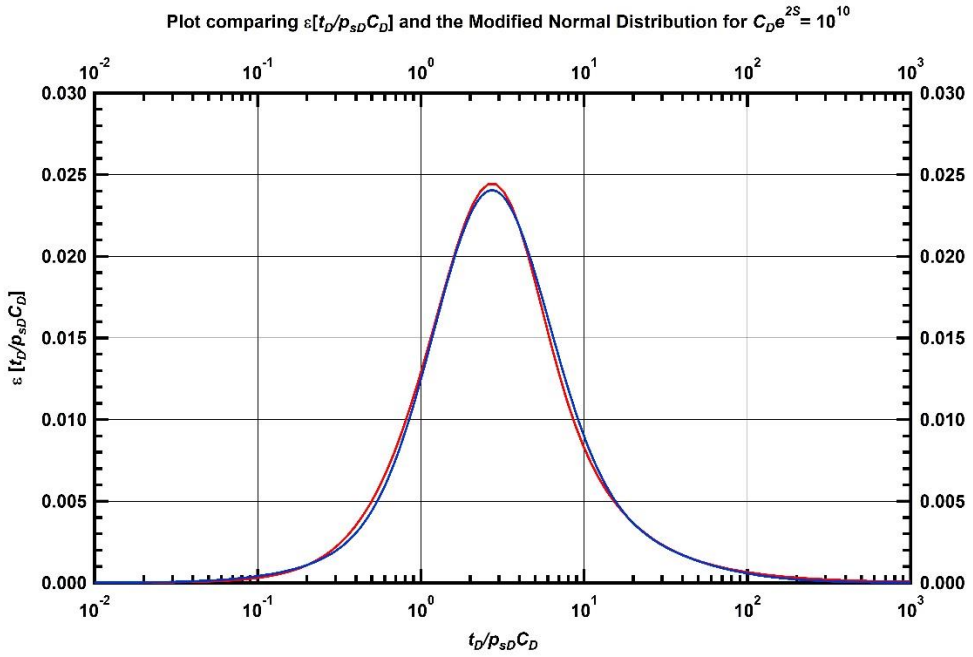

Figure F.24 — Plot comparing $\varepsilon[t_D/(p_{sD}\, C_D)]$ and the Modified Normal Distribution for $C_De^{2s} = 10^{10}$.

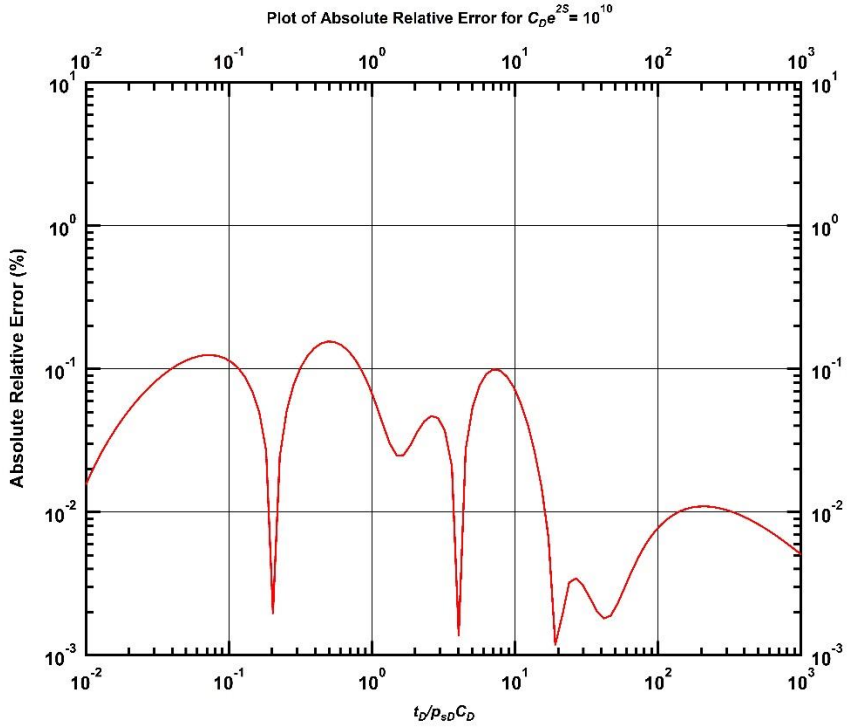

Figure F.25 — Absolute Relative Error Plot for $C_De^{2s} = 10^{10}$ (Modified Normal Distribution).

Figures F.26 and **F.27**show type curve plots of $p_{wCD}(t_D)$. While Figure F.26 shows a type curve plot of $p_{wCD}(t_D)$ obtained numerically compared with that obtained from Eq. F.27, Figure F.27 shows a type curve plot of $p_{wCD}(t_D)$ obtained from Eq. F.27. It can be observed that the match is good, as corresponding C_De^{2s} curves lie on top of each other almost perfectly.

Figures F.28 and **F.29** show type curve plots of $p_{wCD}'(t_D)$. While Figure F.28 shows a type curve plot of $p_{wCD}(t_D)$ obtained numerically compared with that obtained from the numerical differentiation of the $p_{wCD}(t_D)$ in Eq. F.27, Figure F.29 shows a type curve plot of $p_{wCD}(t_D)$ obtained from Eq. F.27. It can be observed that both the pressure and derivative curves are very good matches.

This implies that this approximation is an accurate representation of $p_{wCD}(t_D)$ and a deconvolution aimed at determining $p_{sD}(t_D)$ from this $p_{wCD}(t_D)$ can be attempted.

Deconvolution, in this case, means the determination of $p_{sD}(t_D)$ from Eq. F.18. This cannot be done by hand and requires the use of some software package. Wolfram Mathematica was used in the deconvolution calculations in this work.

Figures F.30 and **F.31** show type curve plots of $p_{sD}(t_D)$. While Figure F.30 shows a type curve plot of $p_{sD}(t_D)$ obtained numerically compared with that obtained from Eq. F.18, Figure F.31 shows a type curve plot of $p_{sD}(t_D)$ obtained from Eq. F.27. It is clear that the $p_{sD}(t_D)$ determined using deconvolution does not match the one obtained numerically. The attempted deconvolution has not yielded an accurate $p_{sD}(t_D)$ approximation.

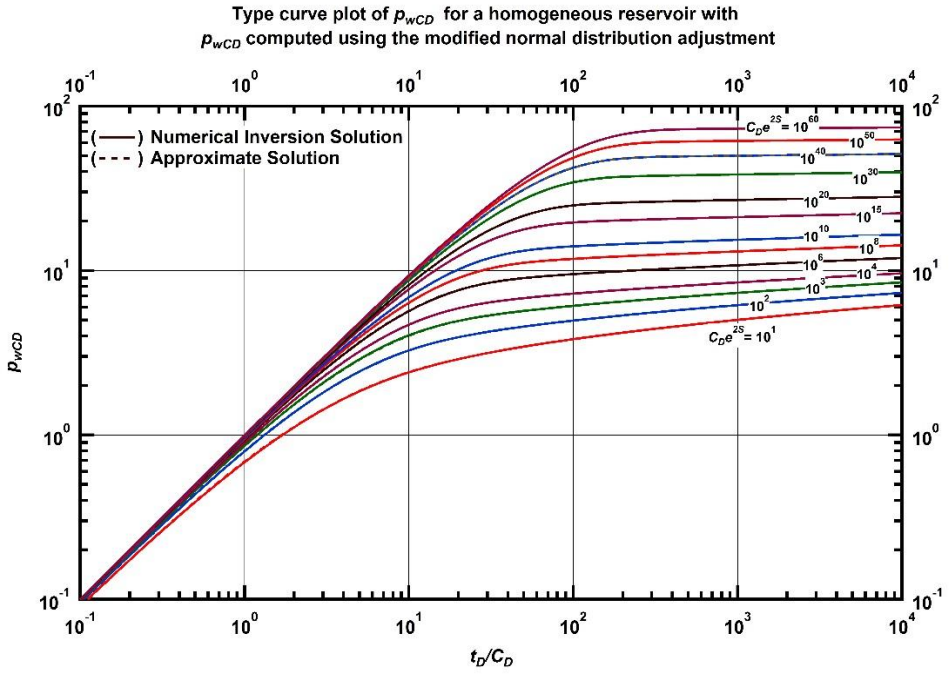

Figure F.26 — Type curve plot of p_{wCD} for a homogeneous reservoir. p_{wCD} computed using the modified normal distribution adjustment.

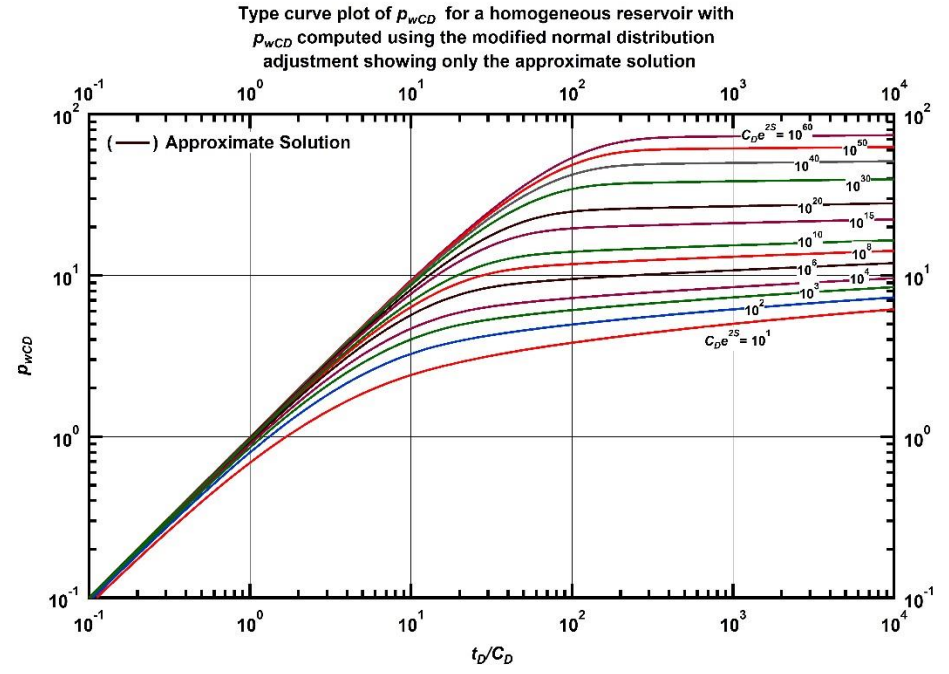

Figure F.27 — Type curve plot of p_{wCD} for a homogeneous reservoir. p_{wCD} computed using the modified normal distribution adjustment showing only the approximate solution.

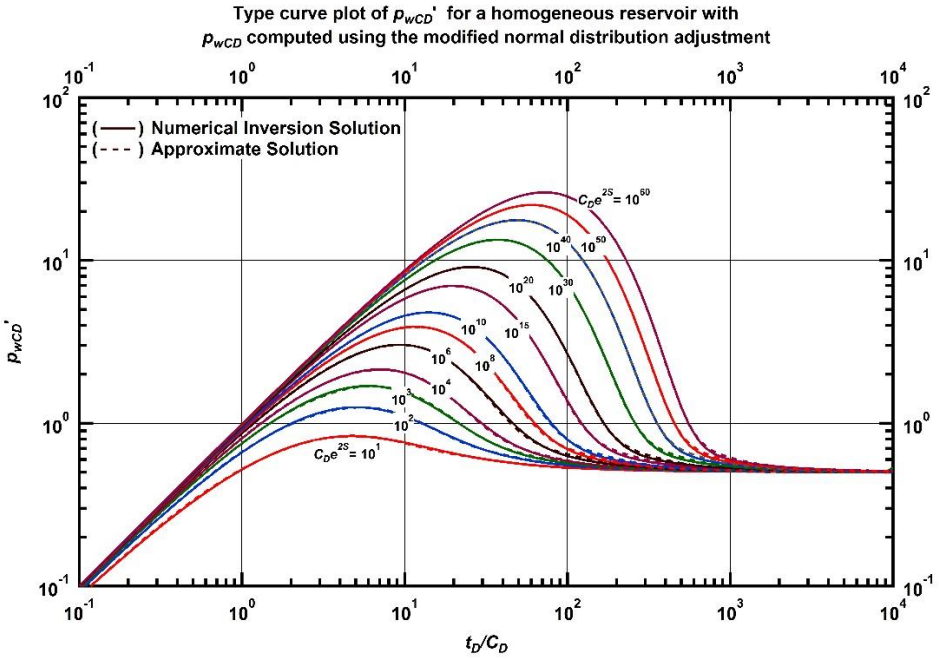

Figure F.28 — Type curve plot of p_{wCD}' for a homogeneous reservoir. p_{wCD} computed using the modified normal distribution adjustment.

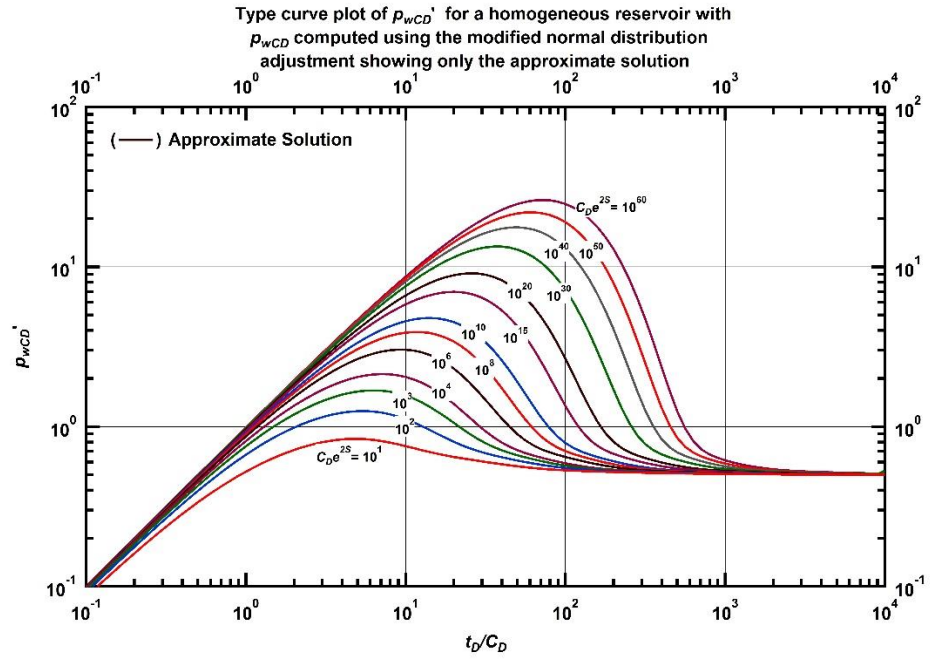

Figure F.29 — Type curve plot of p_{wCD}' for a homogeneous reservoir. p_{wCD} computed using the modified normal distribution adjustment showing only the approximate solution.

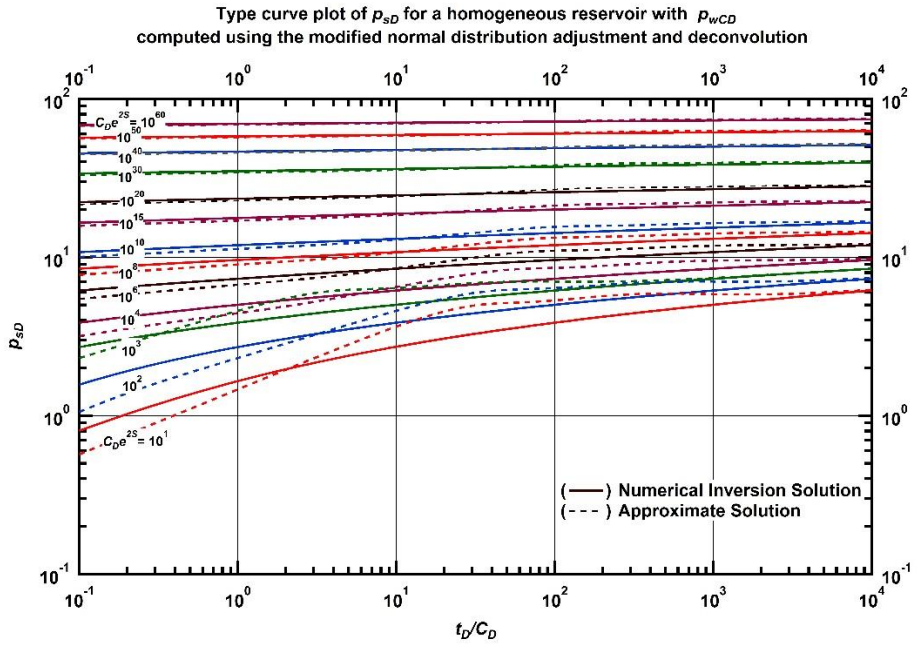

Figure F.30 — Type curve plot of p_{sD} for a homogeneous reservoir. p_{wCD} computed using the modified normal distribution adjustment and deconvolution.

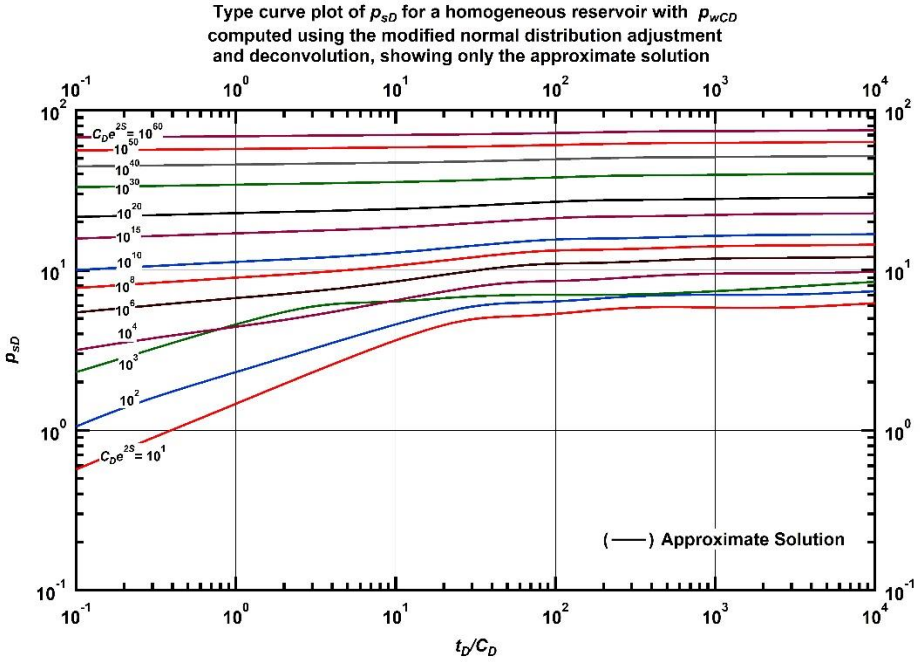

Figure F.31 — Type curve plot of p_{sD} for a homogeneous reservoir. p_{wCD} computed using the modified normal distribution adjustment and deconvolution, showing only the approximate solution.

APPENDIX G

DERIVATION OF DECONVOLUTION APPROXIMATION FOR $p_{sD}(t_D)$ BASED ON $p_{wCD}(t_D)$ DERIVED USING THE LINEAR $p_{sD}(t_D)$ ASSUMPTION

It has been shown that the constant rate bottomhole pressure affected by wellbore storage and skin effects can be written as a convolution integral given by

$$p_{wCD}(t_D) = \int_0^{t_D} \frac{d}{d\tau}\left[q_{wCD}(\tau)\right] p_{sD}(t_D - \tau)\, d\tau \,, \quad \text{(G.1)}$$

where

$$q_{wCD}(t_D) = 1 - C_D \frac{d}{dt_D}\left[p_{wCD}(t_D)\right], \quad \text{(G.2)}$$

and

$$p_{sD}(t_D) = p_D(t_D) + s \,. \quad \text{(G.3)}$$

Eq. G.1 can be approximated as

$$p_{wCD}(t_D) = \frac{y}{x}\left[1 - \exp(-xt_D)\right] + \frac{z}{x^2}\left[\exp(-xt_D) + xt_D - 1\right] \quad \text{(G.4)}$$

where

$$x = \frac{1 + C_D b}{C_D a} \quad \text{(G.5)}$$

$$y = \frac{1}{C_D} \quad \text{(G.6)}$$

$$z = \frac{b}{aC_D} \quad \text{(G.7)}$$

and

$$b = \frac{d}{dt_D}\left[p_{sD}(t_D)\right] \quad \text{(G.8)}$$

$$a = p_{sD}(t_D) - t_D \frac{d}{dt_D}\left[p_{sD}(t_D)\right] \quad \text{(G.9)}$$

Substituting Eqs. G.8 and G.9 into Eqs. G.5, G.6 and G.7, we obtain

$$x = \frac{1 + C_D\left[\frac{d}{dt_D}\left[p_{sD}(t_D)\right]\right]}{C_D\left[p_{sD}(t_D) - t_D\frac{d}{dt_D}\left[p_{sD}(t_D)\right]\right]} \quad \text{.....(G.10)}$$

$$z = \frac{\frac{d}{dt_D}\left[p_{sD}(t_D)\right]}{C_D\left[p_{sD}(t_D) - t_D\frac{d}{dt_D}\left[p_{sD}(t_D)\right]\right]} \quad \text{.....(G.11)}$$

$$\frac{y}{x} = \frac{a}{1 + C_D b} = \frac{p_{sD}(t_D) - t_D\frac{d}{dt_D}\left[p_{sD}(t_D)\right]}{1 + C_D\left[\frac{d}{dt_D}\left[p_{sD}(t_D)\right]\right]} \quad \text{.....(G.12)}$$

$$\frac{z}{x^2} = \frac{C_D ab}{(1 + C_D b)^2} = \frac{C_D\left[p_{sD}(t_D) - t_D\frac{d}{dt_D}\left[p_{sD}(t_D)\right]\right]\left[\frac{d}{dt_D}\left[p_{sD}(t_D)\right]\right]}{\left[1 + C_D\left[\frac{d}{dt_D}\left[p_{sD}(t_D)\right]\right]\right]^2} \quad \text{.....(G.13)}$$

Therefore, Eq. G.4 becomes

$$p_{wCD}(t_D) = \frac{p_{sD}(t_D) - t_D\frac{d}{dt_D}\left[p_{sD}(t_D)\right]}{1 + C_D\left[\frac{d}{dt_D}\left[p_{sD}(t_D)\right]\right]}\left[1 - \exp\left[-\frac{t_D + C_D t_D\left[\frac{d}{dt_D}\left[p_{sD}(t_D)\right]\right]}{C_D\left[p_{sD}(t_D) - t_D\frac{d}{dt_D}\left[p_{sD}(t_D)\right]\right]}\right]\right]$$
$$+\left[\frac{C_D\left[p_{sD}(t_D) - t_D\frac{d}{dt_D}\left[p_{sD}(t_D)\right]\right]\left[\frac{d}{dt_D}\left[p_{sD}(t_D)\right]\right]}{\left[1 + C_D\left[\frac{d}{dt_D}\left[p_{sD}(t_D)\right]\right]\right]^2}\right]$$
$$\left[\exp\left[-\frac{t_D + C_D t_D\left[\frac{d}{dt_D}\left[p_{sD}(t_D)\right]\right]}{C_D\left[p_{sD}(t_D) - t_D\frac{d}{dt_D}\left[p_{sD}(t_D)\right]\right]}\right] + \left[\frac{t_D + C_D t_D\left[\frac{d}{dt_D}\left[p_{sD}(t_D)\right]\right]}{C_D\left[p_{sD}(t_D) - t_D\frac{d}{dt_D}\left[p_{sD}(t_D)\right]\right]}\right] - 1\right]$$

.....(G.14)

$$p_{wCD}(t_D) = \left[\frac{C_D\left[p_{sD}(t_D) - t_D \frac{d}{dt_D}[p_{sD}(t_D)] \right]\left[\frac{d}{dt_D}[p_{sD}(t_D)] \right]}{\left[1 + C_D\left[\frac{d}{dt_D}[p_{sD}(t_D)] \right] \right]^2} - \frac{p_{sD}(t_D) - t_D \frac{d}{dt_D}[p_{sD}(t_D)]}{1 + C_D\left[\frac{d}{dt_D}[p_{sD}(t_D)] \right]} \right]$$

$$\exp\left[- \frac{t_D + C_D t_D\left[\frac{d}{dt_D}[p_{sD}(t_D)] \right]}{C_D\left[p_{sD}(t_D) - t_D \frac{d}{dt_D}[p_{sD}(t_D)] \right]} \right] +$$

$$\left[\frac{p_{sD}(t_D) + (1 - t_D)\frac{d}{dt_D}[p_{sD}(t_D)]}{1 + C_D\left[\frac{d}{dt_D}[p_{sD}(t_D)] \right]} + \frac{C_D\left[p_{sD}(t_D) - t_D \frac{d}{dt_D}[p_{sD}(t_D)] \right]\left[\frac{d}{dt_D}[p_{sD}(t_D)] \right]}{\left[1 + C_D\left[\frac{d}{dt_D}[p_{sD}(t_D)] \right] \right]^2} \right] \quad \text{.....(G.15)}$$

$$p_{wCD}(t_D) = \frac{p_{sD}(t_D) + C_D t_D\left[\frac{d}{dt_D}[p_{sD}(t_D)] \right]^2}{\left[1 + C_D\left[\frac{d}{dt_D}[p_{sD}(t_D)] \right] \right]^2}$$

$$+ \exp\left[- \frac{t_D + C_D t_D\left[\frac{d}{dt_D}[p_{sD}(t_D)] \right]}{C_D\left[p_{sD}(t_D) - t_D \frac{d}{dt_D}[p_{sD}(t_D)] \right]} \right] \left[\frac{t_D \frac{d}{dt_D}[p_{sD}(t_D)] - p_{sD}(t_D)}{\left[1 + C_D\left[\frac{d}{dt_D}[p_{sD}(t_D)] \right] \right]^2} \right] \quad \text{.....(G.16)}$$

The type curve plot, shown in **Figure G.1**, comparing $p_{wCD}(t_D)$ obtained using Eq. G.16 (explicit p_{wCD} equation) and that obtained from applying Eqs. G.4 to G.9 (linear p_{sD} approximation solution) directly shows that the results are one and the same. Therefore, $p_{wCD}(t_D)$ obtained using the explicit equation is an accurate approximation for $p_{wCD}(t_D)$.

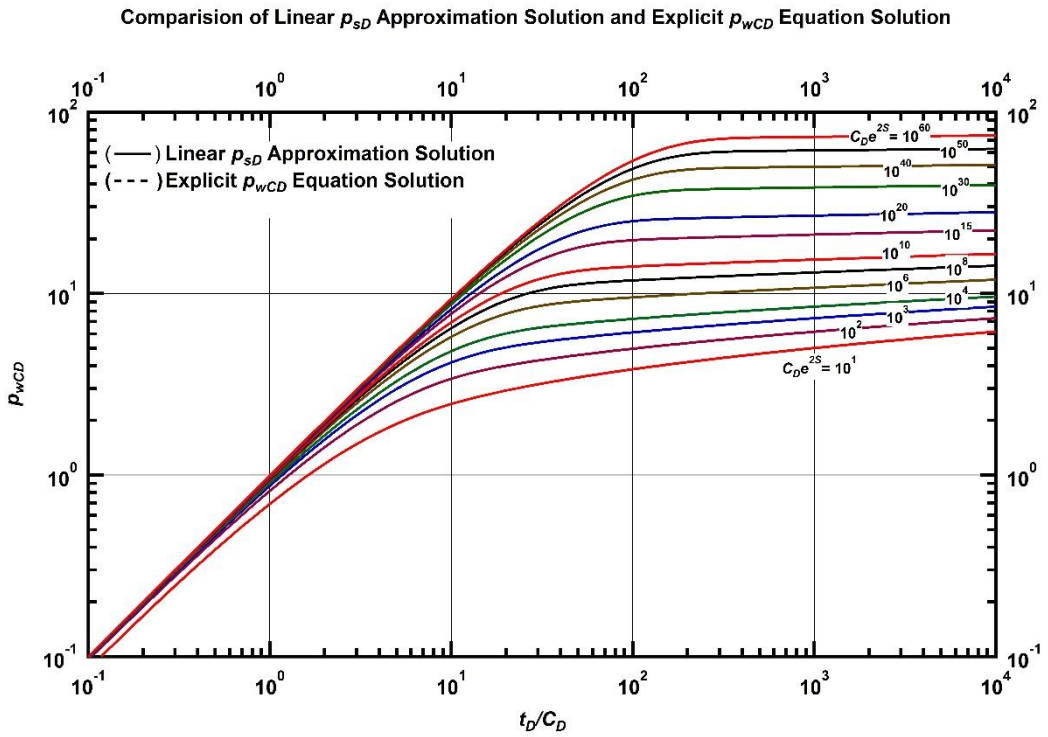

Figure G.1 — Type curve plot of p_{wCD} for a homogeneous reservoir comparing p_{wCD} computed using the explicit p_{wCD} equation and the linear p_{sD} approximation solution.

Deconvolution of $p_{wCD}(t_D)$ for an unfractured well in an infinite-acting homogeneous reservoir

The deconvolution of Eq. G.1 is the determination of $p_{sD}(t_D)$ from Eq. G.16. This would be impossible to achieve without specifying a value for or an expression of the derivative of $p_{sD}(t_D)$ with respect to t_D.

For a vertical, unfractured well in a homogenous reservoir, the log approximation solution to the diffusivity equation for radial flow is given as

$$p_{sD}(t_D) = \frac{1}{2}\ln\left[\frac{4}{e^{\gamma}}\frac{t_D}{{r_D}^2}\right] \quad \text{.....(G.17)}$$

Differentiating Eq. G.17 with respect to t_D,

$$\frac{d}{dt_D}\left[p_{sD}(t_D)\right] = \frac{1}{2t_D} \quad \text{.....(G.18)}$$

Substituting Eq. G.18 into G.16, we obtain,

$$p_{wCD}(t_D) = \frac{p_{sD}(t_D) + C_D t_D \left[\frac{1}{2t_D}\right]^2}{\left[1 + C_D\left[\frac{1}{2t_D}\right]\right]^2} + \exp\left[-\frac{t_D + C_D t_D\left[\frac{1}{2t_D}\right]}{C_D\left[p_{sD}(t_D) - t_D\left[\frac{1}{2t_D}\right]\right]}\right]\left[\frac{t_D\left[\frac{1}{2t_D}\right] - p_{sD}(t_D)}{\left[1 + C_D\left[\frac{1}{2t_D}\right]\right]^2}\right] \quad \text{.....(G.19)}$$

Simplifying Eq. G.19,

$$p_{wCD}(t_D) = \frac{p_{sD}(t_D) + \frac{C_D}{4t_D}}{\left[1 + \frac{C_D}{2t_D}\right]^2} + \frac{t_D\left[\frac{1}{2t_D}\right] - p_{sD}(t_D)}{\left[1 + \frac{C_D}{2t_D}\right]^2} \exp\left[-\frac{t_D + \frac{C_D}{2}}{C_D\left[p_{sD}(t_D) - \frac{1}{2}\right]}\right] \quad \text{.....(G.20)}$$

Eq. G.20 can be solved iteratively for $p_{sD}(t_D)$ with the help of spreadsheet packages.

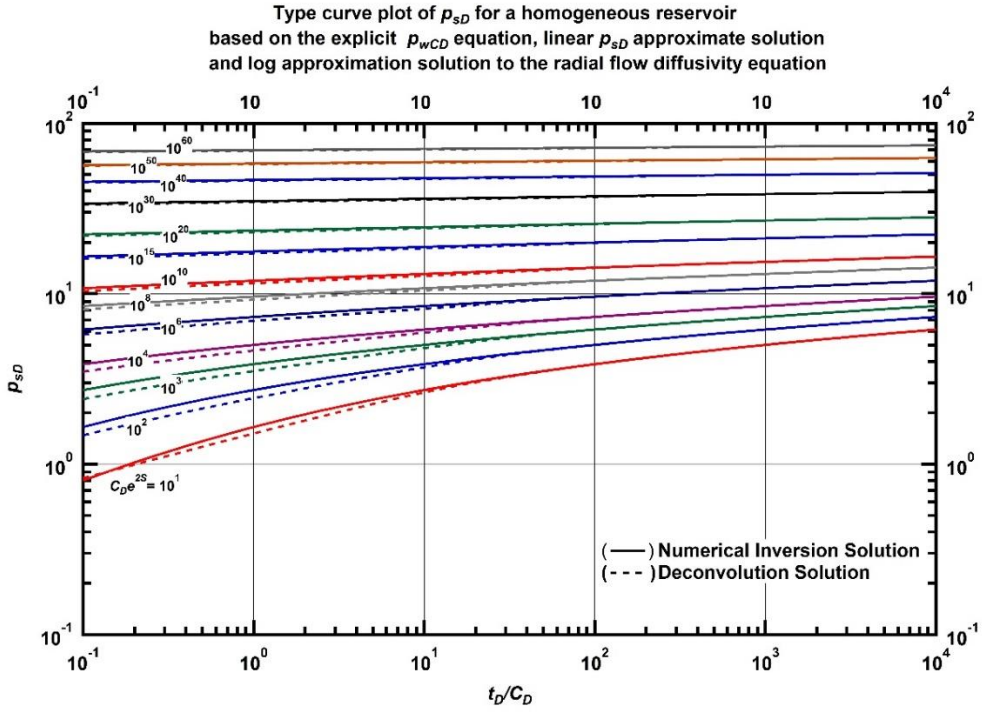

Figure G.2 — Type curve plot of p_{sD} for a homogeneous reservoir comparing p_{sD} computed using the explicit p_{wCD} equation, the linear p_{sD} approximate solution and the log approximation solution to that computed using numerical laplace transform inversion.

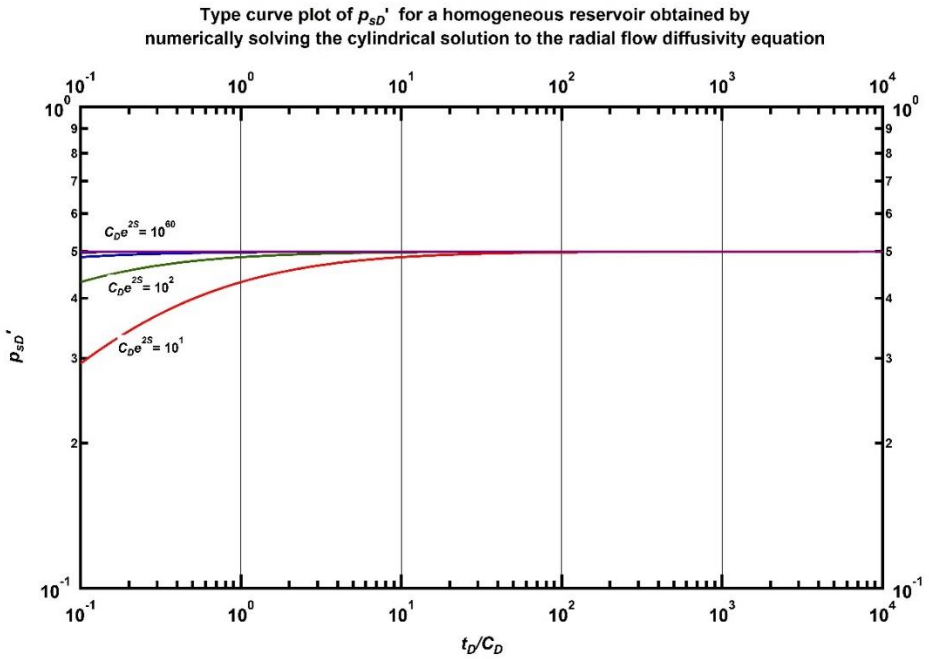

Figure G.3 — Type curve plot of p_{sD}' for a homogeneous reservoir, computed using numerical Laplace transform inversion.

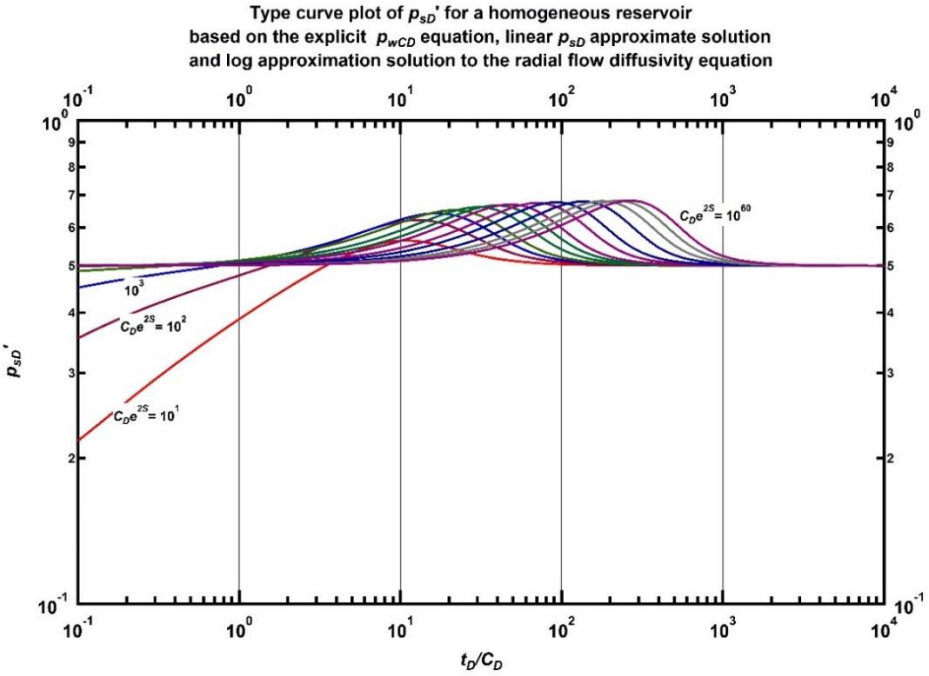

Figure G.4 — Type curve plot of p_{sD}' for a homogeneous reservoir, computed using the explicit p_{wCD} equation, the linear p_{sD} approximate solution and the log approximation solution

Figure G.2 shows the type curve plot of $p_{sD}(t_D)$ comparing results obtained from the numerical Laplace transform inversion and Eq. G.20. While at mid to late times the match is good, at early times, the match is not very good. **Figures G.3** and **G.4** show the derivatives of $p_{sD}(t_D)$ obtained by numerical Laplace transform inversion and Eq. G.20 respectively. It is clear that these two plots do not match each other.

This shows that we have been unable to successfully carry out deconvolution for a vertical well in an infinitely-acting homogeneous reservoir.